POLITECNICO DI MILANO

Facoltà di Ingegneria Industriale e dell'Informazione

Corso di Laurea Magistrale in

Ingegneria Biomedica

Design and validation of a novel experimental set-up for the detection of volitional intention during motor tasks functional imaging

Relatore: Prof. Alessandra Laura Giulia PEDROCCHI

Correlatore: Ing. Marta GANDOLLA

Ing. Simona FERRANTE

Tesi di Laurea di:

Alice FERRARI

Matr. 800935

Martina LOCATELLI

Matr. 798472

Anno Accademico 2013-2014

Table of contents

Sommario

1. Introduzione

Negli ultimi anni molti studi di letteratura si sono focalizzati sui meccanismi di recupero neuro-motorio valutando sia il sistema nervoso centrale (CSN) che il movimento periferico. L'acquisizione multi-modale di imaging di risonanza magnetica funzionale (fMRI) ed elettromiografia (EMG) rappresenta un prezioso strumento per analizzare le interazioni centrali e periferiche durante il processo di recupero. Queste misure simultanee correlano le mappe di attivazione corticale e i cambiamenti della performance del movimento eseguito. In aggiunta al sistema di acquisizione EMG, può essere ottenuta un'informazione più completa con l'introduzione del sistema di analisi del movimento che rileva in modo accurato il movimento eseguito e la cui origine, ovvero l'attività muscolare, è espressa in maniera quantitativa dal segnale EMG. L'interferenza reciproca tra le tecniche EMG e fMRI rappresentano un importante aspetto da analizzarsi sia dal punto di vista della qualità delle immagini funzionali quando è presente la strumentazione EMG che da quello del deterioramento del segnale EMG registrato all'interno della scanner room. Studi di letteratura dimostrano che l'influenza della strumentazione EMG sulle immagini MR sia dovuta alla presenza di componenti metalliche estranee (elettrodi, cavi, ecc.) nella stanza di risonanza e al rumore elettromagnetico irradiato dal dispositivo EMG che possono indurre un forte deterioramento del rapporto segnale-rumore (SNR) delle immagini [1]. D'altro canto, il segnale EMG è compromesso dagli artefatti causati dall'interazione tra i cavi degli elettrodi e i campi magnetici tempo-varianti presenti nella stanza di risonanza, secondo la legge di induzione di Fraday-Lenz. Gli impulsi di radiofrequenza (RF) e i campi magnetici gradiente accesi durante l'esame fMRI causano enormi artefatti nel segnale EMG alla frequenza principale e alle armoniche dei tempi di ripetizione (TR) dei loop di acquisizione della sequenza imaging considerata [2]. Il presente studio vuole affrontare i problemi descritti in modo sistematico e valutare la praticabilità di un innovativo set-up sperimentale che consenta, durante l'indagine fMRI, di registrare simultaneamente sia le caratteristiche del movimento, utilizzando un sistema di analisi del movimento (per compatibilità con fMRI vedi [3]), che il contributo volontario del soggetto (la contrazione muscolare), utilizzando un sistema di acquisizione EMG. Diversamente dai sistemi EMG fMRI-compatibili in commercio, il sistema presente nel set-up proposto non è ancora stato validato per l'uso in ambiente fMRI. E' inoltre adatto a fare da controllore FES (stimolazione elettrica funzionale: tecnica riabilitativa neuro-motoria che induce contrazione in muscoli privati del controllo neurale). I meccanismi centrali di riabilitazione neuro-motoria (rilevabili con fMRI) sono di interesse nel definire il training e il contributo volontario del soggetto (FES EMG-pilotata o miocontrollata) durante la riabilitazione è elemento chiave del suo successo.

2. Materiali e metodi

Il set-up sperimentale è composto da uno scanner CV/I 1.5 T , un dispositivo per la registrazione del segnale EMG Porti7, e un sistema di analisi del movimento Smart μg^{TM} (fig I).

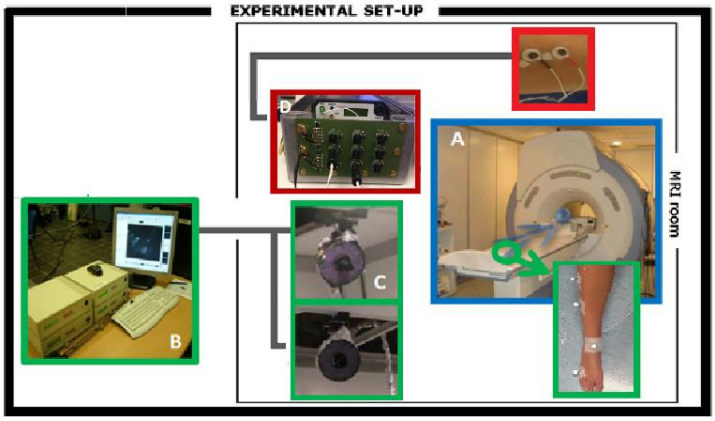

Figura I. Set-up sperimentale. (A) Scanner MRI GE CV/I 1.5 T; (B) Sistema di analisi del movimento Smart μg^{TM} con (C) due telecamere e marker riflessivi; (D) dispositivo Porti7 TMSi posto all'interno di una box prototipo e connesso agli elettrodi di registrazione da cavi in carbonio attorcigliati.

Il sistema di acquisizione EMG (frequenza di campionamento=2048Hz) è utilizzato in una configurazione stand-alone poiché il Porti7 è alimentato da un set di batterie (per prevenire il rumore indotto da MR sul cavo di alimentazione) e i dati EMG acquisiti sono salvati su una flash card. Il Porti7 è posto in un box in alluminio che protegge il sistema dall'accensione dei capi elettromagnetici (EM). I cavi degli elettrodi, essendo in carbonio, non sono immuni al rumore legato alla frequenza di rete (50Hz) e al movimento dei cavi. Gli elettrodi EMG, disposti in una configurazione bipolare, sono applicati al muscolo tibiale anteriore e al muscolo estensore ulnare del carpo poiché il soggetto esegue due compiti motori: dorsiflessione volontaria della caviglia destra (ADF) e estensione volontaria del polso destro (WE). Il protocollo totale dura 10 min e ciascun compito motorio consiste in dieci blocchi ON/OFF, dove ogni blocco è composto da 20s di esecuzione del task e da 10s di riposo. La frequenza di ripetizione del task motorio è posta a 0.5 Hz. Per ricostruire il movimento del soggetto all'interno della stanza di risonanza con il sistema di analisi del movimento (frequenza di campionamento=120 Hz), otto marker riflettenti sono posti sul dito medio della mano destra, sulla gamba destra e sul lettino di risonanza. All'esterno della stanza di risonanza, viene posto un elettrogoniometro sul polso e uno sulla caviglia destra per ottenere misure cinematiche analoghe.

Test di compatibilità MRI-EMG - La valutazione del rapporto segnale-rumore (SNR) su immagini di phantom pesate T1 con (MRI+K+EMG) e senza (MRI+K) la presenza del dispositivo di registrazione EMG è stata fatta per prima (K = cinematica). L'SNR è calcolato, su ogni fetta

dell'immagine MR del phantom, come il rapporto tra l'ampiezza media del segnale in un'area omogenea e la media delle deviazioni standard dell'ampiezza del segnale di background in 4 aree selezionate. Per ogni fetta è calcolata la percentuale di perdita di SNR tra la condizione di riferimento (MRI+K) e la condizione di test (MRI+K+EMG) e comparata con valori accettabili di qualità delle immagini riportati in letteratura (12%).

Test di compatibilità fMRI-EMG – La valutazione dell'SNR su immagini fMRI pesate T2* (TR=3s) del soggetto che esegue i task motori descritti con (fMRI+K+EMG) e senza (fMRI+K) la presenza del dispositivo di registrazione EMG.

Le immagini fMRI sono processate con il toolbox SPM8 di Matlab®. Le immagini vengono riallineate con la prima fetta di ogni volume. Un'immagine media fMRI riallineata viene co-registrata con l'immagine anatomica del soggetto. Le immagini (sia anatomiche che funzionali) vengono normalizzate allo spazio standard MNI. Infine, uno smoothing spaziale è eseguito usando un filtro Gaussiano FWHM di 8 mm. Un'analisi statistica viene eseguita con un general linear model, per ottenere l'attivazione corticale rilevata durante l'esecuzione dei tasks motori con il set-up sperimentale proposto (fMRI+K+EMG). La design matrix è ottenuta con due repressori: gli onset derivati dalla cinematica per i movimenti di ADF e WE. Per valutare la compatibilità fMRI-EMG, l'SNR delle immagini fMRI è calcolato confrontando la condizione di riferimento (fMRI+K) e la condizione di test (fMRI+K+EMG) in 4 regioni di interesse (ROIs) fortemente attivate durante l'esecuzione dei compiti motori [4,5]: la corteccia motoria primaria (M1), la corteccia motoria premotoria e supplementare (PM/SMA), la corteccia somatosensoriale primaria (S1) e l'area somatosensoriale secondaria. Un'analisi preliminare circa l'omogeneità di ciascuna ROI in termini di SNR è svolta utilizzando il coefficiente di variazione (CV), per una data condizione sperimentale (fMRI+K e fMRI+K+EMG), calcolato come la percentuale della deviazione standard dei valori di SNR rispetto alla media dei valori di SNR di ogni ROI, più basso è il valore migliore è l'omogeneità in termini di SNR per quella considerata ROI [6]. La deviazione standard dei CV è calcolata per ogni ROI per comparare i CV ottenuti per i tre soggetti nella stessa condizione sperimentale ovvero per valutarne la riproducibilità inter-soggettiva. Il test di Mann-Whitney è applicato per comparare, per ogni ROI, i CV di tutti i soggetti nelle due condizioni sperimentali ovvero per valutare la riproducibilità inter-condizione. La percentuale di SNR perso tra la condizione di test e la condizione di riferimento è calcolata sulla base del valor medio di SNR per ogni ROI. Dato che per uno scanner di 1.5T i cambiamenti di segnale BOLD rilevabili sono nell'intervallo dell'1-2% [3], sono create mappe di SNR per le immagini funzionali nelle due condizioni sperimentali, imponendo cinque soglie di SNR minimo [7] per il rilevamento di altrettanti cambiamenti di segnale BOLD (0.25%, 0.50%, 0.75%, 1%, 2%). Poi, per ogni ROI, viene calcolato il numero di voxel che possiede abbastanza SNR per rilevare un ΔS=1%-2% e

viene condotto un confronto tra la condizione di test e la condizione di riferimento. Inoltre, l'attivazione cerebrale relativa al compito motorio viene valutata utilizzando le immagini funzionali acquisite nella condizione test (fMRI+K+EMG).

Test di compatibilità EMG-fMRI – I segnali EMG acquisiti nelle diverse condizioni sperimentali, ovvero fuori dalla stanza di risonanza (EMG-Out), all'interno della stanza di risonanza con la sequenza fMRI spenta (B0+K+EMG) e all'interno della stanza di risonanza con la sequenza fMRI accesa (fMRI+K+EMG), vengono comparati. I segnali EMG acquisiti nelle tre condizioni sperimentali sono processati in due modalità differenti poiché l'EMG nella condizione fMRI+K+EMG necessita dell'applicazione di un algoritmo per la rimozione degli artefatti indotti da fMRI, ovvero il FARM (Artifact Reduction For Motion), sviluppato da van der Meer e colleghi [8]. Questo algoritmo filtra passa-banda i dati EMG grezzi (30-250 Hz) per rimuovere gli artefatti indotti da B0, le cui frequenze possono raggiungere i 30 Hz. Il dataset EMG viene poi processato utilizzando EEGLAB su Matlab®. Per creare il modello dell'artefatto da sottrarre ai dati EMG, il FARM usa una finestra mobile composta da 50 segmenti-fetta e seleziona i 12 artefatti-fetta che hanno la più alta correlazione con l'artefatto-fetta che deve essere corretto. In questo modo, se la forma dell'artefatto cambia, a causa di movimento durante l'acquisizione, questa procedura assicura che gli artefatti-fetta danneggiati dal movimento non vengano usati nella costruzione del modello di fetta e quindi la rimozione degli artefatti viene migliorata rispetto all'approccio standard di sottrazione del template di artefatto (AAS, [9]). L'algoritmo conduce un'analisi a componenti principali (PCA) sull'EMG corretto per rimuovere eventuali artefatti mantenutisi ad alta frequenza.
I segnali EMG grezzi nella condizione di riferimento (EMG-Out) e di test (B0+K+EMG) vengono filtrati passa-banda con lo stesso range di frequenze applicate nell'algoritmo FARM per rendere i segnali EMG delle diverse condizioni comparabili. La scelta di una così alta frequenza di taglio (30 Hz) è giustificata anche dall'uso di cavi non schermati attivamente che introducono nel segnale EMG rumore da artefatti di movimento che può raggiungere i 25-30 Hz.
Gli EMG delle tre condizioni sperimentali, vengono poi processati attraverso passi comuni:
- rettificazione full-wave del segnale per mantenerne tutta l'energia [10];
- smoothing con un filtraggio passa-basso (filtro Butterworth del quinto ordine, con frequenza di taglio a 5 Hz) per ottenere l'inviluppo del segnale;
- normalizzazione dell'ampiezza del segnale utilizzando il picco di massima ampiezza registrato all'interno della medesima acquisizione EMG [11];
- finestratura del segnale EMG (ovvero rilevamento di ogni attivazione muscolare) basata sugli onset della cinematica;
- normalizzazione temporale di ogni attivazione muscolare a 100 campioni ed estrazione delle caratteristiche EMG.

Vengono considerati tre indici EMG per comparare la condizione di riferimento (EMG-Out) con le altre due condizioni di test (B0+K+EMG e fMRI+K+EMG): il coefficiente di correlazione tra l'EMG medio ottenuto nelle tre condizioni sperimentali che dà indicazioni del mantenimento della forma caratteristica del segnale EMG senza la distorsione introdotta dall'ambiente MR; il picco di massima ampiezza e l'area integrata sotto il segnale. Il test statistico ANOVA a due vie viene applicato per gli ultimi due indici separatamente per ogni task motorio (ADF e WE) per valutare se vi è una significativa differenza nella media dei dati CV tra condizioni e tra soggetti. Poi, per gli stessi due indici e separatamente per ogni soggetto, viene eseguita un'analisi sulla variabilità EMG tra le condizioni sperimentali utilizzando il coefficiente di variazione (CV), valido per la comparazione intra-soggettiva sullo stesso muscolo [12]. Il CV è calcolato per ciascuno dei due indici (area sotto il segnale e ampiezza di picco) considerando il valore medio dell'indice ottenuto in ciascuna condizione sperimentale come la caratteristica del segnale EMG su cui calcolare la variabilità intra-soggettiva.

Considerando, ad esempio, l'indice area, il CV è definito come segue:

$$\mathrm{CV}_{\mathrm{area}} = \frac{std(area)}{mean(area)} \qquad \text{(eq. I)}$$

dove la media e la deviazione standard vengono definite rispetto alle tre condizioni sperimentali a cui viene sottoposto ogni soggetto.

3. Risultati

Test di compatibilità MRI-EMG – La perdita percentuale di SNR tra la condizione di riferimento (MRI+K) e quella test (MRI+K+EMG) è uguale a (media ± std): 5.7 ± 3.4 %.

Test di compatibilità fMRI-EMG – Per ogni ROI considerata, i valori di CV dell'SNR delle immagini funzionali nelle due condizioni sperimentali di riferimento (fMRI+K) e test (fMRI+K+EMG) sono calcolate e, in media, il loro valore si assesta intorno al 40% per ogni ROI in entrambe le condizioni. I valori di deviazione standard, calcolati per ogni ROI per paragonare i CV ottenuti per i tre soggetti nella stessa condizione sperimentale, sono sempre inferiori al 5%. Il test Mann-Whitney, applicato per paragonare i CV di ogni soggetto tra le due condizioni sperimentali, ha sempre un p-value > 0.05 per ciascuna ROI.

Come atteso, la condizione di riferimento (fMRI+K) ha un valore di SNR medio, per ogni ROI, maggiore di quello della condizione test (fMRI+K+EMG) con la differenze statistica stabilita con un t-test (p-value < 0.05). La tabella I presenta la perdita percentuale di SNR in ogni ROI per tutti i soggetti e una loro media.

La fig. II presenta un esempio delle mappe di SNR, con le 5 soglie di SNR minimo imposte, in entrambe le condizioni sperimentali.

Tabella I. Perdita percentuale di SNR delle immagini funzionali tra condizione di riferimento e di test.
I valori sono presentati sia per soggetto che mediati.

PERDITA SNR (%)	**Soggetto 1**	**Soggetto 2**	**Soggetto 3**	**Media**
M1(b4)	16.60%	10.77%	15.43%	14.43% ± 3.08%
PM/SMA (b6)	14.80%	6.18%	10.28%	10.42% ± 4.31%
S1(b2-b3)	20.03%	15.93%	9.68%	15.21% ± 5.21%
SII (b5-b7)	12.13%	21.22%	4.88%	12.74% ± 8.18%

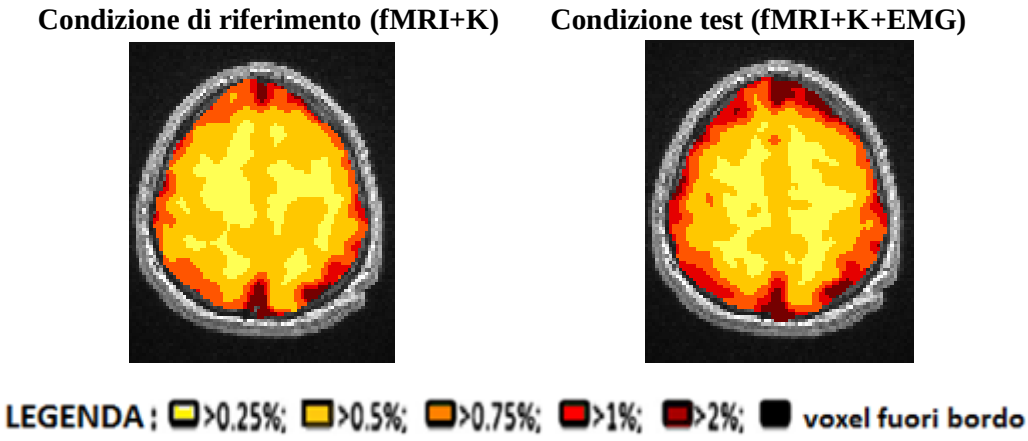

Figura II. Mappe di SNR, nella condizione di riferimento e in quella di test, ottenute per il soggetto 3.

La percentuale di voxel in ogni ROI che presenta un SNR alto abbastanza da permettere di osservare una variazione del segnale BOLD uguale all'1-2% è calcolato: una percentuale maggiore del 89% considerando l'1% di variazione del segnale BOLD e una percentuale maggiore del 97% per il 2% di variazione del segnale BOLD sono ottenute per tutti i soggetti e per ciascuna delle ROI considerate.

In fig. III si mostrano rappresentative mappe di attivazione corticale, ottenute considerando le immagini funzionali acquisite nella condizione test, per entrambi i compiti motori (ADF e WE).

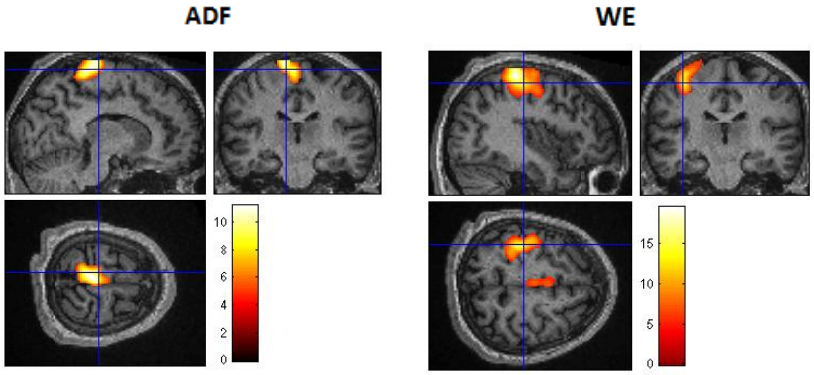

Figura III. Mappe di attivazione corticale ottenute, per il soggetto 3, durante l'esecuzione di un'ADF e di una WE. I risultati sono corretti con FWE (p-value < 0.05) e il numero minimo di cluster è imposto a 10.

Test di compatibilità EMG-fMRI – La fig. IV mostra, per un soggetto rappresentativo, le forme d'onda dell'EMG medio nelle tre condizioni sperimentali (EMG-Out, B0+K+EMG, fMRI+K+EMG).

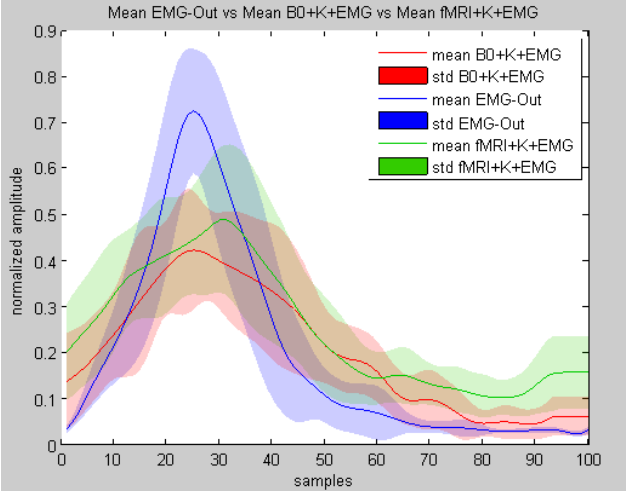

Figura IV. Forme d'onda dell'EMG medio nelle tre condizioni sperimentali considerate. Il compito motorio rappresentato è l'ADF, eseguito dal soggetto 3.

I coefficienti di correlazione delle forme d'onda del segnale EMG paragonando la condizione di riferimento (EMG-Out) con le altre due condizioni di test (B0+K+EMG e fMRI+K+EMG) sono, rispettivamente, maggiori di 0.76 e di 0.78 per ogni soggetto e per entrambi i compiti motori (p-value associato < 0.05). I due indici EMG scelti, area del segnale e ampiezza di picco, sono calcolati per ogni soggetto nelle tre condizioni sperimentali. Un test ANOVA a due vie applicato separatamente a questi indici dà un p-value < 0.05 sia per la differenza inter-soggettiva che per quella inter-condizioni e il risultato è lo stesso per entrambi i compiti motori.
Infine, separatamente per ogni soggetto, è calcolato il CV tra condizioni sperimentali per entrambi gli indici considerati. CV per l'area del segnale è sempre minore del 29% mentre il CV per l'ampiezza di picco è sempre minore del 20% considerando entrambi i compiti motori.

4. Discussione

L'obiettivo di questo lavoro è la progettazione e la validazione di un innovativo set-up sperimentale per l'acquisizione dell'intenzione volontaria del soggetto durante uno scanning fMRI a compiti motori. Il mantenimento della qualità dei dati acquisiti, fMRI ed EMG, è stata valutata.
Test di compatibilità MRI-EMG – Si è mostrato che la perdita di SNR indotta nelle immagini di risonanza magnetica dal set-up sperimentale progettato è trascurabile. Infatti, per ogni fetta di un'immagine MR, la perdita percentuale di SNR tra la condizione di riferimento (MRI+K) e quella di test (MRI+K+EMG) è 5.7 ± 3.4 %. Riferimenti bibliografici [13] mostrano che l'SNR di

immagini di risonanza magnetica, calcolato come nel presente lavoro, diminuisce in maniera inversamente proporzionale all'aumento del numero di elettrodi presenti nella scanner room. La perdita percentuale di SNR rispetto alla condizione di riferimento (senza elettrodi) ritenuta accettabile è dell'11-12%.

Test di compatibilità fMRI-EMG – Quattro ROI corticali, consistentemente attivate durante l'esecuzione di compiti motori, sono state considerate. Un indice di omogeneità (CV) è calcolato per ciascuna di queste ROI nella condizione di riferimento (fMRI+K) e in quella test (fMRI+K+EMG). Questa preventiva analisi di omogeneità è fatta per creare una base per le considerazioni successive sull'SNR, sia tra soggetti che tra condizioni, che sono in primo luogo basate sul valor medio. I dati CV, 40% in media, sono più alti di quelli ottenuti in letteratura [14] ma la loro riproducibilità tra soggetti (std < 5% [3]) e tra condizioni è stata verificata.

Tutti i soggetti mostrano una significativa perdita percentuale di SNR tra le due condizioni sperimentali (t-test con un p-value < 0.05) con la condizione di riferimento avente, come atteso, un valore di SNR maggiore per ogni ROI considerata. Questa perdita di SNR è, in media, attorno al 16 % con una std del 5% per ogni ROI. Nonostante questa generale perdita di SNR delle immagini funzionali, le mappe di SNR create sogliando a 5 valori di SNR minimo, mostrano una significativa diminuzione di segnale solo ai bordi del cervello con un restringimento dell'area che permette la rivelazione di una variazione di segnale BOLD dello 0.75%. Soprattutto, almeno nell'89% delle ROI analizzate è stato possibile rilevare una variazione del segnale BOLD dell'1% e nella quasi totalità della ROI (97%) è rilevabile una variazione del 2%. Quindi il set-up proposto permette di individuare correttamente i cambiamenti di segnale BOLD per mappature statistiche parametriche. Questa ultima assunzione è stata valutata ottenendo le mappe delle attivazioni cerebrali utilizzando le immagini funzionali acquisite nella condizione di test. Per tutti i soggetti, i compiti di ADF e WE danno luogo, chiaramente, a un'attivazione nelle aree controlaterali della corteccia motoria primaria (M1) e della corteccia somatosensoriale primaria (S1). Le attivazioni nei due compiti motori mostrano l'attesa organizzazione somatotopica di entrambe queste aree.

Test di compatibilità EMG-fMRI – Nel presente lavoro, l'uso di una box, esplicitamente progettata per schermare da artefatti indotti da sequenze MRI, in cui alloggiare il sistema di acquisizione EMG non ha comunque permesso una diretta analisi del segnale EMG acquisito durante lo scanning fMRI e, perciò, un algoritmo per rimozione degli artefatti si è reso necessario.

L'analisi spettrale dei dati EMG grezzi acquisiti durante uno scanning fMRI mostra gli attesi componenti-artefatto a 12 Hz (e relative armoniche) che corrispondono al tempo di ripetizione dell'acquisizione di una fetta di immagine funzionale [2], per la specifica sequenza fMRI considerata.

Come ottenuto in letteratura [8], il paragone spettrale the i segnali EMG grezzi acquisiti nella condizione di riferimento (EMG-Out) a nella prima condizione test (B0+K+EMG) mostra che gli artefatti indotti dal movimento dei cavi EMG nel campo magnetico statico B0 sono concentrati a frequenze inferiori ai 30 Hz. Quindi, possiamo confermare che il filtraggio passa-alto applicato nei primi passi del processamento del segnale EMG (fcut = 30Hz) è adatto a ridurre non solo gli artefatti da movimento dei cavi non schermati ma anche quelli indotti dal loro movimento in B0.

Nel presente lavoro, l'algoritmo FARM esegue un'efficace correzione degli artefatti fMRI su ogni segnale EMG registrato in condizione fMRI+K+EMG fatta eccezione per uno dove l'applicazione dell'algoritmo riduce solamente l'ampiezza degli artefatti ma non permette un appropriato riconoscimento delle attivazioni EMG. La ragione del fallimento dell'algoritmo è da ricercarsi nell'errata costruzione del modello di artefatto da sottrarsi al segnale EMG. Ulteriori analisi sono richieste per migliorare la prestazione dell'algoritmo e, tra queste: uno studio accurato sulla struttura del modello di artefatto per ogni fetta fMRI, specialmente alla transizione da un volume fMRI al successivo, diversi test su varie larghezze di finestra e numeri di artefatti-fetta su cui basarsi per costruire il modello di artefatto da sottrarre.

La letteratura offre molti indici, sia in tempo che in frequenza, per valutare la qualità e la riproducibilità delle misura del segnale EMG. Nel presente lavoro, tre caratteristiche temporali del segnale sono state scelte e analizzate per paragonare la condizione sperimentale di riferimento con le altre due condizioni test: coefficiente di correlazione tra la forma media del segnale, area del segnale e ampiezza di picco.

Per tutti i soggetti, la forma d'onda dell'EMG medio nelle tre condizioni sperimentali sono altamente correlati (p-value < 0.05) con valori del coefficiente di correlazione, per la condizione fMRI+K+EMG, maggiori dello 0.75. Quindi possiamo affermare che i segnali EMG acquisiti nella camera di risonanza, con lo scanner MRI considerato, durante l'applicazione della sequenza fMRI, non sono influenzati o significativamente distorti nella loro forma caratteristica.

Per quanto riguarda gli altri due indici EMG, area del segnale e ampiezza di picco, il test ANOVA a due vie, applicato separatamente a ogni indice, mostra una significativa differenza nella media dei valori (p-value < 0.05) tra condizioni sperimentali ma anche tra soggetti. Data l'ampia variabilità intra- e inter-soggettiva del segnale EMG, preventivamente ossia durante il processamento, il segnale era stato normalizzato in ampiezza per poter condurre una ragionevole comparazione tra condizioni sperimentali (EMG-Out, B0+K+EMG, fMRI+K+EMG) e tra soggetti. Tuttavia l'approccio più conveniente per la normalizzazione di segnali EMG in contrazioni dinamiche è un punto di discussione in letteratura [11] a una significativa variabilità del segnale EMG tra prove, funzione del tipo di normalizzazione applicata, deve comunque essere considerata [12,15,16]. I dati di CV ottenuti per entrambi gli indici in entrambi i compiti motori si assestano sotto il 30%.

Come è dimostrato da letteratura, un'ampia gamma di valori di CV intra-soggettivi sono ottenuti in base al muscolo analizzato, al tipo di contrazione (isometrica, dinamica, massimale, sub-massimale, ecc.), al tipo di processamento applicato al segnale EMG e alla caratteristica descrittiva del segnale considerata: dal 9% [12] al 52% [14].

Oltre a questa intrinseca variabilità del segnale EMG tra prove, si deve considerare che, nel presente lavoro, le contrazioni non erano rigidamente controllate in termini di ampiezza quindi l'ipotesi che un soggetto esegua tutte le contrazioni EMG, acquisite in diverse condizioni ambientali (tre condizioni sperimentali) ma soprattutto in diversi momenti temporali, con lo stesso impegno (in termini di forza applicata alla contrazione) è molto debole. Perciò, nonostante vi sia una significativa differenza statistica tra condizioni sperimentali nelle medie dei valori dei due indici EMG presentati, questa discrepanza (testata attraverso CV) è inclusa nella variabilità intra-soggettiva del segnale EMG e può quindi essere considerata come trascurabile in questo contesto.

5. Conclusioni e prospettive future

L'analisi condotta dimostra la fattibilità, senza significative alterazioni o distorsioni di nessuno dei segnali considerati (fMRI ed EMG), di un'acquisizione combinata fMRI-sistema di analisi del movimento-EMG (adatto come controllore FES). In conclusione, lo studio corrente convalida l'applicazione di un innovativo set-up sperimentale che permetta di acquisire l'intenzione volontaria del soggetto (attività muscolare) e l'effettivo movimento svolto durante uno scanning di imaging funzionale in cui vengono eseguiti compiti motori. L'attuabilità di un esame fMRI combinato a una terapia FES pilotata tramite EMG del soggetto potrebbe aumentare la conoscenza del processo di riabilitazione motoria ed essere un'efficace strumento per valutare i cambiamenti nei pattern di attivazione cerebrale in studi su pazienti affetti da diverse disabilità motorie.

Bibliografia

[1] Krakow K. et al. Human Brain Mapping 10, 2000.
[2] Hoffmann A. et al. Magn Reson Med 44, 2000.
[3] Gandolla M. et al. Medical Engineering & Physics 33, 2011.
[4] Johannsen, P. et al. J. Physiol. 535, 2001.
[5] Dai T.H. et al. Exp. Brain Res. 140, 2001.
[6] Tjandra T. et al. Neuroimage 27, 2005.
[7] Parrish T.B. et al. Magn Reson Med 30, 2000.
[8] van der Meer J.N. et al. Clinical Neurophysiology 121, 2009.
[9] Allen P.J. et al. Neuroimage 12, 2000.
[10] Basmajian J.V. and De Luca C.J. Baltimore: Williams & Wilkins. 5th edition, 1985.
[11] Halaki M. and Ginn K. Edited by Ganesh R. Naik. Publisher: InTech. Chapter7, 2012.
[12] Yang J.F. and Winter D.A. Arc Phys Med Rehab 64, 1983.
[13] Scarff C.J. et al. NeuroImage 23, 2004.
[14] Francis et al. NeuroImage 44, 2009.
[15] Knutson L.M. et al. J Electromyogr Kines 4, 1994.
[16] Araujo et al. Electromyogr. Clin. Neurophysiol. 40, 2000.

Summary

1. Introduction

In the last years, taking into account the increase in population aging, many literature studies have focused on the neuro-motor recovery mechanisms evaluating both the central nervous system (CNS) and the peripheral outcomes. Functional magnetic resonance imaging (fMRI) and electromyography (EMG) multi-modal acquisition is a precious tool to analyze the central and peripheral interactions during the recovery process. These simultaneous measurements correlate cortical activation maps and the changes of the performance of the executed movement. Furthermore, more complete information can be obtained with the introduction, in addition to the EMG acquisition, of a motion capture system to accurately detect the actual executed movement whose origin, i.e. muscle activity, is reported by the EMG signal quantitatively. The mutual interference between EMG and fMRI techniques represent an important aspect which has to be analyzed: functional images quality with the EMG equipment and EMG signal deterioration recorded inside the MR scanner need to be evaluated. Studies in literature argue the influence of the EMG equipment to the MR images is due to the presence of extraneous metal components (electrodes, cables, etc.) in the scanner environment and the electromagnetic noise radiating from the EMG device which can induce a strong deterioration of the images signal-to-noise ratio (SNR) [1]. On the other hand, the EMG signal is impaired by artifacts caused by the interaction between electrodes leads and the time-varying magnetic fields in the scanner room, according to the Faraday-Lenz's induction law. Radio-frequency (RF) pulses and gradient magnetic field switched on during the MR scanning cause huge artifacts in the EMG signal (some orders of amplitude greater than the EMG signal) occurring at the main frequency and at the harmonics of the repetition time (TR) of the acquisition loops of the considered imaging sequence [2].

This study wants to deals with the described issues systematically and to assess the feasibility of a novel experimental set-up which allows, during fMRI scanning, to simultaneously record the movement characteristics (i.e. amplitude, velocity, etc.) using a motion capture system (whose fMRI-compatibility was assessed in literature [3]) and the volitional contribution of the subject (i.e. muscle contractions) using an EMG acquisition system. Differently from the fMRI-compatible EMG systems already available commercially, the EMG system present in the proposed set-up hasn't yet been validated for use in fMRI environment. It's also suitable for being a FES-controller (functional electrical stimulation, i.e. a clinical neuro-motor rehabilitation practice able to induce contraction in muscles deprived of neural control). Neuro-motor rehabilitation central mechanisms of action (fMRI-detectable) are of great interest in defining a proper training and subject volitional contribution (EMG piloted or myocontrolled FES) during rehab is a key feature for its success.

2. Materials and methods

The designed experimental set-up is composed by a CV/I 1.5 T scanner, a Porti7 EMG recording equipment and a motion capture system Smart μg^{TM} (fig I).

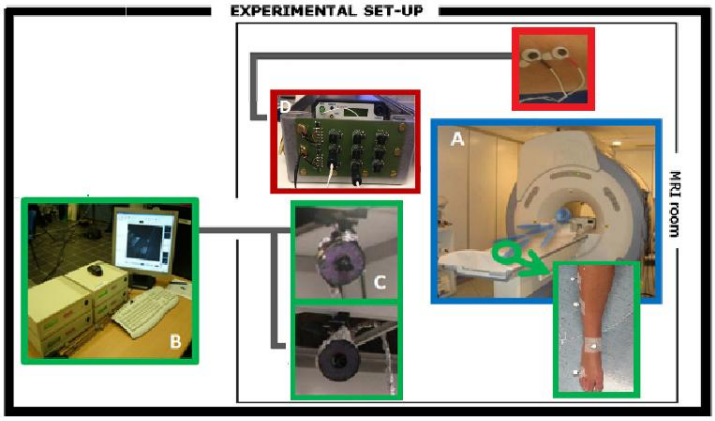

Figure I. Experimental set-up. (A) MRI scanner GE CV/I 1.5 T; (B) motion capture system Smart μg^{TM} with (C) two cameras and reflective markers; (D) Porti7 TMSi system located inside a prototype box and connected to the recording electrodes by twisted carbon cables.

The EMG recording system (sampling rate=2048Hz) is used in a stand-alone configuration, as Porti7 is powered by a set of batteries (to prevent MR noise on the power supply cables) and the acquired data are stored on a PC-card flash disk. Porti7 is placed in an aluminum prototype box which protects the system against the switching EM fields. The electrode leads are in carbon material, not immune to the cable movement artifacts and to power supply noise (at 50Hz). The EMG electrodes, arranged in a bipolar configuration, are applied to the tibialis anterior muscle and to the extensor carpi ulnaris muscle, as the subjects performs two tasks: voluntary dorsiflexion of the right ankle (ADF) and voluntary extension of the right wrist (WE). The total experimental protocol lasts 10min and each motor task consists in ten ON/OFF blocks where every block is composed by 20s of task execution and 10s of rest. The motor task repetition frequency is set to 0.5Hz.

In order to track the movement of the subjects inside the scanner room with the motion capture system (sampling rate=120Hz), eight reflective markers are placed on the right hand middle finger, on the right leg (two on the tibia axis, one on the malleolus and one on the foot little finger) and three on the MR-bed. Outside the scanner room, electrogoniometers are applied on the right ankle and on the right wrist to gather analogous kinematic measures.

MRI-EMG compatibility test – The evaluation of the signal-to-noise ratio (SNR) on phantom T1-weighted images with (MRI+Kinematics+EMG) and without (MRI+K) the presence of the EMG recording device has been first assessed.

SNR is calculated over the slices of the phantom acquisitions, as the ratio between the mean amplitude of the signal on a homogeneous area and the mean of the standard deviation of the background signal amplitude on four selected ROIs. For each image slice the percentage loss of SNR between the reference (MRI+K) and the test (MRI+K+EMG) condition is computed and compared with acceptable values for images quality reported in literature (12%).

fMRI-EMG compatibility test – The evaluation of the SNR on T2*-weighted fMRI images (TR=3s) of the subject who performs the described motor tasks with (fMRI+K+EMG) and without (fMRI+K) the presence of the EMG recording device.

fMRI images are pre-processed with SPM8 running on Matlab®. Images are unwarped and realigned to first scan of each volume. An average realigned fMRI image is co-registered with the subject anatomical one. Imaging data (both functional and anatomical) are normalized to standard MNI space. At last, a spatial smoothing is performed using an 8 mm Full-Width Half-Maximum Gaussian filter. A statistical analysis is carried out through a general linear model, to obtain cortical activation during the execution of the motor tasks detected with the proposed experimental set-up (fMRI+K+EMG). The design matrix is obtained with two regressors, i.e. the kinematics-derived onsets for each motor task, ADF and WE.

To evaluate fMRI-EMG compatibility, SNR of the fMRIs is computed compared between reference (fMRI+K) and test (fMRI+K+EMG) conditions in four regions of interest (ROIs) consistently activated during motor tasks executions [4,5], i.e. primary motor cortex (M1), premotor and supplementary motor cortex (PM/SMA), primary somatosensory cortex (S1) and second somatosensory area (SII). A preliminary analysis of each ROI homogeneity in terms of SNR is made using the coefficient of variation (CV) for a given experimental condition (fMRI+EMG+K and fMRI+K) calculated as : the percentage of the standard deviation of the signal across sessions with respect to the mean of the signal across sessions, the lower the value, the better the SNR homogeneity for a considered ROI [6]. The CV standard deviation is computed for each ROI to compare the CVs obtained for the three subjects in the same experimental condition, i.e. to assess the inter-subject CV reproducibility. A Mann-Whitney test is applied to compare, for each ROI, the CVs of all the subjects between the two experimental conditions, i.e. inter-conditions reproducibility assessment. The SNR percentage loss between reference and test condition is calculated on the basis of the mean values of the ROIs'SNR. Then, given that for an MR scanner of 1.5T the BOLD signal changes detectable are around 1-2% [3], SNR maps are created, for the fMRIs in the two experimental conditions, imposing five minimum SNR thresholds [7] for the

detection of as many BOLD signal changes (0.25%, 0.50%, 0.75%, 1%, 2%). So, for each ROI, the computation of number of voxels which has enough SNR to detect ΔS=1%-2% is performed and a comparison between reference and the test condition is conducted. Moreover, the actual task-related cerebral activation is assessed analyzing the images obtained in the fMRI+K+EMG condition.

EMG-fMRI compatibility test – The EMG signals acquired in experimental conditions, i.e. outside the MR room (EMG-Out), inside the MR room with the fMRI sequence off (B0+K+EMG) and inside the MR room with the fMRI sequence on (fMRI+K+EMG) were compared.

The EMG signals acquired in the three experimental conditions are processed in two different ways because the EMG in the condition fMRI+K+EMG needs the application of an fMRI artefacts removing algorithm, i.e. the FARM (Artifact Reduction For Motion) one, developed by van der Meer and colleagues [8]. This algorithm band-pass filters the raw EMG (30-250 Hz) to remove the B0-induced artefacts whose frequency may reach the 30 Hz. Then the EMG dataset is processed using EEGLAB, running on Matlab® . To create the artefact template to be subtracted from the EMG data, FARM uses a sliding window composed of 50 slice-segments and selects the 12 slice-artefacts which have the highest correlation with the slice-artefact to be currently corrected. In this way, if the shape of the artefact changes due to motion during the acquisition, this procedure ensures those "motion-impaired" slice-artefacts are not used in the slice-template construction and then the artefacts removal is improved with respect to the standard artefact template subtraction approach (AAS, [9]). The algorithm conducts an additional 4-principal components analysis on the corrected EMG dataset to remove residual high frequency artifacts.

The raw EMG signals in the reference (EMG-Out) and in the test condition (B0+K+EMG) are band-pass filtered with the same frequency range applied in the FARM algorithm to make EMG in different experimental conditions comparable. The choice of such a high cut-off frequency (30Hz) is justified also by the use of not-active-shielded cables which introduce motion-artefact noise in the EMG signal that may reach the 25-30Hz.

Afterwards, the three experimental conditions datasets, undergo common steps:

- full-wave rectification of the signal to retain the whole energy of the signal [10];
- smoothing with a low pass filtering (5th order Butterworth filter, cut off frequency 5 Hz) to obtain the signal envelope;
- amplitude normalization of the signal with reference to the recorded maximum amplitude peak within the current EMG acquisition [11];
- windowing of the EMG signal (i.e. detection of every actual muscle activation) based on kinematic onsets;
- time normalization of each muscular activation at 100 samples and EMG features extraction.

Three EMG indices are considered to compare the reference condition (EMG-Out) with the two test conditions (B0+K+EMG and fMRI+K+EMG): the correlation coefficient among the average EMG waveforms obtained in the three experimental conditions which provides indication on the maintenance of the EMG characteristic form without distortions induced by the MR-environment; the maximum amplitude peak and integrated area under the signal.

A statistical two-ways ANOVA test is applied on these last two indices for each motor task separately (ADF and WE) to evaluate whether there is a significant inter-condition and inter-subject means difference. Then, for the same two indices and separately for each subject, an analysis on the EMG variability among experimental conditions is made calculating the coefficient of variation (CV) for EMG intra-subject comparisons on the same muscle [12]. In the current discussion, CV is computed, for each of the two indices (area and peak amplitude), considering the index average value obtained in every experimental condition as the EMG feature on which to calculate the intra-subject variability. Then, considering, for example, the area index, the CV is defined as follows (eq. I):

$$\mathrm{CV}_{\mathrm{area}} = \frac{std(area)}{mean(area)} \qquad \text{(eq. I)}$$

where the mean and the standard deviation are defined with respect to the three experimental conditions that each subject undergoes.

3. Results

MRI-EMG compatibility test - The SNR percentage loss between reference (MRI+K) and test (MRI+K+EMG) condition is equals to (mean ± std): 5.7 ± 3.4 %.

fMRI-EMG compatibility test - For each cortical ROI, the CVs of the functional images SNR for the three subjects in the two experimental conditions (fMRI+K and fMRI+K+EMG) are calculated and, on average, their value is set around 40% for every ROI in both conditions. The standard deviation values, computed for every ROI to compare the CVs obtained for the three subjects in the same experimental condition, are always lower than 5%. The Mann-Whitney test, applied to compare the CVs of each subject between the two experimental conditions, has always p-value > 0.05 for every ROI.

As expected, the reference condition (fMRI+K) has a mean SNR value, for each ROI, higher than the test condition (fMRI+K+EMG) one with the statistical difference assessed by a t-test (p-value < 0.05). Table I presents the SNR percentage loss in every ROI for all subjects and an average of it.

In fig. II an example of the SNR maps, with the five minimum SNR thresholds, in both the reference and test conditions, is presented.

Table I. Functional images SNR percentage loss between reference and test condition separately for each subject and an average of this SNR loss.

SNR LOSS (%)	**Subject 1**	**Subject 2**	**Subject 3**	**Average**
M1(b4)	16.60%	10.77%	15.43%	14.43% ± 3.08%
PM/SMA (b6)	14.80%	6.18%	10.28%	10.42% ± 4.31%
S1(b2-b3)	20.03%	15.93%	9.68%	15.21% ± 5.21%
SII (b5-b7)	12.13%	21.22%	4.88%	12.74% ± 8.18%

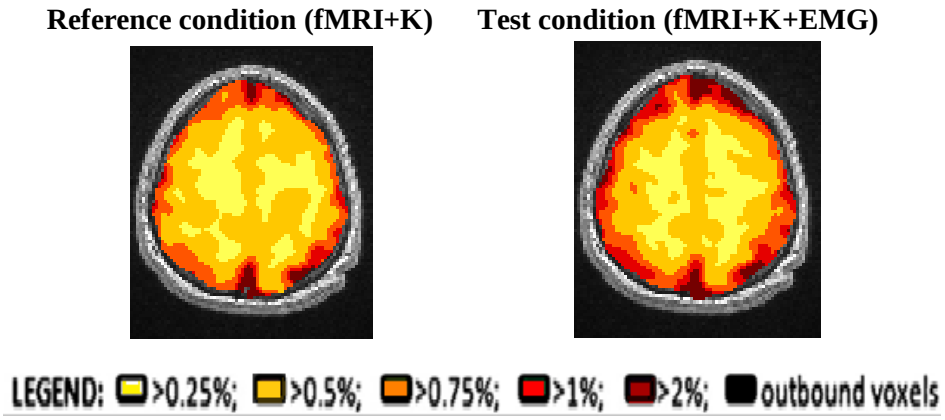

Figure II. SNR maps obtained for the subject number 3 in reference and test condition.

The percentage of each ROI which have an SNR value high enough to observe a BOLD signal change equal to 1-2% is computed: a percentage higher than 89% considering a 1% BOLD signal change and a percentage higher than 97% for the 2% BOLD signal change are obtained for all the subjects in every considered ROI.

In fig. III it is shown one representative cortical activation map for both the ADF and WE motor task obtained considering the functional images acquired in the test condition (fMRI+K+EMG).

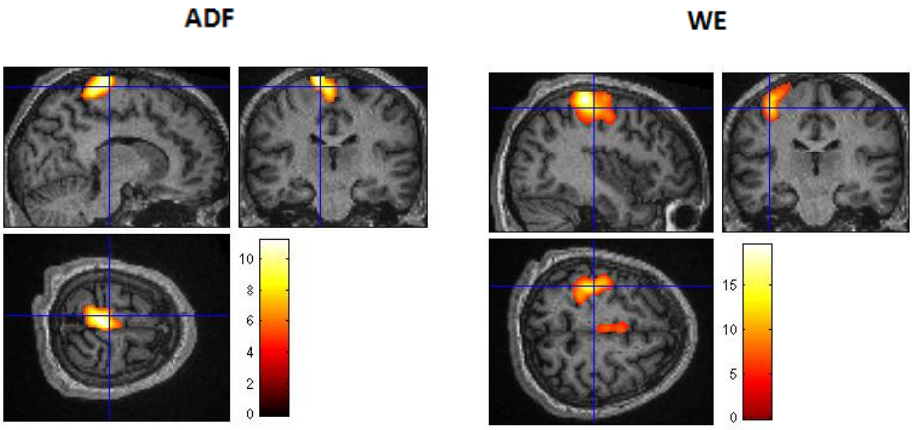

Figure III. Cortical activation maps obtained, for the third subject, during the ADF and a WE motor task performance. The results are FWE corrected (p-value < 0.05) and the cluster number is set at 10.

EMG-fMRI compatibility test- Fig. IV shows, for a representative subject, the average EMG waveforms in the three experimental conditions (EMG-Out, B0+K+EMG, fMRI+K+EMG).

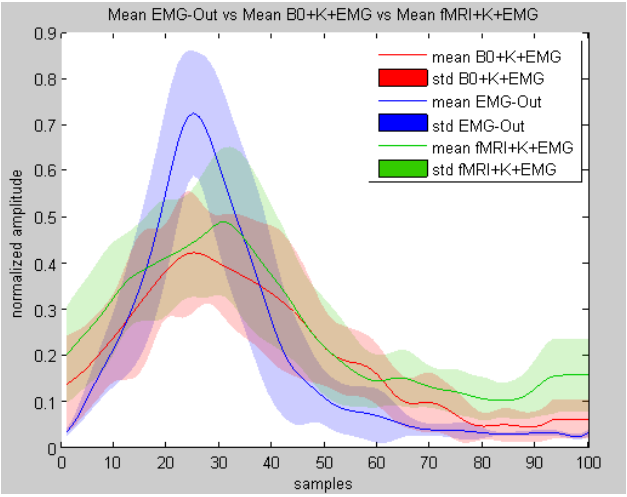

Figure IV. Average EMG waveforms in the three experimental conditions (EMG-Out, B0+K+EMG and fMRI+K+EMG) with respect to the ADF motor task performed by the third subject.

The correlation coefficients of the EMG waveforms comparing the reference condition (EMG-Out) with the other two test conditions (B0+K+EMG and fMRI+K+EMG) are higher respectively than 0.76 and than 0.78 for every subject and for both motor tasks with an associated p-value<0.05. The two defined EMG indices, area under the signal and peak amplitude, are calculated for every subject in the three experimental conditions. The two-way ANOVA test performed on these indices separately works out a p-value < 0.05 for both the inter-subject and the inter-condition test and the result is the same for the two motor tasks. Lastly, the inter-condition CVs of both indices are calculated for every subject separately. CV for the area is always lower than 29% and CV for the peak amplitude is always lower than 20%, with respect to both motor tasks.

4. Discussion

The aim of this work was the design and the validation of a novel experimental set-up for the detection of volitional intention during motor tasks functional imaging. The maintenance of data quality for both fMRI and EMG has been evaluated.

MRI-EMG compatibility test - It was shown that the SNR loss induced in the magnetic resonance images by the designed experimental set-up is negligible. In fact, for each MRI slice, the SNR percentage loss between reference (MRI+K) and test condition (MRI+K+EMG) is 5.7 ± 3.4 %. Indeed, it is used as reference a literature study [13] where it is shown that magnetic resonance

image SNR, computed as we did, decreases as the number of electrodes increases and with respect to the imaging data quality is given as acceptable an images SNR loss of 11-12%.

fMRI-EMG compatibility test - Four cortical ROIs, consistently activated during motor tasks executions have been considered. A homogeneity index (CV, coefficient of variation) was computed for every ROI in the two experimental conditions including fMRI scanning (i.e., fMRI+K and fMRI+K+EMG). This homogeneity analysis is made to create a valuable background for the following SNR considerations which are both inter-subject and inter-condition and mean-based. CV data, 40% on average, were a bit higher than those in literature [14] but the reproducibility among subjects (std < 5% [3]) and among experimental conditions was verified. All subjects show a significant percentage SNR loss between the two conditions (t-test, p-value < 0.05), with the reference one having the highest SNR values as expected. This loss, on average, settles below the 16% with a std of 5% for each considered ROI. Despite this general functional images SNR loss between the two scanning conditions (fMRI+K and fMRI+K+EMG), the thresholded SNR maps show a significant signal drop only at the edges of the brain with a shrinkage of the area with a minimum SNR such as to allow the detection of a BOLD signal change greater than 0.75%. Above all, at least in the 89% of all selected ROIs it was still possible to detect a 1% BOLD signal change and almost in the whole considered ROIs volume (97%) a 2% BOLD signal change can be revealed for both reference and test scanning condition. Therefore the proposed experimental set-up allows to correctly detect the BOLD signal changes for statistical parametric maps analysis.

This last assumption was assessed obtaining the actual cerebral activation maps from the functional images acquired in the test condition. For all subjects, ADF and WE elicited clear activation respectively in the leg and hand contralateral primary motor (M1) and primary somatosensory (SI) areas. Cerebral activations obtained for the two protocol motor tasks show the expected somatotopical -structure of the motor and somatosensory areas.

EMG-fMRI compatibility test - In the present work the use of a prototype box, explicitly designed to shield the EMG acquisition system from fMRI-induced artefacts, doesn't allow a direct analysis of the EMG signals recorded during MRI scanning and the application of an fMRI artefacts reduction algorithm was necessary. The spectral analysis of the raw EMG acquired during an fMRI scanning shows the expected artefact components at 12 Hz (and at its harmonics) which corresponds to the slice-timing of the fMRI [2]. As obtained in literature [8], the spectral comparison of raw EMG acquired in the reference (EMG-Out) and in the first test (B0+K+EMG) condition shows that the artefacts induced by the EMG wires movements in the main B0 fields are concentrated at frequencies lower than 30 Hz. So, we can confirm that the high-pass filter applied

in the first EMG processing step (fcut = 30 Hz) is suitable to reduce not only movement artefacts due to the not-active-shielded cables but also the artefacts induced by their movement in B0.

In the present work, the FARM algorithm performs an effective fMRI artefacts correction on every EMG dataset, except for one where the application of the algorithm only reduces the amplitude of the artefacts but doesn't remove enough superimposed fMRI-noise to allow a proper EMG activations detection. The reason of this failed artefacts removing deals with a wrong slice-artefacts template construction performed by the algorithm. Further analysis is required to improve FARM performance: a detailed analysis of each slice template, especially at the transition from an fMRI acquired volume to the following one, some tests on different slice-neighbouring width and on the number of slices to construct the slice-artefacts template might improve the artefacts removal.

The literature offers many indices, both in time and in frequency, to evaluate the EMG measurement quality and reproducibility. Three time features of the EMG were chosen to be analyzed to compare the experimental reference condition (EMG-Out) to the other two test conditions (B0+K+EMG and fMRI+K+EMG): correlation coefficient among average EMG signal shape, area under the EMG curve and peak amplitude. For all the subjects, the mean EMG signal waveforms in the three conditions are highly correlated (p-value < 0.05) with correlation coefficient values, for the fMRI+K+EMG condition, higher than 0.75. So, we can be confident that the EMG signal acquired inside the considered scanner room with the fMRI scanning on it is not affected or significantly distorted in its characteristic waveform.

For what is concerning the other two EMG indices, area under the signal and peak amplitude, the two-way ANOVA test, applied on each index separately, shows a significant difference in the indices means (p-value < 0.05) among the experimental conditions but also among subjects. Given the large intra- and inter-subject EMG signal variability, preventively, i.e. in the processing steps, the EMG signal amplitude was normalized to reasonably perform comparison among conditions (i.e. EMG-Out, B0+K+EMG, fMRI+K+EMG) and subjects. However, the most convenient normalization approach for EMG signal in dynamic contractions is a questionable point in literature [11] and a significant EMG variability among trials, function of the normalization applied, must still be considered [12,15,16]. The CVs obtained for both indices for both motor tasks (ADF and WE) set below the 30%. As various studies argue, according to the muscle analyzed, the type of contraction (isometric, dynamic, maximal, sub-maximal, etc.), the EMG processing applied and the descriptive EMG feature considered, a wide range of intra-subject CV are obtained: from 9% [12] to 52%[15].

In addition to this intrinsic EMG variability, it has to be considered that, in the present work, the contractions weren't strictly controlled in terms of amplitude. Therefore, the hypothesis that a

subject performs all the EMG contractions, acquired in different environmental conditions but, above all, in different time moments, with the same commitment and effort is very weak.
So, even though there is a statistical difference among conditions in the means of the two presented EMG indices, this discrepancy (tested by CV) is included in the variability which affects the intra-subjective reproducibility of EMG signal and can be considered as negligible in this context.

5. Conclusions and future perspectives

The conducted analysis shows the feasibility, without significant alterations or distortions of any data, of a combined fMRI-motion capture system-EMG acquisition with respect to a specific EMG recording system suitable to be a FES-controller. In conclusion, the current study validates the application of a novel integrated set-up which allows to detect the subject volitional intention and the effective executed movement during motor-tasks functional imaging. The practicability of a combined fMRI scanning and of an EMG-piloted FES could increase the information on the motor rehabilitation process and be an effective way to evaluate the changes in cerebral activation patterns in studies on patients affected by different kinds of motor disabilities.

References

[1] Krakow K. et al. Human Brain Mapping 10, 2000.
[2] Hoffmann A. et al. Magn Reson Med 44, 2000.
[3] Gandolla M. et al. Medical Engineering & Physics 33, 2011.
[4] Johannsen, P. et al. J. Physiol. 535, 2001.
[5] Dai T.H. et al. Exp. Brain Res. 140, 2001.
[6] Tjandra T. et al. Neuroimage 27, 2005.
[7] Parrish T.B. et al. Magn Reson Med 30, 2000.
[8] van der Meer J.N. et al. Clinical Neurophysiology 121, 2009.
[9] Allen P.J. et al. Neuroimage 12, 2000.
[10] Basmajian J.V. and De Luca C.J. Baltimore: Williams & Wilkins. 5th edition, 1985.
[11] Halaki M. and Ginn K. Edited by Ganesh R. Naik. Publisher: InTech. Chapter7, 2012.
[12] Yang J.F. and Winter D.A. Arc Phys Med Rehab 64, 1983.
[13] Scarff C.J. et al. NeuroImage 23, 2004.
[14] Francis et al. NeuroImage 44, 2009.
[15] Knutson L.M. et al. J Electromyogr Kines 4, 1994.
[16] Araujo et al. Electromyogr. Clin. Neurophysiol. 40, 2000.

Introduction

Combined acquisition of different modalities

The worldwide increase in population aging enhanced the importance and the social impact of neuro-motor disabilities motivating the interest in finding advanced methods for their rehabilitation.

Therefore, recently, many literature studies have had the aim to investigate the neuro-motor recovery mechanisms considering both the central nervous system (CNS) and the peripheric outcomes (muscles contractions). The need for providing accurate, quantitative and repeatable measures of these rehabilitation processes has brought the practice of the multi-modal acquisition set ups. Concurrent acquisition of electroencephalogram (EEG) and functional magnetic resonance imaging (fMRI) is used, clinically, since the late 1990ies and is traditionally called multi-modal neuroimaging acquisition. This allows to combine the strengths of both methods and to complete the fragmentary information provided by either one of them [1]. EEG and EMG recordings are based on similar principles and the recording equipment for EMG is very similar to that already in place for EEG and can often be used for both purposes. EMG is a clinical modality which gives the information on muscle electrical activity through the measure of biopotentials due to muscle contraction. The EMG signal provides timing and amplitude information from individual muscles during dynamic or static (isometric) contractions [2]. The most used kind of EMG in multi-modal acquisition is the surface one: it means that the electrical signals of the muscle contractions are recorded with electrodes placed on the skin surface.

The addition of EMG to fMRI presents several advantages to experiments focused on motor control. The EMG can be used to examine if subjects have actually performed the tasks as they were instructed [3] or to enable localization of brain areas that modulate (pathological) muscle activity [4,5].

Moreover, simultaneous measures of effectively executed movement during scanning correlate activation maps and their changes to the exact performance of the movement [6]. In fact the aim of neuro-motor rehabilitation process is the motor recovery (the efficiency of muscle contraction), which can be obtained through a central neural reorganization and relearning.

It can be concluded that fMRI-EMG multi-modal acquisition is a very useful tool to analyze the central and peripheric interactions during rehabilitation process.

Challenges

The two main aspects to keep into consideration in a fMRI-EMG multi-modal acquisition are the safety of the subject inside the MR (magnetic resonance) scanner and the mutual interference of both methods that might impair the acquired data. Furthermore, in the EMG case there is also the problem of the subject motion. In fact the movement is not only unavoidable but necessary to measure the muscle contraction and this complicates the artifact issue in both acquired data. Analyzing the first issue, it has to be considered that the EMG leads are ferro-metals elements and therefore electrical conductors. They act as antennas (electrical devices resonant at the same frequency of the caught signal) which pick up the time-varying electromagnetic (EM) signals used for the imaging process. This can lead, theoretically and in the worst case, to heating of the recording electrodes up to many Celsius degrees [7], although other experimental studies [8,9] show that the most employed fMRI sequence (echo planar imaging, EPI) leads to an increase of less than 1°C.
For what is concerning the mutual interference, it has to be analyzed in detail in literature from both points of view i.e. evaluating the fMRI image quality with the EMG equipment present and acquiring in the scanner room and the maintenance of the EMG features when the signal is recorded inside the MR environment.
The EMG signal deterioration has been demonstrated to be caused by the rapidly varying electromagnetic fields applied during the MRI acquisition with the appearance of very large artifacts superimposed on the EMG. On the other hand, the influence of the EMG equipment to the functional MR images is due to presence of extraneous metal components (electrodes, cables, etc.) in the scanner environment and electromagnetic noise radiating from the EMG device which can the strong deterioration of the images signal-to-noise ratio (SNR).
Lastly, the motion of the subject and, consequently, of the leads connecting the surface electrodes to the acquisition device during the scanning process worsen the quality of both acquired signals. In fact, closed conducting loops, like the ones created by the electrical wires, which move inside time-varying EM fields, suffer from the induction of electromotive forces (EMF) inside them.

This kind of EMF are described by the Faraday-Lenz's law of induction and consist in the voltage, measured in volts (V), which is determined by the rate of change of a magnetic flux through the circuit. In this particular case, the change in the magnetic flux linkage is produced by the movement of the conducting coil (the loop of the leads) in a stationary magnetic field (inside the MR scanner during the imaging sequence).

Aim of the work

The present study wants to systematically asses the feasibility of a novel experimental set-up which allows, during fMRI scanning, to simultaneously record the movement characteristics (i.e., amplitude, velocity, etc.), using a motion capture system (whose fMRI-compatibility was assessed in a previous work, [6]) and the volitional contribution of the subject (i.e., muscle contractions) throughout the session, using an EMG acquisition system. Moreover, as our set-up is composed of a EMG recording device, not yet validated methodically for an use in fMRI environment, which is suitable for being a FES-controller (functional electrical stimulation) because of its technical features (i.e. the absence of embedded pre-amplifiers, the high ADCs'resolution and the fast recovery time), this work could be a valid background for the future practicability of a EMG-piloted FES test during an fMRI acquisition. EMG-controlled FES is a clinical neuro-motor rehabilitation practice which, when rehabilitated muscles are not completely paralyzed, exploits the features of the residual EMG signals of the paretic limb to control the timing and the intensity of the stimulation patterns [10]. FES procedure has been used long in clinical practice, but if its peripheral effects on muscles themselves are well known, possible mechanisms about central therapeutic benefits of FES have only been hypothesized. Only recently the fMRI scanning of subjects undergoing FES-induced motor tasks has been conducted [11].

Therefore, since the neuro-motor rehabilitation central mechanisms of action (fMRI-detectable) are of great interest in the definition of a proper patient training and it is widely accepted that volitional contribution of the subject (EMG-detectable) during rehab is a key feature for its success, the proposed experimental set-up enables the integration of both aspects in a single examination session.

Furthermore, the methodical assessment of the usability inside the MR scanner of an experimental set-up not expressly designed to be MR-compatible is an effective and useful goal not only from the economical point of view (an MR-compatible EEG/EMG recording

system can easily costs more than double the price of a not compatible one) but also from the technological point of view to set up potentially innovative hardware approaches.

In order to address all the presented issues, this work is organized in five chapters.
Chapter 1, Background, introduces and discusses the scientific context in which this work inserts taking into consideration the general characteristics of the signals occurring in this work i.e. the EMG signal, the functional magnetic resonance imaging, the kinematic data. Furthermore the chapter presents the state of art about safety and artifacts appearance in combined modality acquisition.
Chapter 2, Materials and Methods, focuses on the novel designed experimental set-up, presented in this study, including an fMRI scanner, a motion capture system to accurately detect the effectively executed movement and a particular EMG acquisition system (suitable to be a FES-controller) to obtain data about the actual subject contribution to the movement. Also this chapter deals with the protocol and the methods implemented to process the recorded data and to get to signals (fMRI and EMG) quality indices on which drawing conclusions about the compatibility of a simultaneous EMG-fMRI acquisition.
Chapter 3, Results, includes all the quantitative data obtained in the experiments conducted for this work, through the materials and the methods described in the previous chapter.
Chapter 4, Discussion, the relationship between the work hypothesis and the results is discussed.
Chapter 5, Conclusions and future perspectives, draws conclusions about the presented work and proposes future applications and developments of the designed experimental set-up.

Chapter 1. Background

1.1 EMG signal features and recording concerns

Electromyography (EMG) is a technique which measures electrical potentials formed in a muscle during its contraction. These potentials are caused by the depolarization of the muscle fibers in response to the electrical impulses which arrive at the neuromuscular synapse (fig. 1.1).

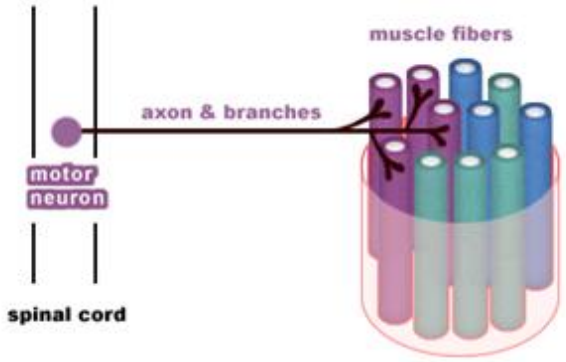

Figure 1.1. Neuromuscular synapse.

There are two kinds of EMG in widespread use: surface EMG (sEMG) and intramuscular (needle and fine-wire) EMG. Even if it provides a detailed few fibers information, no cross-talk and no electrode-skin movement problem, intramuscular EMG is considered too invasive or unnecessary in most cases. Instead, surface EMG, based on the recording of the muscle electrical activity through superficial electrodes attached to the skin of the subject, may be used to monitor the general picture of muscle activation as opposed to the activity of only few fibers, as observed using an intramuscular EMG.

Indeed, as it is shown in fig. 1.2, sEMG signals are essentially made up of superimposed motor unit action potentials (MUAPs) from several motor units (one motor neuron and all of the muscle fibers it innervates).

sEMG provides information to detect muscle activation intervals as well as to study neural control strategies and neuromuscular system properties [12].

The most important properties of the sEMG include non-invasiveness, low costs, easiness of application and detection of superficial muscles.

It may be concluded that compared to the electromyography based on needles, superficial technique provides more global information about the muscle observed, but it avoids the risks given by the use of needles.

In the present work we concentrate on surface EMG since it is the most used in the clinical practice to evaluate the muscle condition and the potential progress in its rehabilitation.

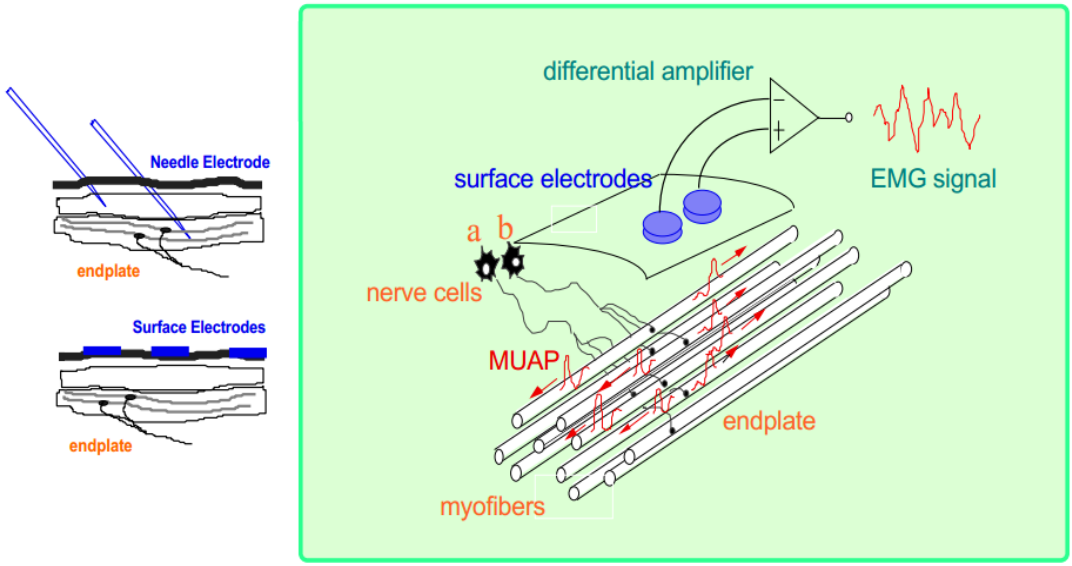

Figure 1.2. On the left: intramuscular and surface EMG. On the right: sEMG detection [13].

The amplitude of the detected sEMG signal is intrinsically stochastic in nature [2] and the standard deviation of this stochastic signal is a function of the number of activated motor units. The amplitude of the sEMG signal ranges from 50uV to 10 mV peak-to-peak, depending on the muscle under observation [14]. The usable energy of the signal is limited to the 10 to 500 Hz frequency range (fig. 1.3), with the dominant energy being in the 50-150 Hz range.

Usable signals are those with energy above the electrical noise level [14].

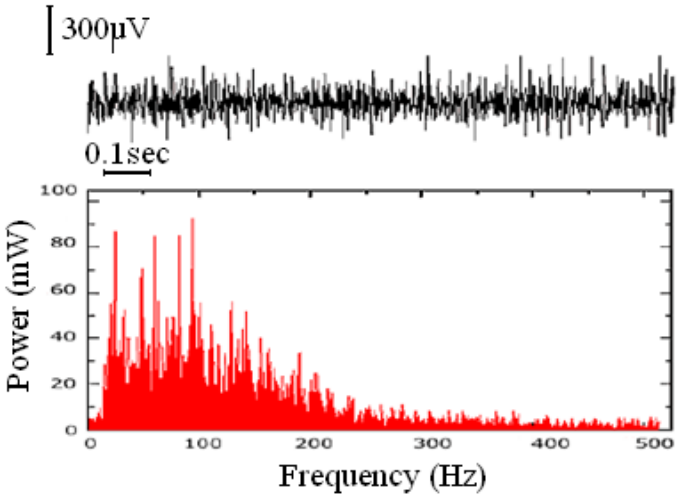

Figure 1.3. Upper: Raw sEMG detected from the Tibialis Anterior (TA) muscle during a constant force isometric contraction at 50% of voluntary maximum. Bottom: Frequency spectrum of the same sEMG signal [15].

When detecting and recording the EMG signal, there are two main issues of concern that influence the reliability of the detected signal. The first is the signal to noise ratio (SNR), that is the ratio of the energy in the EMG signal and the energy in the noise signal. In general, noise is defined as electrical signals that are not part of the EMG signal which carries information about muscles activity. The other concerning issue is the distortion of the signal, meaning that the relative contribution of any frequency component in the EMG signal should not be altered by the recording [14]. The detection of sEMG signals is performed through superficial electrodes. A sEMG electrode can be defined either as a sensor of the electrical activity of a muscle or as a transducer of the ionic current, flowing in the tissue, into the electronic current, flowing in the metal wires [12].

A surface electrode is characterized by physical dimension, shape, technology and constituent materials. All these factors may strongly influence the recorded sEMG signal and, obviously, the reliability of the EMG signal detected by the electrode influences all subsequent treatment of the signal. Electrodes may be used in two principal configurations (fig. 1.4): monopolar configuration, where an active electrode is placed in correspondence of the muscle to be examined and the other one on a reference or neutral point; bipolar configuration, where two active electrodes are placed on the muscle to be studied and the difference of the signal between the two electrodes is then reported to the ground electrode.

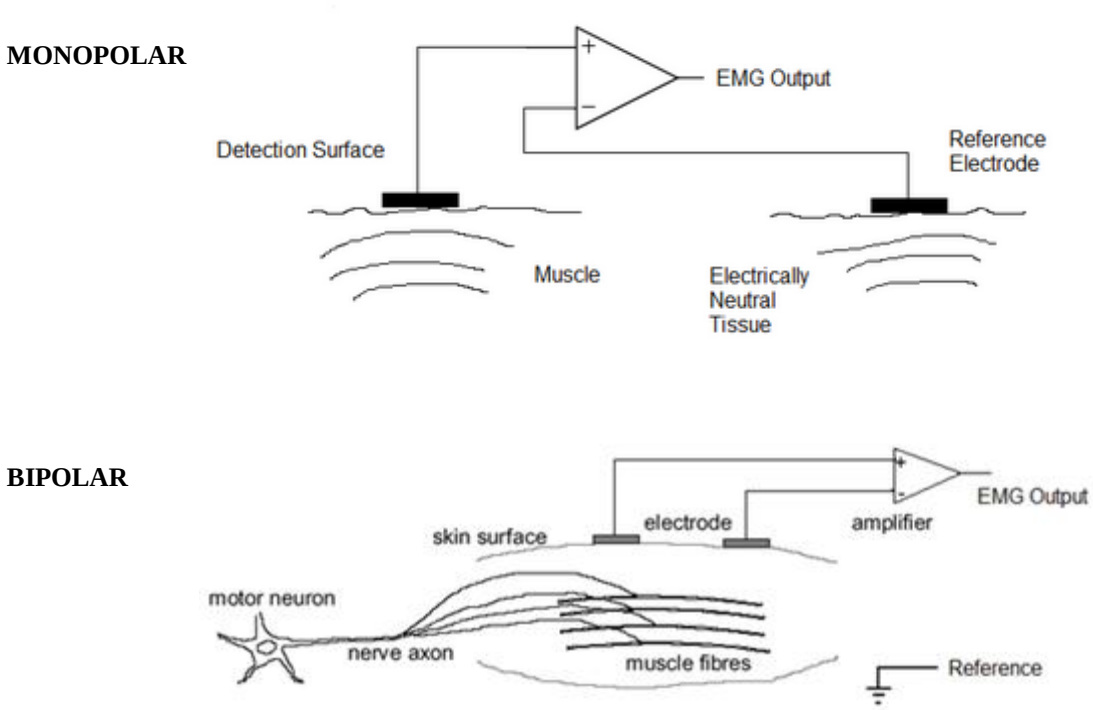

Figure 1.4. Upper: **monopolar** configuration where one electrode is place over the belly of the muscle and one electrode somewhere farther as the reference and the signal between the two electrodes is amplified and recorded. Bottom: **bipolar** configuration. Two electrodes are placed over the belly of the muscle within 1-2 cm from each other and one electrode somewhere farther as the reference and the signal between the two electrodes over the belly of the muscle is amplified differentially respect to the reference electrode (NR Sign Inc. EEG & EMG solution website).

In the present study, bipolar electrodes are used: these are most commonly employed because they allow to substantially reduce the potentially much greater noise superimposed on the sEMG signal (common mode noise). The signal-to-noise ratio is much better in this configuration. The sEMG signal is detected at two sites: electronic circuitry subtracts the two signals and then amplifies the difference. As a result, any signal that is common to both detection sites is removed and signals that are different at the two sites have a differential that is amplified.

This explanation requires the availability of a highly accurate "subtractor". For this reason, the amplifier choice is a very important issue in the sEMG recording. The accuracy with which the differential amplifier can subtract the signals is measured by the Common Mode Rejection Ratio (CMRR). A perfect subtractor would have an infinite CMRR.

A CMRR of 90 dB (decibel) is generally sufficient to suppress extraneous electrical noises. In order to prevent attenuation and distortion of the detected signal due to the effects of input loading, the input impedance of the differential amplifier should be as large as possible. The balance between the impedances of the two detection sites is also of great importance [14].

1.2 fMRI: features and physical principles

Brain imaging techniques

Brain imaging techniques may be divided considering the information they provide. Referring to this approach, two categories may be identified: the anatomical and functional imaging. The aim of anatomical imaging is to obtain the most detailed picture possible considering the structure and the anatomy of the brain, whereas the functional imaging gives information about the activation of brain areas in different conditions. Nowadays, the magnetic resonance imaging (MRI) is one of the most widely used procedure in hospitals for medical diagnosis, staging of disease and for follow-up because of the flexibility and effectiveness but, above all, because of its non-invasivity compared to the classical nuclear medical imaging techniques X-rays (TAC), computed tomography (CT), etc. In fact, since MRI doesn't imply any exposure to ionizing radiation, its use is recommended in preference to CT when either modality can yield the same clinical information. On the other hand, TAC and CT, for anatomical images, and positron emission tomography (PET) and single photon emission tomography (SPECT), for functional images, provide an higher spatial resolution than MRI and fMRI (functional magnetic resonance imaging). In general, MR images can be acquired with a discrete spatial and temporal resolution and recent technological developments, such as the use of intense static magnetic fields and multichannel radio frequency receiving, have made possible to increase the spatial resolution on the scale up to few millimeters (fig. 1.5).

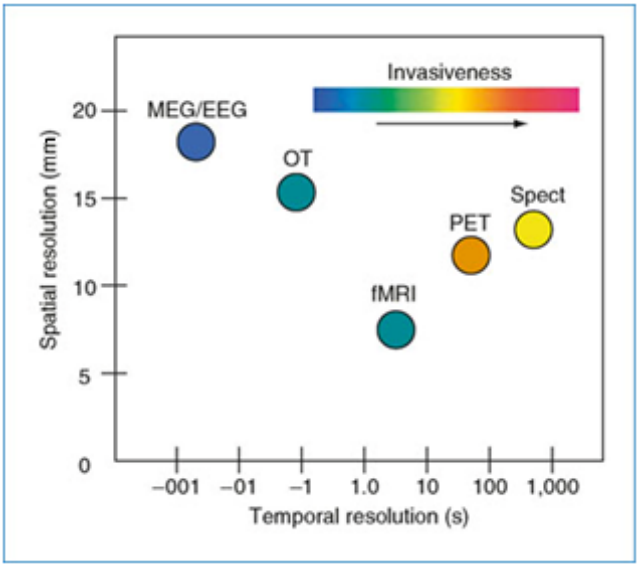

Figure 1.5. Comparison of the spatial, temporal resolution and invasiveness of different neuroimaging methods. SPECT; PET; fMRI; OT (optical topography); MEG (magneto encephalography; EEG) [16].

MRI

The MRI is based on a strong static magnetic field (B_0) which is created by the main magnet around the area to be imaged and on the radio frequency (RF) signal emitted by particular excitable nuclei in the subject body (^{1}H is the most common one) recorded after the stimulation from an oscillating magnetic field (RF pulses emitted by RF coils) at an appropriate resonant frequency (Larmor frequency). The spatial detection of the image is obtained by varying the main static magnetic field switching on and off some gradient coils. In fig. 1.6 is illustrated, in a schematic way, the structure of a common MR imaging scanner.

Biological tissues are predominantly made of ^{12}C, ^{16}O, ^{1}H and ^{14}N. Hydrogen is the most abundant atom in the body (the majority of hydrogen is in water) and is the major species that is MR sensitive. The hydrogen nucleus contains no neutrons but contains only one proton, so it is a spinning, positively charged particle.

When the nuclei are not exposed to an external magnetic field, the spins are randomly oriented in different directions. In the magnetic field, the energy levels for a nucleus of a spin number I will split into 2*I+1 energy levels. For example H^1 nucleus can have two discrete energy levels (I= 1/2), a lower and a higher energy state.

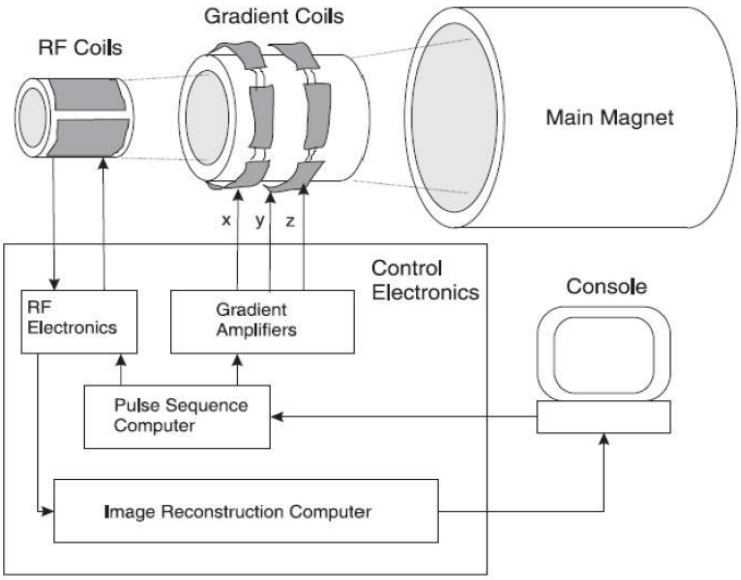

Figure 1.6. Typical structure of an MRI scanner. The shape and frequency of the RF pulses and the timing of gradient field switching are set from a computer placed outside the scanner room [17].

If the sample is placed in a static magnetic field, the spins tend to orient themselves along the field: when the nuclear magnetic moment is oriented parallel to the external field, the nucleus is in the lower energy state and when the nuclear magnetic moment is oriented antiparallel to the external field, the nucleus is in the higher energy state. This situation crates a NMV (Net Magnetization Vector, the vector sum of all the nuclear spins in the sample) lined up and oriented parallel to the external field B_0. A small B_0 produces a small net magnetization M, while a larger B_0 produces larger net magnetization M.

Moreover, due to the influence of B_0, the hydrogen nucleus "wobbles" or precesses, in details the axis of the nucleus forms a path around B_0 known as the "precessional path", which is random or "out of phase" for the individual nucleus. The speed at which hydrogen precesses depends on the strength of B_0 and is called the "precessional frequency". It can be found from the Larmor relationship:

$$\omega = \gamma * B_0 \qquad \text{(eq. 1.1)}$$

where ω is the Larmor frequency (2π times the precessional frequency), B_0 is the static magnetic field strength and γ is a property of the particle called gyromagnetic ratio.

Because the gyromagnetic ratio for ^{1}H is 42.577 MHz/T, the Larmor frequency in a 1.5 T magnet is approximately 63.86 MHz. Irradiating a spin population with a radiofrequency (RF) pulse of the spin resonant frequency, can induce energy transitions between the two spin stages, so the net nuclear magnetic moment vector is perturbed away from the equilibrium. In fact if a pulse of radio-frequency (RF) energy at the Larmor frequency is applied to the system, the particles absorb energy and the precessional axes rotate. They could rotate 90° or until the point where they precisely reverse the direction of alignment (a full 180°). Because the RF energy and the pulse width determine this angular shift, the pulses are called simply 90° or 180° RF pulses. We can conclude that during a RF pulse, the hydrogen atoms starts to precess "in phase" and they flip, in order to align with the RF's magnetic field (B1). When the RF pulse is turned off, the net magnetization vector NMV starts to spin along a spiral path back to the z-axis and to the equilibrium, it "relaxes" back to B0. This relaxation time will be longer for a longer pulse. According to Faraday's law, a time-varying magnetic field produces a current to a conductor and, thus, also the transverse component of the spinning magnetization vector induces a weak current to a receiver coil. This is how the NMR signal is detected. During time, if the spins are not excited again the signal decays exponentially. This phenomenon is called free induction decay (FID).

The relaxation process is characterized by two constants: a longitudinal or spin-lattice relaxation time constant (flipped nuclei realign with the magnetic field B0) and a transverse or spin-spin relaxation time constant (caused by nuclei that quickly become incoherent, out of phase). The longitudinal relaxation time constant, T1, determines the recovery rate of the longitudinal component; in detail because the phenomenon is exponential, after time T1, the longitudinal component has recovered to 66% and after three T1 periods to 99% of its maximum value. The transverse relaxation time constant, T2, determines the decay rate of the transverse component. These time constants are quite long, ranging from several milliseconds to seconds, and they depend on the type of particles and the surrounding material. Eq. 1.2 and eq. 1.3 describe, respectively, the relaxation of longitudinal and transverse magnetization, while in fig. 1.7 the two relaxation curves are shown.

$$M_z(t) = M_0 * (1 - e^{-\frac{t}{T_1}}) \quad \text{(eq. 1.2)}$$

$$M_{xy}(t) = M_0 * e^{-\frac{t}{T_2}} \quad \text{(eq. 1.3)}$$

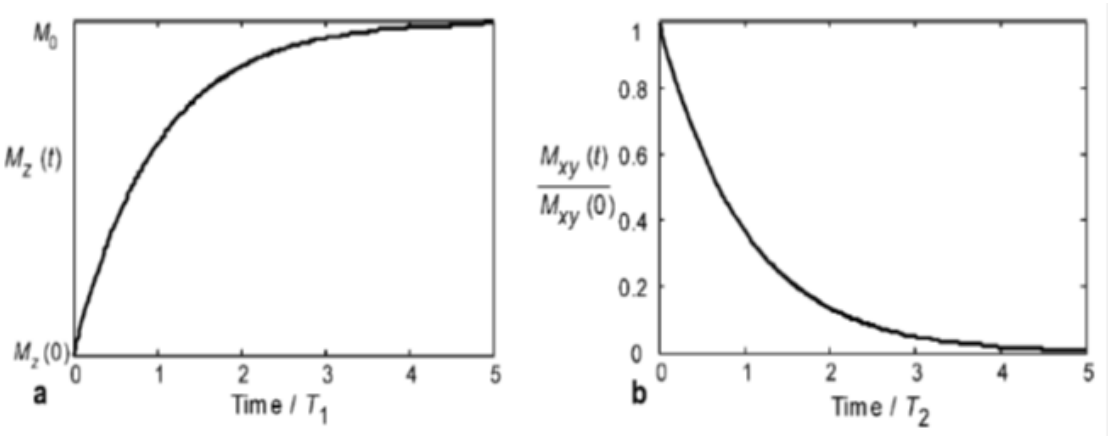

Figure 1.7. Relaxation of a) longitudinal magnetization component and b) transverse magnetization component [17].

The relaxation time constant T2* take into account the magnetic susceptibility and all the disturbances of the magnetic field. Spin coherence is sensitive to the fact that the magnetic field is not completely uniform: this inhomogeneities cause some protons to spin at slightly different frequencies, so that they lose coherence faster. Factors that change local magnetic field (susceptibility) can change T2* decay. Different tissues have different relaxation times: these differences can be used to generate image contrast.

Now, it is given a general description of the method used to form the image in the MRI [9]. To achieve an MR image, a gradient is added to the static magnetic field. Actually three different gradient fields are used to provide a three-dimensional image: Gs or Gz (slice–select), Gp or Gy (phase-encode) and Gr or Gx (readout or frequency encode). Firstly a slice-selective gradient Gz is applied in the direction of the static magnetic field B_0 and the z-axis. Thus in the iso-centre of the MR scanner the magnetic field strength is B_0, in one end it is (B_0–Gz*z), where z is the spatial distance from the iso-centre, and in the other end it is (B_0+Gz*z). Then an RF pulse of a specific frequency band is applied to excite the spins of a specific volume slice. This is possible because, with the gradient application, the nuclei in every slice along the z-axis have a specific stimulation frequency.

After the excitation, the received MR signal comes only from this specified slice. To construct a two-dimensional image of the selected slice, two more gradients, Gx and Gy, are needed. One of the most used imaging sequence is the echo-planar technique. It is a very fast acquisition approach to MR imaging and therefore often used in functional imaging (fMRI). In EPI, the imaging time is reduced by measuring all or most of the MR image spatial frequencies necessary to fill the complete image data during a single RF stimulation period. In slower conventional sequences, such as, for example, spin echo e gradient echo, only one line of the whole spatial frequency space (called k-space) is filled in a stimulation period (called repetition time, TR, and settable parameter of the sequence) and then the imaging time is a multiplication of this duration. The lines number of the spatial frequency space is given by the chosen steps for Gy (or phase-encode gradient). Figure 1.8 shows the difference between a conventional MR sequence and the EPI sequence.

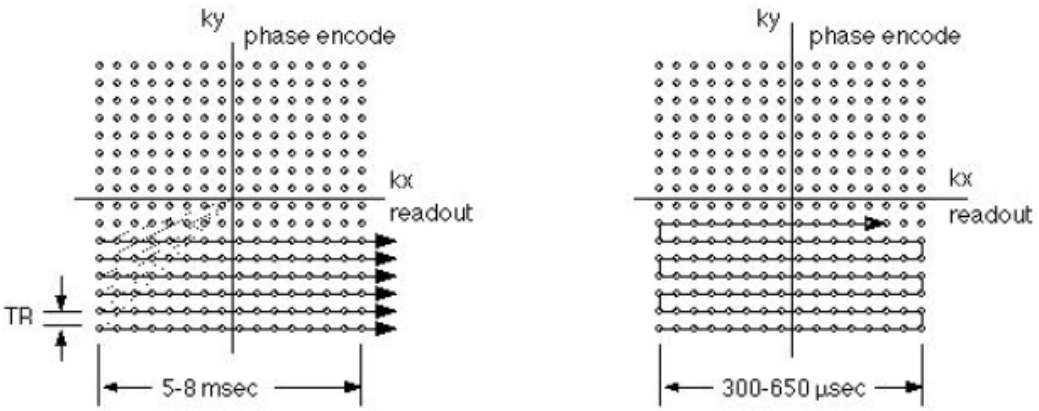

Figure 1.8. On the left: conventional imaging sequence where a single line in k-space is measured every RF stimulation period (TR). On the right: EPI sequence where the whole k-space can be covered during one RF stimulation period by cycling the frequency and phase-encode gradients. Imaging time difference between the two approaches are shown [18].

In EPI sequence, there is a first selective RF pulse combined with the slice-select gradient. Then, there is an initial frequency-encode gradient pulse (Gx) and an initial phase-encode gradient pulse (Gy) that position the nuclei at the beginning of the k-space to be filled, as it happens in any sequence.

After that, in EPI, during the same RF pulse period the phase-encode gradient is periodically applied while the frequency-encode gradient is cycled reversing its value continually and an MR signal is recorded at each step. In this way, the whole k-space is covered and the image can be reconstructed. Figure 1.9 illustrates the RF stimulation and gradients application in standard EPI sequence.

With EPI sequence the acquisition of one image takes about 100 ms and thus a whole-brain study covering about 20 slices can be performed in 2-3 seconds [19].

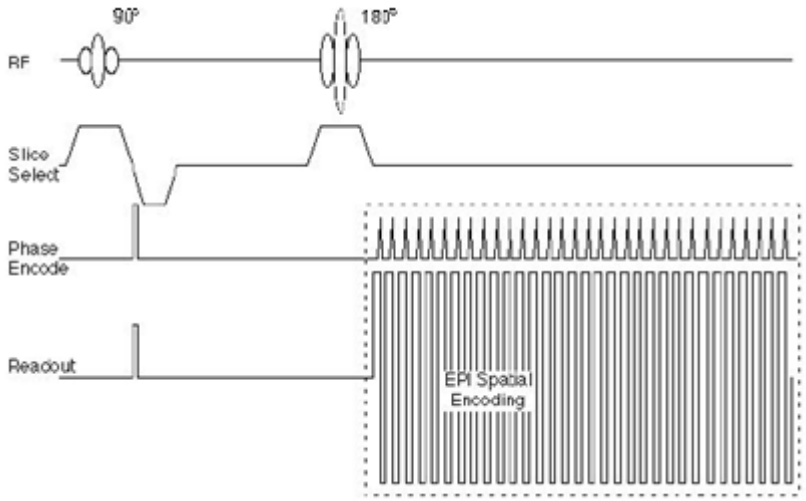

Figure 1.9. EPI pulse sequence diagram. A single RF event comprises both the 90° and 180° pulse to stimulate nuclei. First, a slice-select gradient is applied. Then, after an initial frequency- and phase-encode gradient pulse to position the spins at the beginning of the k-space, during signal acquisition the phase- and frequency-encode gradients are cycled to fill the whole k-space [18].

fMRI

fMRI is a non-invasive functional imaging technique which utilizes the magnetic resonance EPI sequence to image neural activity. It is able to view the hemodynamic response (changes of the content of oxygen in parenchyma, the functional parts of an organ in the body, and capillaries surrounding the organ) in man or in other animals. It's well known that changes in blood flow and blood oxygenation are indirect measures of brain activity.

In fact the increase of the electrical neuronal activity has as a consequence a greater demand of oxygen. The carrier molecule of oxygen in the blood is hemoglobin (Hb). In the inactive state neural cells pick up a certain amount of oxygen from oxygenated hemoglobin (oxyhemoglobin, HbO2) which then becomes deoxygenated hemoglobin (deoxyhemoglobin, Hbr). In the active state the request of oxygen by neurons increases, and thus the blood flow will bring a greater amount of oxygenated hemoglobin compared to the inactive state.

In the active areas, therefore, there will be a net increase of the concentration of oxyhemoglobin. The oxygenated hemoglobin and the non oxygenated hemoglobin have different magnetic properties, in particular oxyhemoglobin is diamagnetic (insensitive to the magnetic field) and deoxyhemoglobin is paramagnetic (paramagnetic materials are characterized at the atomic level by magnetic dipoles which align with the applied magnetic field that weakly attracts them).

The presence of paramagnetic Hbr cause the distortion of the static magnetic field B_0; the spins in a non uniform magnetic field precess at different frequencies, causing a greater dispersion of phase coherence and therefore a more rapid decay of the recorded MRI signal.

This effect is called blood oxygenation level dependent (BOLD) signal [20].

The change of oxygenation in the blood causes a local cortical variation of the magnetic parameter T2* compared to the brain rest condition. The T2*is the time constant which takes into account the decay of inducted spin (nuclei) magnetization due to the inhomogeneous magnetic field and to the spin-spin interaction. Thus, a change in this parameter leads to a variation of the MR image intensity (T2*-weighted contrast).

Below a schematic summary and the table 1.1 show this cascade of physical changes inside the brain cortex during neural activation.

Baseline state:

- ✓ normal blood flow;
- ✓ baseline level of Hbr;
- ✓ baseline blood volume (CBV);
- ✓ acquired baseline-signal.

Active state:

- ✓ higher blood flow;
- ✓ lower level of Hbr;
- ✓ increase of blood volume (CBV);
- ✓ increase of the acquired baseline-signal signal.

Table 1.1.Variation of MR parameters due to cortical activation as result of a stimulus.

MR Parameters	Variation
Blood flow	↑↑↑
O_2 consumption	↑
O_2 blood level	↑↑
Deoxyhemoglobin level	↓↓
B_0 distortion	↓↓
Magnetization dispersion	↓↓
Actual decay speed ($1/T_2^*$)	↓↓
T_2^* - weighted signal	↑↑

.

During a scanning session, therefore, functional images are acquired in the absence of stimuli, which are used as comparison images (baseline level, resting BOLD signal), and during a stimulation protocol. The presented stimuli may be: sensory, motor or cognitive task.

In easy terms, the final functional image is obtained by a subtraction between the image acquired during the absence of stimuli and the image during stimuli. In this way we obtain a differential image which is then superimposed on the anatomical one to detect the activated brain areas.

In conclusion, the BOLD signal is generated by the total cerebral blood flow coming from large arteries and veins, small arterioles, venues and capillaries. Experimental results indicate that the BOLD signal can be estimated from smaller vessels, thus closer to the active neurons, using more intense magnetic fields.

For example, while about 70% of the BOLD signal is derived from the larger vessels in a 1.5 Tesla scanner, about 70% comes from the smaller vessels in a 4 Tesla scanner. Furthermore, the magnitude of the BOLD signal varies approximately in proportion to the square of the intensity of the magnetic field. So, there was an increase of the attention about scanner with more intense magnetic field, to improve the localization of measures and to increase the detectable signal. In the last few years, have been created 7 Tesla scanners (experimental scanner of 8 and 9 Tesla are in development).
Figure 1.10 shows the hemodynamic response exploited in the fMRI technique.

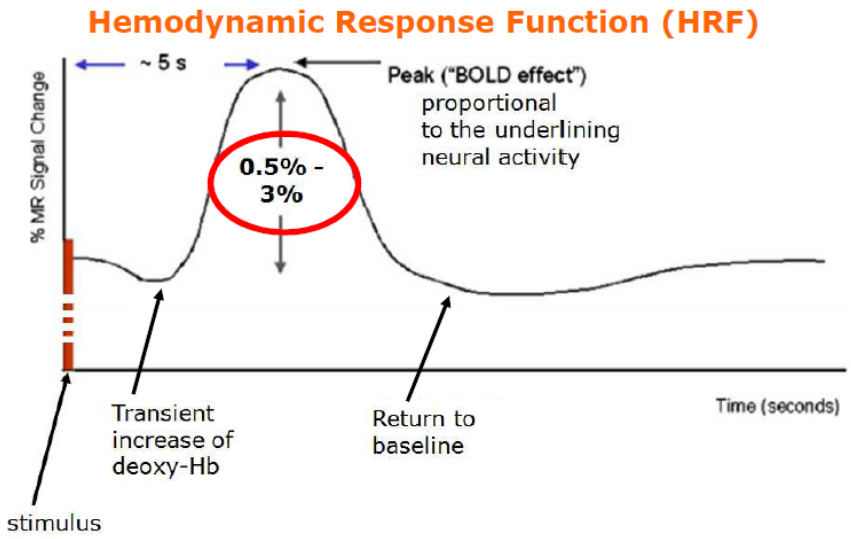

Figure 1.10. The BOLD peak value is expressed in percentage of the baseline MR signal and it depends on, beyond the greater or lesser neural activation, the static magnetic field strength applied during the imaging scanning [21].

1.3 – Motion capture: optoelectronic system with passive markers

Introduction

Motion capture is a process of recording the movement of objects or people. The device used for the acquisition of the movement is a photogrammetric system, consisting of a system of multiple cameras (at least two), operating in the visible range or in the near-infrared region, and markers of reflective material (fig. 1.11).

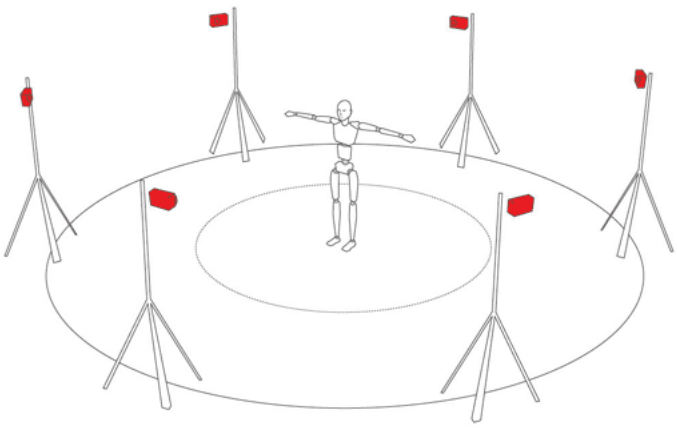

Figure 1.11. System of multiple cameras. (Image of ATPM system)

The optoelectronic systems are the most widespread technological solution to this necessity.

Movement acquisition is based on the recognition and three-dimensional reconstruction of passive retro-reflective markers in each instant of time. This allows to get all kinematic information such as trajectories, speed, joint angles in the three main floors (sagittal, transverse and frontal), etc.

The markers, spherical or hemispherical, are placed on the subject on specific landmark, and the light reflected by these is seen by the cameras as a bright spot on the system.

In order to reconstruct the three-dimensional position of a marker, the position and the orientation of each camera must be known. The system, which must be composed of at least two cameras, is able to combine the two-dimensional images from each camera and elaborate a final three-dimensional image.

As we have already said the kinematic system is used to track quantitatively the movement of the subject and as a sort of gold standard for windowing the EMG data.

Motion capture system has many advantages: three cameras allows a reliable reconstruction of 3D positions of the markers, it's flessible and compatible with the MRI environment.

On the other hand lots of markers are needed if the movement is difficult to reconstruct and the cameras are not positioned with the optimal mutual orientations, because of the major priority to put them on the ceiling at the maximal distance from the bore.

1.4 Safety aspects

Besides the safety precautions for standalone-MR [22], there are the additional issues of the combined data acquisition with EMG. This safety risk is due to induced currents in EMG conductors which can be caused by the static magnetic field, switching magnetic gradient fields or RF interaction [8]. A theoretical study [7] reviewed all these possible mechanisms that might induce currents in electrical wires used for combined electrophysiological recording inside the MR scanner and the associated risks for the patient, demonstrating that the most important potential hazard is due to the inducted currents by RF pulses.

The authors concluded that recording an EEG (or EMG) during MRI acquisition is safe if series resistors, with specific values for each MRI sequence, are added to limit the current value inside the EEG (EMG) leads and so the local heating and possibly burning of the subject's tissue.

This shrewdness is especially necessary when the combined acquisition is done during MRI sequences with maximum specific absorption rate (SAR) value permitted. In fact, the temperature increase strongly depends on the SAR of the MR sequence: the SAR describes the rate of RF deposition on the subject's body.

The actual temperature rise at any time depends on the balance between the energy absorbed and the energy transferred from the region of the body concerned [23].

SAR increases with field strength, radio frequency power and duty cycle, and body size. The doubling of the field strength from 1.5T to 3T leads to a quadrupling of SAR. SAR can be reduced by lower flip angle and longer repetition times, which could potentially affect image contrast (MR-Technology Information Portal).

The addition of current-limiting resistor in series with each EMG electrode leads represents a serious concern because its value is a trade-off between two effects: attenuation of the current flowing through the leads (high resistance value for limiting heating and burning) versus maximization of the EEG signal-to-noise ratio (low resistance value) [7].

Then, because of the potentially compromised quality of the EMG signal recording, some studies focuses on the experimental examination of the actual temperature rise of the electrodes wires to determine whether, without additional resistors, there is an extreme temperature rise or not.

A study [8] shows that EEG signals can be safely acquired inside the magnet during an fMRI sequence without the need of additional serial resistors. In fig. 1.12 are represented the measured temperature rise for five of the eleven healthy subjects which have been tested in the Lazeyras's study.

The temperature rise for EPI sequence (the most used one in functional imaging acquisitions), using a 1.5 T MR scanner, is negligible for every subject ($\Delta Ts < 0.2°$ C).

Another study on the temperature rise in combined EEG-fMRI acquisition (using a 3 Tesla MR scanner) shows the maximum temperature increase measured with the EPI sequence, generally utilized for fMRI, is only 0.85°C [9].

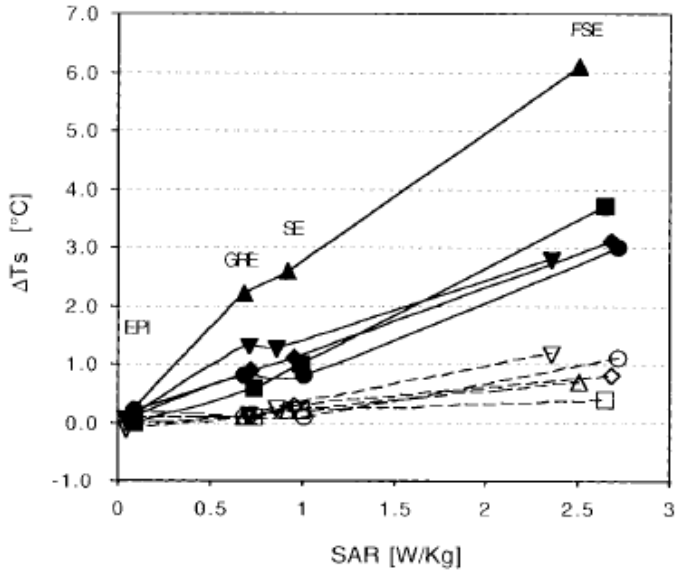

Figure 1.12. Temperature increase as compared to SAR deposition measured in five volunteers. The graph represents the skin temperature rise of four different imaging sequences with increasing SAR. A single subject (the polygonal chain with the steepest slopes) has the peak value over all the tested subjects. The safety limit corresponds to a temperature rise of 8.5°C in these experiments. In the graph the open symbols refer to measurements made without electrodes and the closed symbols refer to measurements made with the EEG system.

1.5 Mutual interference: EMG-fMRI artifacts

Artifacts in MRI data

The introduction in a homogenous magnetic field of objects with magnetic susceptibly value different from that of the surrounding tissue distorts the field and causes local magnetic field inhomogeneities [9]. These inhomogeneities interfere with the imaging gradient fields resulting in local image distortions. As a result of these field gradients, dephasing of excitated nuclei becomes faster which leads to gross signal decrease up to complete signal loss.

So the image is warped in the frequency-encoding direction causing spatial distortion [9]. Since the susceptibility of metal is much higher than that of soft tissue, stronger artifacts are seen around metallic, particularly ferromagnetic objects within scanned portion of the body [24].

The figure 1.13 represents an example of this kind of distortion given by ferromagnetic objects inside the MR scanning field.

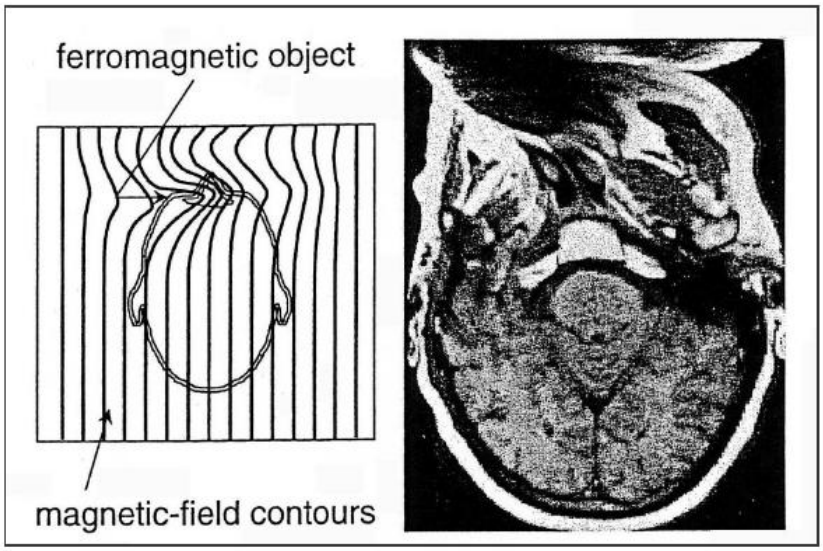

Figure 1.13. Geometric distortion in an MR image. Placing a ferromagnetic object inside the scanner can cause magnetic field perturbations and close to the object MR signals are shifted to different frequencies. The distortion in this figure was caused by steel dental fillings in the subject's teeth [25].

Susceptibility artifacts increase with echo time and field strength and are most prominent in gradient echo and in echo planar imaging [24].

Thus, EMG recording electrodes and wires which are made of conducting materials (ferromagnetic ones) can interfere with the MR image acquisition system [26]. Indeed, the EMG device could radiate spurious electromagnetic noise to its environment and the sensitive receiver coil in MR scanner could pick up this noise resulting in spots or strikes in MR images or the image could even completely vanish [9]. The effect of the EMG equipment noise emission is, then, the degradation of the image signal-to-noise ratio.

Besides, ferromagnetic objects move in the magnet during the EMG recording, and thus causes ghosts in MR images. These ghosts, if sequential, can be represented as replicas of the actual anatomy in the image [25].

Special measures as the choice of conducting materials with suitable magnetic properties should be taken to ensure that these interactions are minimized, to preserve image and EMG signal quality [28].

An important study [27] investigated the effect of individual components of the EEG recording equipment on the quality of echo planar images with a 1.5 Tesla static magnetic field strength. Electrodes, current-limiting resistors, and leads of different material and design are evaluated to identify the most appropriate components for an EEG recording inside the MR scanner.

The results of the Krakow's study [27] shows that most types of EEG electrode give image artifacts which don't exceed the minimum average scalp-cortex distance (the threshold to evaluate a potentially degradation of the fMR image of the cortex).

Conductive gel gives large image artifacts, and as it can be expected that the depth of the signal drop-out and geometric distortion increases with larger amounts of gel, only the minimum amount necessary to give acceptable electrode impedance should be used.

Optimized electrode-wire assemblies lead to artifacts clearly smaller than the minimum scalp-cortex distance so Krakow's analysis concludes that EEG can be recorded inside a MR scanner without compromising the cortex signal by local artifacts [27].

Figure 1.14 illustrates examples of image artifacts caused by EEG components on a phantom.

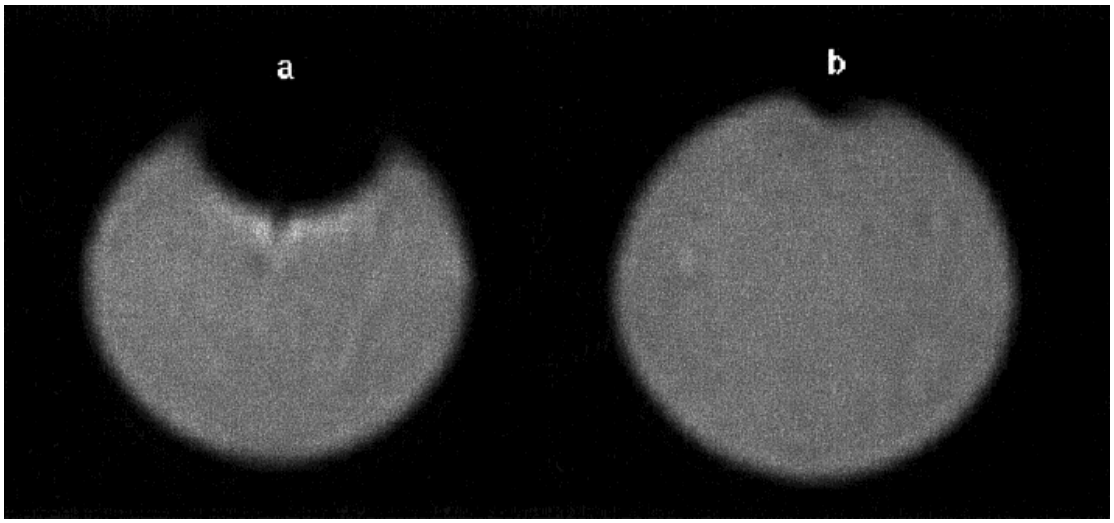

Figure 1.14. Examples of image artifacts caused by current-limiting resistors casused in electrode assemblies. The images show the signal drop out/geometric distortion caused by a carbon composition resistor (a) and by a film resistor by Cermet (b), placed on the top of the phantom (diameter 10 cm) [27].

With regard to electromagnetic noise emitted by the EEG equipment, in Krakow's study [27] is found significant coherent noise in the images if no shielding is used. This noise is likely to be dependent on the type of the EEG equipment, its location in respect to the head-coil and the scanner Larmor frequency (i.e., field strength).

By using an appropriate shielding device (aluminum box and RF filter) the noise could be removed completely for both field strengths.

Obviously, considering the EEG equipment on its own, it compromises the image quality much more than the EMG ones because of its close position to the RF pulse coils (rib-cage coils around the subject's head where the EEG electrodes are put) while the EMG electrodes and leads movements during fMRI data acquisition can produce more motion artifacts in the images.

Artifacts in EMG data

Recording EMG in the MR scanner is challenging because of many interferences on the EMG signal generated by the MR imaging sequence. Large artifacts (many orders of magnitude greater than the mean EMG event) are superimposed on the EMG frequency range and preclude an immediate EMG-fMRI recording.

Completely removing these artifacts is almost impossible but some hardware and software solutions have been shown to reduce them and to allow simultaneous effective recording. Most of the reducing techniques presented below have been developed with respect to electroencephalography (EEG) and fMRI simultaneous recordings, but EEG and EMG are based on similar principles [28] even though some differences in signal amplitude and frequency can be surely detected (EEG range: 5-250 μV; bandwidth: 0-70 Hz, [29]). Therefore, solutions applied to EEG signal filtering may be extended to EMG even if more problems related to subject movements are expected because of the relatively longer EMG wires and, above all, their unavoidably motion during muscle contraction [28].

The imaging artifact sources

Interactions between the imagined subject, EMG electrodes leads and the magnetic fields in the scanner result in artifacts which obscure the EMG signal. The physical principle which underlie the generation of these artifacts is the following: if the magnetic flux through a conductive loop changes, an electromotive force (emf) is induced in that loop. This is called the Faraday-Lenz's induction law and is expressed by the eq. 1.4.

Given a surface A, its perimeter, denoted as ∂A, is made by conductor material and then it creates an electric circuit. A magnetic flux Φ(A) is flowing through this surface. According to the law of induction, the voltage along the perimeter, i.e., in the electric circuit, U(∂A), equals the decrease rate of the magnetic flux through the area [1].

$$U(\partial \mathcal{A}) = -\dot{\Phi}(\mathcal{A}) \qquad \text{(eq. 1.4)}$$

The magnetic flux Φk through a surface is given by the product of the area with the normal projection of the magnetic flux density as shown in eq. 1.5:

$$\Phi(\mathcal{A}) = \int_{\mathcal{A}} B_{\mathrm{n}} \cdot dA. \qquad \text{(eq. 1.5)}$$

From eq. (1.5) two additive causes for a variation of the flux and thus of an induced voltage according to eq. (1.4) are possible:

- ✓ the magnetic flux density ΦB varies while the area A stays constant. This case applies to a changing magnetic field through a stationary conductor;

- ✓ the area A changes its form or position within a constant magnetic field. This case is referred to as moving conductor [1].

Induced voltage consequently adds up to the actual EMG signal creating noise. Ideally, if a bipolar differential recording configuration is used for the EMG signal, (fig. 1.15) the disturbance currents common in the two conductor leads would cancel out each other entirely in the amplifier when the potential difference is measured.
However, in real configuration, this doesn't happen. Even though the resistances of all the EMG wires are made as equal as possible, it is impossible to achieve exactly the same values for the resistance of the two different conductors entering the amplifier.

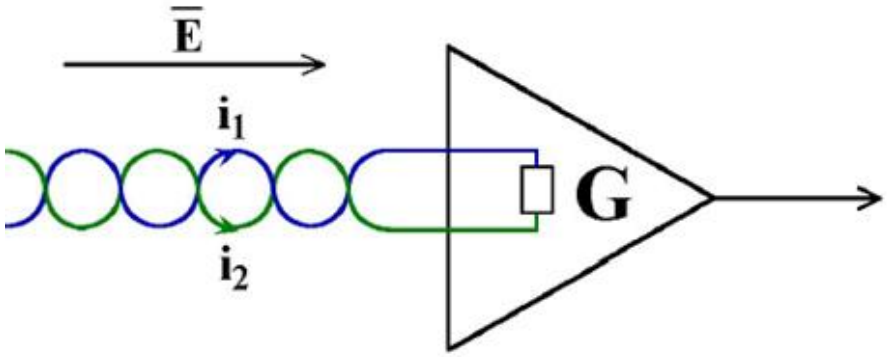

Figure 1.15. Induced voltage (electric field $\bar{E}$) results in induced currents inside the EMG conductors during MR imaging [9].

According to Ohm law, depending on the resistance value R of every conductors, although the induced currents were exactly the same at some moments, there would still remain a small voltage difference between the amplifier input clamps [9], as it is represented in fig. 1.16. This small difference is amplified by the EMG linear amplifier and, thus, the eventual noise collected before the amplification step becomes very large and source of problems for the next signal processing steps.

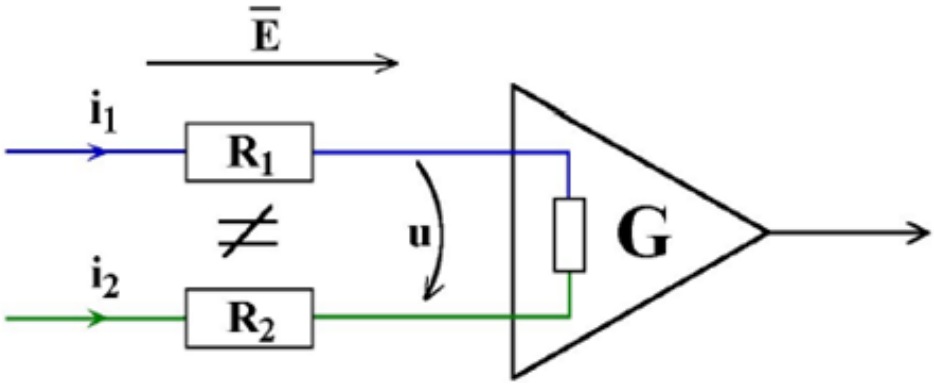

Figure 1.16. Disturbance current in the EMG amplifier end. Because the resistances of two conductors can never be perfectly the same, a small voltage difference between them remains even when the currents i1 and i2 are equal. After amplification the disturbance voltage is large [9].

The induction principle presented above results in the following EMG artifacts when this signal is recorded during an MRI scanning:

- ✓ Outside the magnet bore, the static field (B_0) becomes non-uniform and hence a moving inter-electrode lead loop may experience a change in flux resulting in an induced emf.

By twisting electrode leads together and securely fixing the leads to a stationary surface, this kind of artifact (non-uniform static field) can be minimized [30] because the area of the loop among electrode cables and amplifier and its motion is thus reduced.

- ✓ Movement of the subject and hence the attached electrode leads may change the area of inter-electrode lead loops normal to B_0, resulting in an induced emf in the leads.

This second kind of artifact results from subject movement and the Allen's study [30], on simultaneous EEG and fMRI, it is treated in a way similar to that of artifact caused by B_0 non-uniformity. The proposed solution to fix the subject's head in the imaging head coil and to use a movement detector to help identify head movements in the EEG track in the post processing analysis. In consideration of EMG signal the proposed solution is not feasible since this signal detection is based on the movement (i.e. muscle contraction and relaxation).

- ✓ The switching of magnetic fields applied during image acquisition may induce emfs in the electrode leads independently of subject or lead movement and tilting [30].

The third kind of artifact is the most important and wide-distributed one, and it's difficult to remove. In fact, the amount of artifact reduction and the degree of physiological signal preservation are important complementary performance measures. Reduction of the artifact itself is not a quality measure, since it provides no information on biological signal preservation. Performance differences of post-processing removing algorithms are demonstrated in respect to different spectral bands and therefore the choice of a particular algorithm has to be performed taking into account the characteristics of the electrophysiological signal to be detected [31].

The following paragraph is concentrated on the third kind of artifact: its amplitude and frequency features and the state of art of hardware, software and protocol reduction solutions which have been proposed applied to EEG/EMG signal.

Changing magnetic fields artifacts

Two different fields are applied during image acquisition: RF and gradients. Artifacts induced by the specific RF frequency (~63 MHz for a 1.5 Tesla MR scanner) are out of the EEG and EMG bandwidth and can be therefore effectively reduced by low-pass filtering applied before the EEG amplifier front end [29] or even after the amplification step if the linear amplifier and the ADC have a very large dynamic range.

The own frequency of oscillation of the gradients depends on their rise time (~ hundreds of μs) and, generally, it is ~1 kHz so it can be filtered as mentioned previously.

However, both magnetic fields induced artifacts contain components also in the EMG frequency range because of the main frequency and the harmonics of the repetition time TR of the imaging acquisition loops [32].

Let us consider again the gradient artifacts because of their amplitude that is some orders of magnitude higher than the RF ones. The difference in amplitude between RF and gradient field artifacts has been studied by Hoffmann [32]: RF pulses artifacts have a power less than 5 μV^2/Hz while gradient artifacts have a power over $10^4 \mu V^2$/Hz. The maximal amplitude of the induced gradient artifact is given by eq. 1.6:

$$Vga_{Max} = \left(\frac{dB}{dt}\right)_{Max} * A_{loop_{Max}} \qquad \text{(eq. 1.6)}$$

where $Vga_{\_Max}$ is the maximum amplitude of the induced gradient artifact, $(dB/dt)_{\_Max}$ is the maximum rate of change of gradient field, and $Aloop_{\_Max}$ is the maximum loop area.

To make an approximate estimate of the size of the gradient artifact, we assume an easily generated, average rate of change of magnetic field of 20 T*s^{-1} and an effective loop area of 50 cm^2. This yields an induced noise voltage of 100 mV (200mV pk-pk) [33], which is more than 100 times larger than a typical response in an EMG recording. In general the amplitude of the gradient interference is dependent on all sequence parameters regarding the gradient slope (amplitude at a fixed rise time).

Therefore, reduction of the slice thickness or the field of view (FOV) result in a higher amplitude of interference [32].

The interfering spectrum needs a further investigation. If a signal of any shape and any own frequency is continuously repeated after a time TR, the frequency spectrum of a long period of repetitions of that signal consists of multiples of one frequency that is 1/TR.

MR sequences consist of several repeated loops of RF and gradient switching. In all the spectra of the recorded biological signal with the interference of the applied imaging sequences, multiple discrete frequencies are observed corresponding to TRs of the loops of the MR sequence (harmonics).

This concept is illustrated in the example fig. 1.17 taken from the Hoffmann's paper [32].

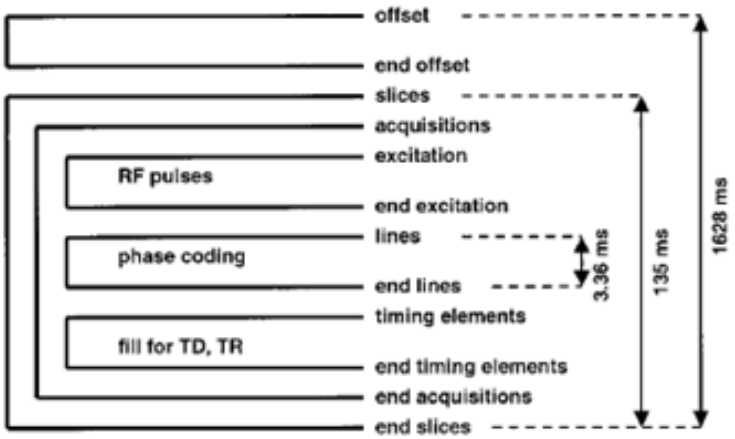

Figure 1.17. Example of a loop structure of an EPI sequence and the TRs of the single loops: 3.36 msec for phase encoding, 135 msec for imaging of one slice, 1628 msec for one whole measurement [32].

Following the Hoffmann's analysis, specific testing sequences are presented to explain the composition of the interfering spectrum in the recorded electrophysiological signal.

Two particular sequences are programmed to apply single components of a whole imaging sequence, such as repeated RF pulses and oscillating gradients, separately. These two sequences are represented, respectively, in fig. 1.18 and fig. 1.19. Later on a standard fMRI sequence, such as spin echo and gradient echo sequences, with different TE and TR values, is performed during EEG recording.

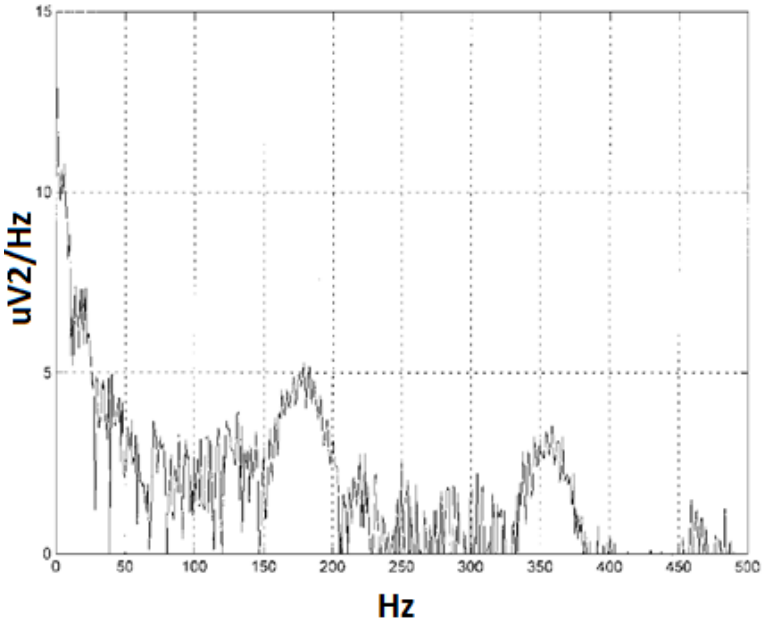

Figure 1.18. Power spectral density of 1 sec of an EEG recorded during repeated saturation RF pulses at 64 MHz. Main frequencies of the RF can be detected at 175 Hz and 350 Hz (the first harmonic) with a bandwidth of about 50 Hz. 175 Hz corresponds to the repetition rate of the saturation pulses used without gradient switching (i.e. 5710 msec) [32].

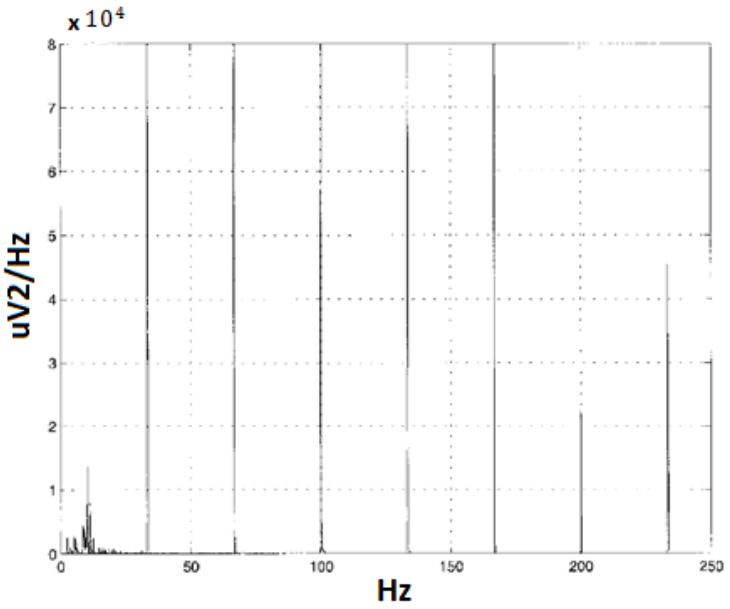

Figure 1.19. Power spectral density of 10 sec of an EEG recorded during a gradient sequence with a TR of 30 msec. The corresponding interfering frequencies at multiples of 33.3 Hz are high, sharp peaks. The minor contributions of the EEG at frequencies between 0 and 30 Hz can be seen also [32].

For the EPI sequence, the spectrum of interfering frequencies is complex, but it can be explained by examining the loop structure of this sequence (fig. 1.17). The most inner loop represents the readout of the image lines. The TR for this loop is 3.36 ms so the frequencies generated by this loop are multiples of 298 Hz.

The next outer loop represents the different slices. Ten slices are imaged and the TR for this loop results in 136 msec. The corresponding frequencies are multiples of 7.36 Hz and affect the EEG signal.

The most outer loop represents the number of measurements performed. In Hoffmann's study are imaged ten slices and the time for one complete measurement is then 1628 msec. The corresponding frequency is 0.61 Hz.

All of these frequencies are found in the power spectrum of an EEG recorded during the EPI sequence [32] (fig. 1.20).

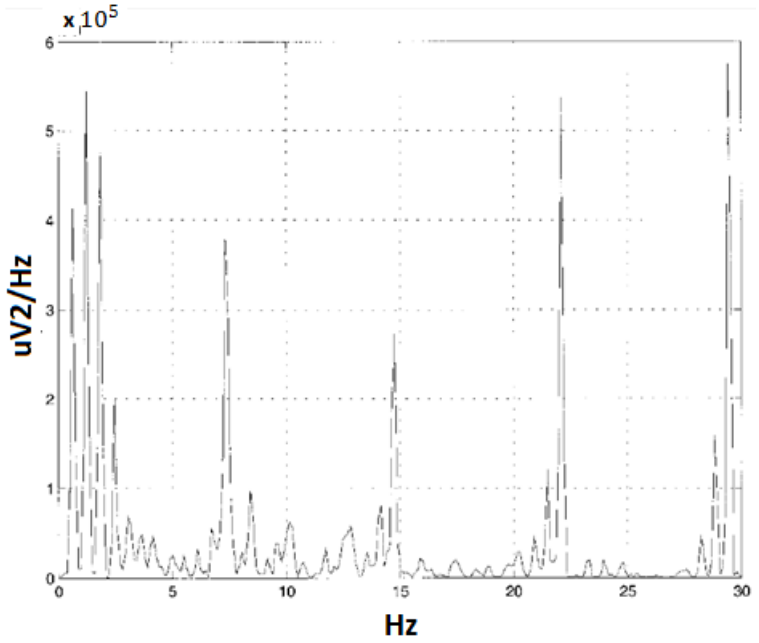

Figure 1.20. Power-spectral density of the interference of the EPI sequence depicted during an EEG recording. Multiples of 0.61 Hz and 7.36 Hz are clearly detectable, corresponding to the TRs of 1628 msec and 135 msec in the loop structure of the sequence. Amplitudes of the interference are five orders of magnitude higher than in the RF itself. The frequencies above the interesting EEG bandwidth (0-30 Hz in the Hoffmann's study) are low-pass filtered (64 MHz and 833 Hz which are the own oscillation frequencies of RF and gradient field respectively; 298 Hz and its harmonics which depend on the TRs of the slice-acquisition) [32].

Post-processing algorithms to reduce artifacts caused by changing magnetic fields

Hoffmann and colleagues [32] propose to restore the EEG signal using an algorithm which compares the frequency power spectrum of the unaffected EEG with the spectrum of a disturbed EEG of the same channel. When high frequency differences are found, a series of band-stop filters which selectively remove the artifacts is applied. Hoffmann uses band-stop filters with frequencies multiples of 7.36 Hz and at neighboring frequencies 0.61 Hz apart in the frequency window of the EEG. The digital filters are of the fourth order, have a Butterworth characteristic and a bandwidth of 0.2 Hz.

The restored EEG is consistent with the EEG of the patient recorded under normal conditions. Obviously, Hoffmann's method to remove the changing magnetic fields artifacts is not feasible for a signal (even the EEG one when, for example, the alpha waves are studied) which contains important frequency components in one or more of the filter band-stop ranges.

In conclusion, the Hoffmann's analysis shows that a simple low-pass or band-pass filtering is not effective to reduce the artifacts in EEG (or EMG in the present work case) caused by the switching of RF and gradient fields but a more complex and radical approach to the artifacts problem is necessary.

A proposed method to reduce gradient artifacts is that described by Laudon [34] and applied to the ECG signal (in this context, EEG and ECG signals have similar spectral content and therefore similar results would be expected for EEG, [29]). Laudon and colleagues use an external loop placed over ECG electrodes to record the induced emfs and then subtracts this electronically from the ECG signal, reducing the artifact to 20%. This approach is impractical for multichannel EEG recordings and the artifact reduction is far too small [29].

Felblinger [35] describes a method which determines the impulse response of the ECG recording system for gradient fields applied individually in the *x*, *y*, and *z* planes during a period of low-amplitude ECG (the ventricular diastole) with the assumption that the signals recorded are entirely induced artifact. These responses are then used to filter the *x*, *y*, and *z* gradient waveforms from the scanner during imaging period and the sum of the filter outputs are subtracted from the ECG signal [29]. This technique appears to be effective for ECG recordings with gradient slew rates of 10 T/m/s. However, an extension of this method to EEG signals (and EMG ones) is ineffective because the gradient slew rates in fMRI are an order of magnitude higher (typically 125 T/m/s) and both EEG and EMG signals have not a "rest-period" during which recording the gradient artifacts in the three planes.

AAS

Average artifact subtraction (AAS) is the most widely algorithm used to remove artifacts in combined EEG/EMG and fMRI analysis (for example EEG, [28]).

It forms an average gradient artifact template and then subtracts this template from each occurrence of the gradient artifact in the EEG data [33]. This approach assumes that the shape of gradient artifacts is constant over time and additive to the physiological signal [31]. A previous assessment of image artifact waveforms recorded from subjects during periodic fMRI suggests that these artifact waveforms have a very low inter-volume

variability and hence subtraction of the image artifact waveform averaged over a number of volume acquisitions might be effective [29].

Allen proposes a feasible and quite simple method for reducing gradient artifacts, avoiding the complication of recording the impulse response for each gradient direction and not requiring a "quiet" period in the detected electrophysiological signal.

The RF artifacts are neglected by Allen because of the low-pass filtering applied to the recording signals before the front end amplification and, probably, because of the difference in amplitude between the two kinds of artifact where the gradient artifacts have a much higher amplitude than the RF ones. Moreover, the AAS algorithm by Allen can deal with artifacts persisting after the cessation of gradients. In fact, artifact sometimes persists after gradients have ceased changing: this is due to small subject movements caused by scanner vibration [29].

The mechanical forces on the gradient coils when their fields are switched in the static magnetic field, induce vibrations in the MRI scanner which are heard as the typical noise. These vibrations transmit to the amplifier and the electrode cables and if they are moved in the static magnetic field, a disturbing signal is induced. These movements take finite time to decay. An hardware solution to deal with this issue is to use a padding under the electrode wires and the amplifier to reduce the mechanical transmission of the vibrations to the EEG system during imaging [32].

The AAS algorithm has two principal sections: an average imaging artifact waveform is calculated over a fixed number of EEG epochs and is then subtracted from the EEG for each epoch; adaptive noise canceling (ANC) algorithm [36] is used to attenuate any residual artifact the majority of which is synchronized to the slice-timing signals (around some Hz value so they can't be removed by linear filtering without affecting an important part of the electrophysiological signal). The algorithm is presented schematically in fig. 1.21.

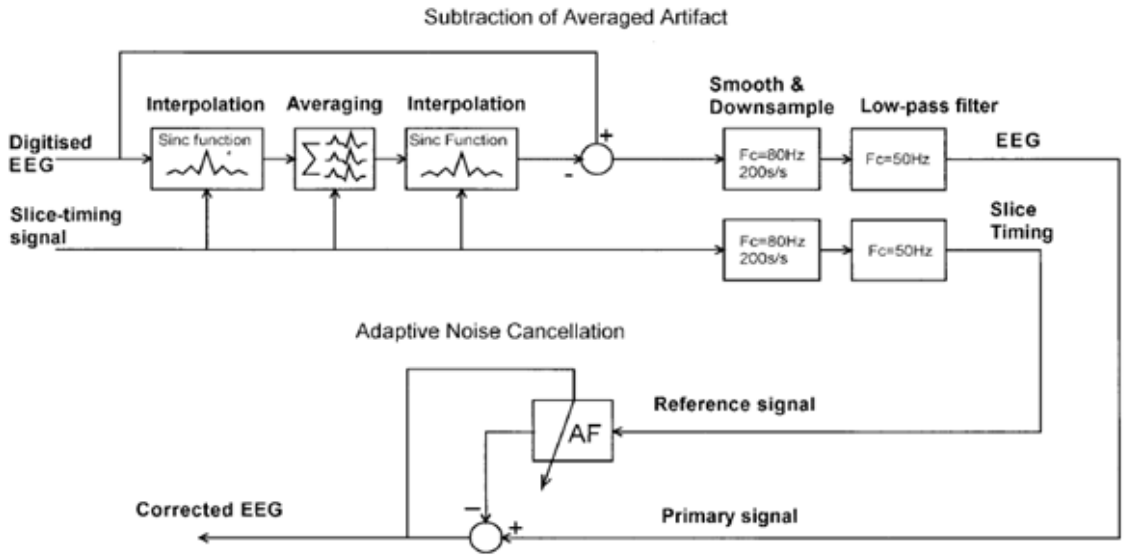

Figure 1.21. Image artifact reduction method presented by Allen [29].

For a periodic fMRI sequence with delays between volume scans, an epoch is defined as the volume repeat time, TR. The EEG recording is divided into sections of epochs over which averaging is performed. It is assumed that EEG is uncorrelated between epochs. Imaging artifact on the recorded signal is nearly perfectly synchronized to the slice-timing signal. After subtracting the average artifact, the signals are smoothed to reduce the likelihood of aliasing in the next process, which is downsampling to 200 Hz, a sampling rate typically used for EEG. Additional low-pass filtering is then performed with fcut = 50 Hz [29]. Although subtracting the averaged artifact followed by low-pass filtering removes most of the artifacts, some residual artifacts, synchronized to the slice-timing signals and then in the Hz order (in the frequency range of interest of EEG), are still present. So, an adaptive noise canceling approach is used to remove the residual artifact [29].

Noise cancelling is a variation of optimal filtering that is highly advantageous in many applications. It makes use of an auxiliary or reference input derived from one or more sensors located at points in the noise field where the signal is weak or undetectable. This input is filtered and subtracted from a primary input containing both signal and noise. As a result the primary noise is attenuated or eliminated by cancellation.

An adaptive filter differs from a fixed filter in that it automatically adjusts its own impulse response. Adjustment is accomplished through an algorithm that responds to an error signal dependent on the filter's output.

Thus with the proper algorithm, the filter can operate under changing conditions and can readjust itself continuously to minimize the error signal. In noise cancelling systems the practical objective is to produce a system output $z = s + no - y$ that is a best fit in the least squares sense to the signal s.

This objective is accomplished by feeding the system output back to the adaptive filter and adjusting the filter through an LMS adaptive algorithm to minimize total system output power [36]. Fig. 1.22 shows the ANC approach.

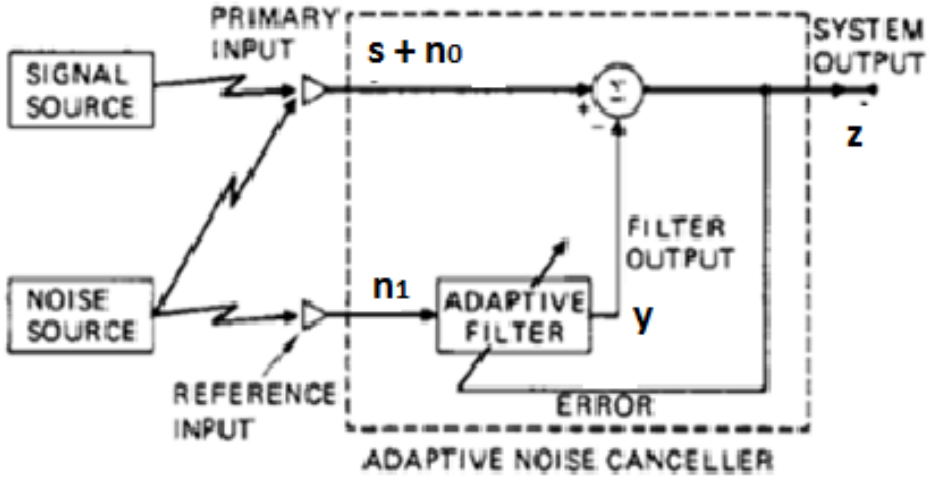

Figure 1.22. The adaptive noise cancelling concept [36].

Before the algorithm application, Allen and colleagues measure a median artifact amplitude of 4000 uV pk-pk, (which is over 400 times larger than the lowest amplitude EEG events). It's important to say that they also apply an hardware low-pass filtering (fcut = 70 Hz) which reduces this interference to 571 uV, but indicating that low-pass filtering alone is not sufficient to remove artifacts caused by fMRI sequences. Subtraction of the averaged artifact (followed by another low-pass filtering, fcut = 50 Hz) reduces this artifact to 11 uV and the ANC reduces this to 8 uV.

Then, the AAS algorithm performs the bulk of the artifact subtraction and ANC suppresses the small amount of residual artifact. The AAS method is implemented offline but, for continuous fMRI, the short averaging period used allows an online implementation.

There is still a residual artifact noise in the recorded electrophysiological signal due to differences between individual epochs on which the template is computed and the average artifact, due to small subject movements and scanner drifts [29].

AAS algorithm requires an accurate sampling of the gradient artifact waveform which means that the artifact must be precisely sampled. The former requirement can be achieved through synchronization of the MR scanner and EEG clocks [37].

In this recently proposed approach two conditions must be met in order to achieve synchronicity between an MRI sequence and the regular sampling pattern of the concurrent electrophysiological signal: the repetition time (TR) of the MRI sequence must be an integer multiple of the EEG sampling interval so the gradient artifacts are constant over time and can be removed by simple artifact template subtraction (AAS); the internal clocks of both systems, EEG and MRI, must be phase locked with a frequency divider and phase-locking device. Obviously, synchronized recordings can be combined with any post-processing method of artifact reduction [37]. However, since synchronization of EEG and MR scanner requires technical modifications that are as yet available in only a few laboratories, the unsynchronized acquisition of EEG and fMRI is still the prevalent method [31].

For this reason, because of the residual noise in the recorded signal, the AAS algorithm is supplemented, in the very last years, by more sophisticated signal processing schemes such as Principal Component Analysis.

Principal Component Analysis (PCA) algorithm

In this section is presented just one of the possible development of the principal components analysis present in literature for the application to the imaging artifact removing from an electrophysiological signal.

MacIntosh and co-workers propose a PC/IC (Indipendent Components) analysis for reducing the gradient and RF artifacts in EMG signal [2].

Typically, component analysis techniques attempt to isolate structured features in the data from noise sources. In the MacIntosh's work is recognized that stochastic EMG muscle signals can be isolated from fMRI-induced highly structured and periodic noise (i.e. the opposite goal) [2].

To ensure data synchronization, EMG acquisition software triggers the MR scanner. The goal of the MacIntosh's approach to the artifact problem is to maximize EMG signals and two alternative component analysis techniques are investigated to separate fMRI-induced contamination from EMG muscle signals of interest. The first one is PCA and the second one is an ICA ''seeded'' by PCA (performed customarily). In fig. 1.23 the results of the next described PC/IC algorithm application to an EMG signal is shown.

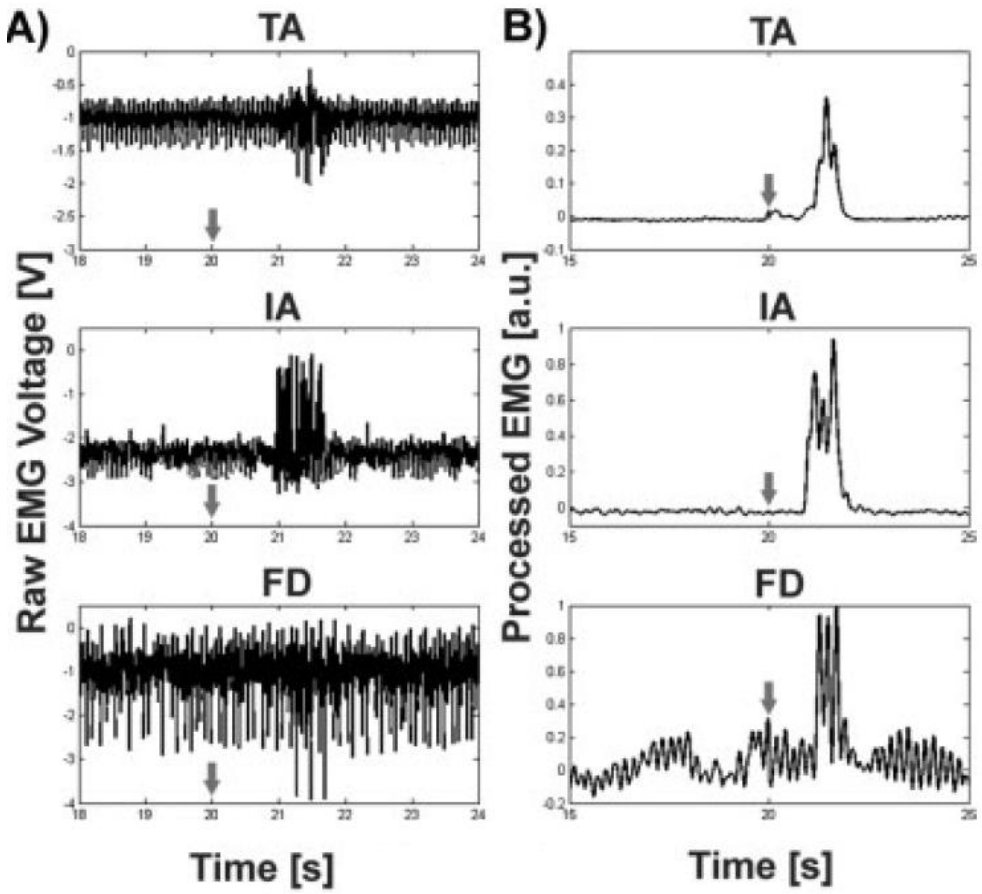

Figure 1.23. EMG during fMRI. **A:** Sample EMG time series from three muscle groups: right tibialis anterior (TA, top), right index abductor (IA, middle), right flexor digitorum (FD, bottom). fMRI induced noise is evident in all three traces to varying amounts. **B:** Processed EMG data for the same three muscles after PCA, rectification, and low-pass filtering clearly delineates muscle burst for TA and IA, whereas results for FD are poorer [2].

Component analysis on EMG data is performed after separating the recordings into the constituent 15 motor task repetitions of 20 s duration, time-locked to the fMRI acquisition. The multiple trials are treated as repeated measures creating the redundancy requirement essential for feature extraction techniques.

EMG data are reconstructed after using an automated power spectrum calculation to select those PCs that reflect the signal contamination.

The mean power and standard deviation are calculated for each component and expressed as a ratio.

If this ratio is less than the average across all the components by an amount greater than 1 Standard Deviation, then the component is removed.

The remaining components are then used to reconstruct the EMG data. A fast ICA algorithm is subsequently used to represent the data as 15 linearly independent components, using the PCA result as the starting input [2].

FARM

Current template-based artifact reduction methods are inadequate to reduce irregular volume and slice-artifacts induced by limb motion in combined (surface) EMG–fMRI (electromyography–functional magnetic resonance imaging) studies. In addition, artifacts are not removed adequately for EMG frequencies above 50 Hz. This algorithm, by van der Meer [38] is an improvement of the AAS algorithm by Allen [29], named artifact reduction algorithm for motion (FARM), which takes into account the changes in fMRI artifacts along the EMG acquisition and integrates a final principal components analysis too.

During an EPI sequence (the fMRI typical imaging sequence), the fMRI artefacts can be divided into periodic volume-artefacts and slice-artefacts. As Allen theorized in his paper [29], the periodicity of these artefacts allows the construction of a template by averaging several slice-segments or volume-segments of the EMG data (which have a stochastic nature and then are not repeatable). However, template subtraction requires that the shape of the artefacts remains constant and that the onset of every slice and volume-artefact can be determined with a high accuracy [38]. The first requirement don't occur when the recorded signal during an fMRI is the EMG one which needs, for its acquisition, limbs movements and then changes in fMRI artefacts collected by the EMG cables.

Template subtraction techniques commonly used for EEG–fMRI remove less fMRI artefact for frequencies above 50 Hz [31]. Surface EMG frequency content ranges up to 500 Hz and is therefore intrinsically more sensitive to high-frequency artefact components.

The motion of the limbs introduces two extra artefacts in the EMG. The first is due to movement of wires and electrodes in the main B_0 field.

This translates into interaction between the wires and the main magnetic field, introducing extra unpredictable components in the signal, whose frequency and amplitude depend on the trajectory and speed of the wires. If motion is fast enough, the frequency of these components can reach 25–30 Hz and the amplitude can be as high as 30 mV. Because the waveform is unpredictable, it cannot be estimated with templates. The second artefact is due to alterations in the spatial orientation of the wires, which in turn alters the shape and size of the slice- and volume-artefacts.

Chapter 2. Materials and Methods

2.1 Subjects

Three healthy right-handed volunteers (23,7 of mean age) are scanned, a female and two males. Experiments are conducted at Villa Beretta rehabilitation center (Costa Masnaga, Italy).

2.2 Experimental set-up

The experimental set-up is composed by a 1.5T MRI scanner, a motion capture system and an EMG recording equipment arranged as shown in fig. 2.1.

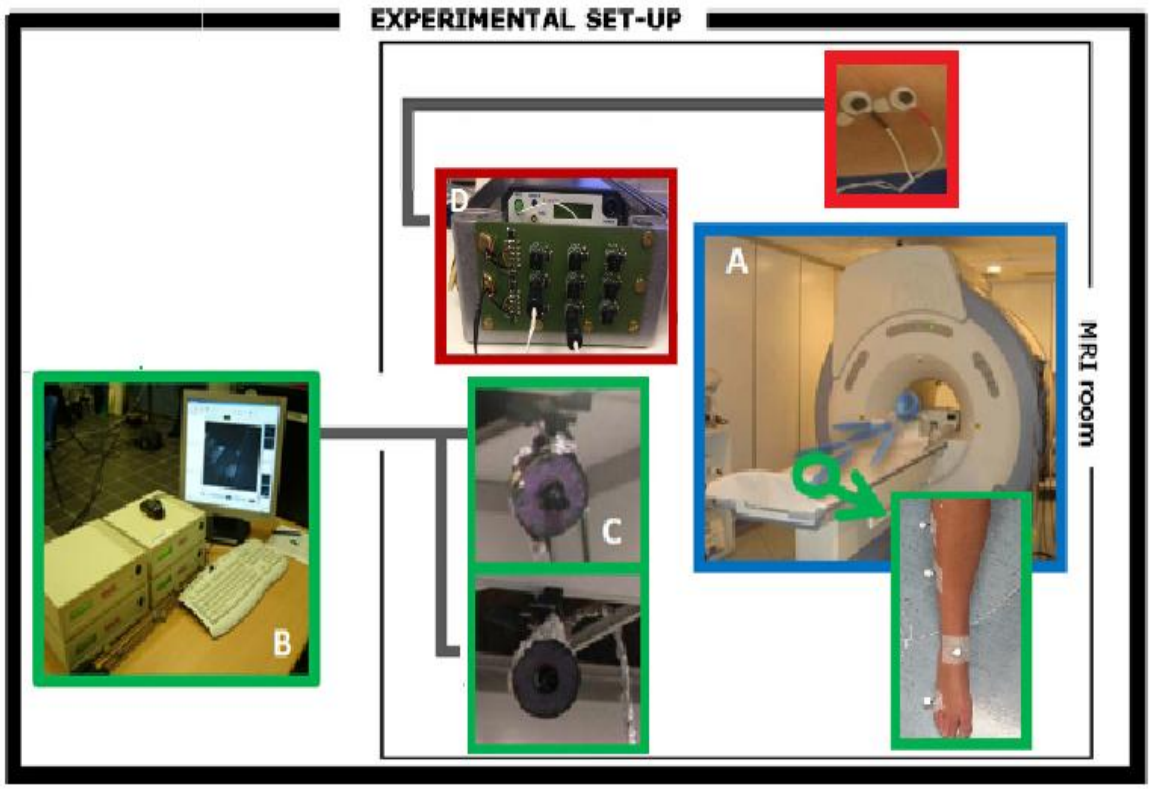

Figure 2.1. Experimental set-up. (A) MRI scanner GE CV/I 1.5T; (B) motion capture system Smart μg^{TM} with (C) two cameras and reflective markers; (D) Porti TMSi system located inside a prototype box with the recording electrodes.

The scanner used for all images acquisition of this study is a GE Medical Systems product: CV/I 1.5 T model.

Motion capture system arrangement is based on a previous study [6].
Thus, an optoelectronic motion analysis system which tracks passive, reflective, markers with two cameras assembled in the resonance room. A previous study validated the feasibility of this technical asset [39].
The commercial motion capture system Smart μg^{TM}(BTS, Italy) is used. Cameras have a LED enlighter emitting at 850 nm and a CCD detector sensible to infrared light. The working frequency is set to 120 Hz.
Aluminum foils, connected to MR room ground, are contiguously applied to all motion capture elements in the MRI room as seen in literature [40] in order to limit the RF interference. Cameras cables are passed through the waveguide of the MRI room, which connects the inside of the scanner room to the outside, to reach the motion capture workstation placed in the operator room.

The recording system for electrophysiological signals is the Porti7 produced by TMS International shown in fig. 2.2. The system has unipolar and bipolar inputs and also auxiliary inputs for physiological signals (e.g. respiration, body position, body movement, temperature, etc.) one of which is used in the present work to acquire inputs from the electrogoniometer.

Figure 2.2. EMG recording system: Porti7 produced by TMS International.

In this work, the system is powered by a set of batteries to prevent MR-sequence induced noise on the power supply cables and the EMG acquired data are stored on a PC card flash disk within the Porti system for a further reading instead of optical fibers.
This choice is made to avoid too many wires to be carried out the scanner room (the waveguide connecting interior to exterior of the MRI room has a very small diameter); in fact optical fibers, which are very delicate, should be connected to a computer placed in the operator room. In this way, thanks to the batteries and to the flash disk, the system is in a stand-alone configuration.
The most relevant Porti7's features are:

- ✓ absence of embedded pre-amplifiers;
- ✓ the input stage for measuring bipolar EMG is configured as an INA with Gain = 20, input range = -150mV / +150mV, CMRR > 90 dB;
- ✓ the input impedance of the active channels is very high (10 TΩ) so the influence of electrode impedance results to be very small.
- ✓ the ADCs inside the Porti7 have a very high resolution (22 bits) so for bipolar inputs, with a gain of 20, one bit of the digital output corresponds to 71.5 nV.
- ✓ the sampling frequency can be set and, in the present work, it is set to 2048 Hz. Inside the ADCs there are also anti-aliasing linear phase digital low pass filterers with fcut = 0.27 * sampling frequency (i.e. 553 Hz with a 2048 Hz sampling rate).

The set-up also includes a prototype box produced by TMS International too where the Porti7 can be placed. The box is made of aluminium but contains some ferromagnetic materials too which may cause the box to be pulled inside the MRI bore: for this reason and for preventing the saturation of the Porti's internal DC-DC converters due to the high static magnetic field of the MRI scanner (B_0) the box is placed quite far from the scanner bore i.e. at the foot of the MRI bed (about 1.5 m). This box acts like a good shield against the switching EM fields such as the RF pulses and the gradient magnetic. There are pi-filters (capacitor-input filters) on the edge of the box and a big ferrite inside which protect the Porti against the RF pulse. The aluminium box isn't grounded because even the thick lead to the ground connection turns into an antenna for the 50-100 MHz RF pulse and into a sort of loop for the gradient field.

Moreover, the aluminium box and the integrated pi-filters (RF pulses filters) are appropriate shielding devices, for a 1.5 T magnetic scanner, to remove the electromagnetic noise emitted by the EMG equipment [27]. This coherent noise may significantly affect the functional images SNR during the concurrent acquisition of fMRI and EMG.

The leads connecting the surface electrodes to the EMG recorder are in carbon materials which are suited for use in MR compatible system because they cause less imaging artefacts [27] and radio frequency heating [41] than metallic components. On the other hand, even if the leads are twisted to minimize gradient artefacts, they aren't shielded, meaning that they are not immune to the capacitive cable movement artefacts and to power supply noise (at 50 Hz) comparing them to the actively shielded ones, normally used in EMG acquisitions with Porti devices. Instead the active-shielded cables, because of their internal structure, are affected by RF-pulse artefacts heavily. Leads choice is done taking into account the trade-off between the RF pulses versus the 50Hz and movement artefacts considering the RF pulse artefacts the most important (and the widest) ones to be limited in the present context.
At last, in this work, no current-limiting resistors are put in series to the EMG wires because of the negligible temperature rise of the surface electrodes during an EPI sequence [8, 9].

2.3 Experimental protocol and acquisition procedures

Task repetition, EMG electrodes placement and acquisition period

Two simple motor tasks have been evaluated within this study, including upper and lower limbs measurements:
1) voluntary dorsiflexion of the right ankle (ADF);
2) voluntary extension of the right wrist (WE).
The EMG electrodes are arranged in a bipolar configuration, with the two active electrodes applied respectively to the tibialis anterior (TA) muscle for the ankle dorsi-flexion and to the extensor carpi ulnaris for the wrist extension.
The reference electrode is applied to the right wrist only for the first subject (who performs only ADF) while for the other two subjects is applied to the left wrist (subjects perform ADF and WE).

The experimental protocol lasts 10 minutes for a single fMRI run, whit 5 minutes for each task (no switching between the two tasks is performed before completing all the 5 minutes of one task).

Each motor task consists in ten ON/OFF blocks where every block is composed by 20 seconds of motor activation and 10 seconds of rest. During the 20 ON blocks, the motor task is performed with a repetition frequency of 0.5 Hz, e.g. an ADF or a WE every 2 seconds (fig.2.3), as reported in literature [11].

So the number of EMG activations for each single task in a whole acquisition is 100 (10 EMG for an ON/OFF block* 10 blocks = 100 EMG).

The order of execution of movement tasks is set to 5 minutes of ADF followed by 5 minutes of WE. The timing of the movements is auditory cued (both inside and outside the scanner room) through a recorded acoustic signal in headphones.

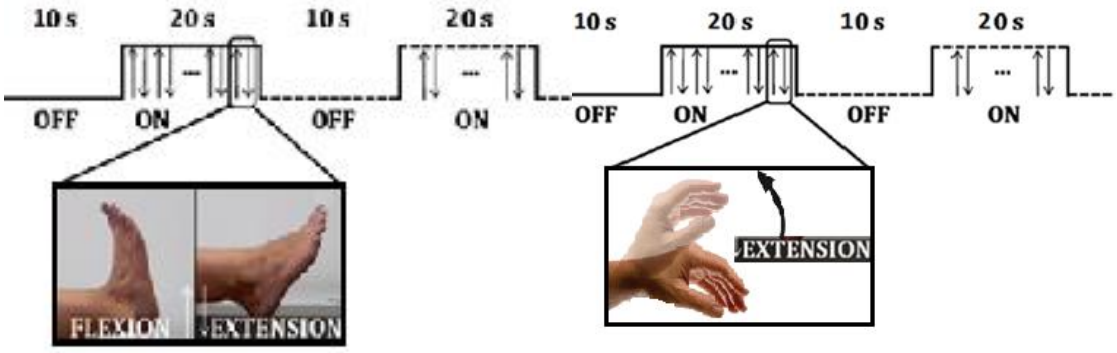

Figure 2.3. Experimental protocol: 30 seconds block design. Each task acquisition (firstly ADF and secondly WE) is composed of by 10 alternate ON/OFF blocks (5 minutes). A total acquisition lasts 10 minutes (20 blocks).

Kinematic measurements

Four passive markers for movement tracking were placed on the right leg of the subjects, two on the tibia axis, one in correspondence of the median malleoulus and the last one on the little finger of the toe (fig. 2.1) and other three markers were placed on the MR-bed and one on the middle finger (fig. 2.4).

Specific markers placement depends on the goal of the study but does not affect the present evaluation [6].

Outside the scanner room, electrogoniometers applied to the right ankle and to the right wrist are used to track the effective movements of the subject limbs during the motor tasks performance. The transfer function between the amplitude of the recorded angle (input) and the voltage measured (output) is linear.

Figure 2.4. Marker placed on the middle finger of the subject.

Experimental conditions

Different experimental conditions has been foreseen in order to test possible images degradation (both for MRI and fMRI sequences) and possible EMG signal degradation. (K = Kinematics)

1) MRI-EMG compatibility test: evaluation of the signal to noise ratio on T1-weighted images with the introduction of the EMG recording device. They are subject-independent acquisitions. In detail:

1.1) 1 phantom acquisition without EMG instrumentation inside the MRI room: reference condition for MRI images (MRI+K);

1.2) 1 phantom acquisition with EMG instrumentation inside the MRI room (MRI+K+EMG).

2) fMRI-EMG compatibility test: evaluation of the signal to noise ratio on T2*-weighted functional images. They are subject-dependent acquisitions. In detail:

2.1) 1 MRI subject acquisition (anatomical images) without EMG instrumentation: reference condition to normalize functional images of the subject;

2.2) 1 fMRI signal acquisition (5 minutes for ADF and 5 minutes for WE) of the subject who performs the motor protocol inside the MR room without the EMG instrumentation: reference condition for fMRI images (fMRI+K);

2.3) 1 fMRI images acquisition (5 minutes for ADF and 5 minutes for WE) of the subject who performs the motor protocol inside the MR room with the EMG instrumentation (fMRI+K+EMG).

3) EMG-fMRI compatibility test: evaluation of the degradation of the EMG characteristics. They are subject-dependent acquisitions. In detail:

3.1) 1 EMG signal acquisition (5 minutes for ADF and 5 minutes for WE) of the subject who performs the motor protocol outside the MR room: reference condition for the EMG signal (EMG-Out);

3.2) 1 EMG signal acquisition (5 minutes for ADF and 5 minutes for WE) of the subject who performs the motor protocol inside the MR room with the fMRI sequence off, i.e. only B_0 is on (B0+K+EMG);

3.3) 1 EMG signal acquisition (5 minutes for ADF and 5 minutes for WE) of the subject who performs the motor protocol inside the MR room with the fMRI sequence on (fMRI+K+EMG).

2.4 Imaging data acquisition parameters

The anatomical data of the phantom and of the subjects are acquired with a standard sequence of 3D gradient echo in T1-weighted images: echo time (TE) = 4.28 ms; repetition time (TR) = 10.58 ms; flip angle =12°; matrix 512×512; field of view (FOV) = 26 cm; voxel size = 1×1×1 mm^3.

Functional images are acquired with sequence of gradient EPI T2*-weighted: TE = 50 ms; TR = 3 s; flip angle = 90°; matrix 128×128; FOV = 24 cm; voxel size = 1.8×1.8×4 mm^3.

An fMRI acquisition sequence lasts 10 minutes (as the protocol duration) and then collects 200 volumes of the entire brain (total duration/TR = 600s/3s = 200) with 36 slices for each volume.

2.5 Data processing

Kinematic data

The 3D kinematic data acquired for each marker in the scanner room are obtained by ElsTracker software and processed using Matlab: they are interpolated to obviate the time periods during which some markers may not be seen by one of the cameras.
The kinematic data, once combined the 3D coordinates in the movement trajectories (ADF and WE), are used to window the EMG signal, i.e. to distinguish the EMG activity which produce an actual limbs movement.

Imaging data

Processing

Functional images are converted from DICOM to Analyze format with the MRIcro software [42].
fMRI images undergo a standard pre-processing analysis carried out with SPM8® (Wellcome Trust Centre for Neuroimaging, London UK) running on Matlab 8.4. Images are unwarped and realigned to first scan of each volume and realignment parameters are assessed for excessive motion.
Then, an average realigned fMRI image is co-registrated with the subject-specific anatomical image using an optimization algorithm which maximize the mutual information between fMRI and MRI. At this point a segmentation of the anatomical image is performed: SPM8 creates cerebrospinal fluid, gray and white matter images.
Imaging data (both fMRI and MRI) are then normalized to standard Montreal Neurological Institute (MNI) space. In neuro-imaging the spatial normalization is a common processing step consisting in a registration between the actual recorded images and a reference template. In fact, human brains differ in size and shape and, thus, the aim of spatial normalization is to deform human brain scans to bring them to a common space in which different brains can be compared. Fig. 2.5 shows the normalization of a functional images.

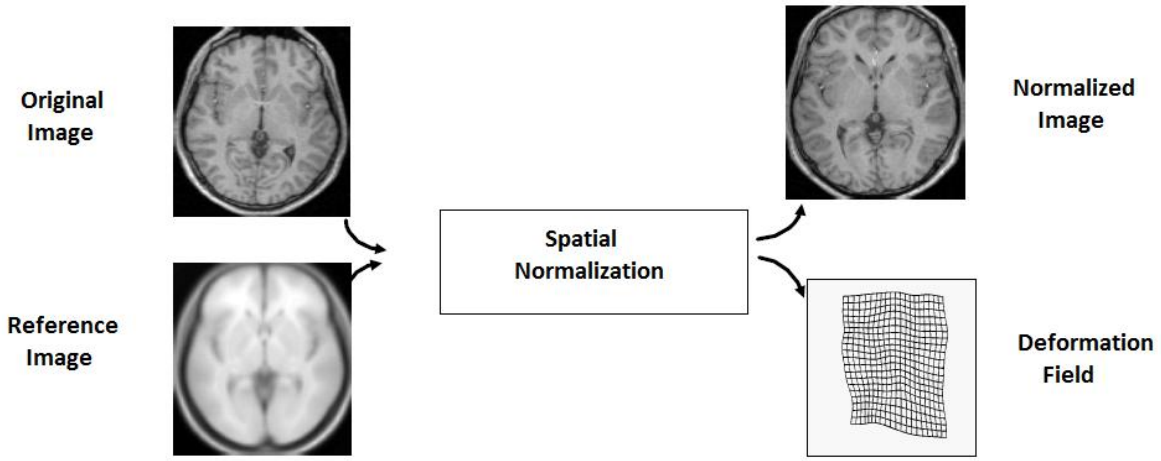

Figure 2.5. fMRI spatial normalization.

Next a spatial smoothing is performed using a Full-Width Half-Maximum (FWHM) Gaussian filter of 8 mm. The purpose of spatial smoothing is to cope with functional anatomical variability that is not compensated by spatial normalization and to improve the signal to noise ratio. Spatial smoothing means that data points are averaged with their neighbors. This has the effect of a low pass filter meaning that high frequencies of the signal are removed from the data while enhancing low frequencies: the result is that sharp "edges" of the images are blurred. The standard procedure of spatial smoothing is employed by convolving the fMRI signal with a Gaussian function of a specific width (FWHM). This so called Gaussian kernel is a kernel with the shape of a normal distribution curve [6].

Statistical parametric maps

Once the scans pre-processing is done, a statistical analysis is carried out in order to obtain a map of activated areas during the execution of the experimental tasks. Every voxel of the fMR images is considered independently from each other in its time evolution and a general linear model (GLM) is applied (fig.2.6). This model can be seen as an extension of multiple regression: multiple regression characterises the relationship between several independent variables, called regressors, X_1, X_2, X_3 etc, and a single dependent variable, Y, which represents the acquired data (eq. 2.1).

$$Y = \beta_1 X_1 + \beta_2 X_2 + \ldots\ldots + \beta_L X_L + \varepsilon \qquad \text{(eq. 2.1)}$$

The X variables are combined linearly and each has its own regression coefficient β (weight) which reflects the independent contribution of each regressor, X, to the value of the dependent variable, Y. The regression consists in estimating the regressors weights (β_L) in order to minimize the error ε.

In this contest, multiple regression only looks at one Y variable while GLM allows to analyse several Y variables in a linear combination (time series in voxel).

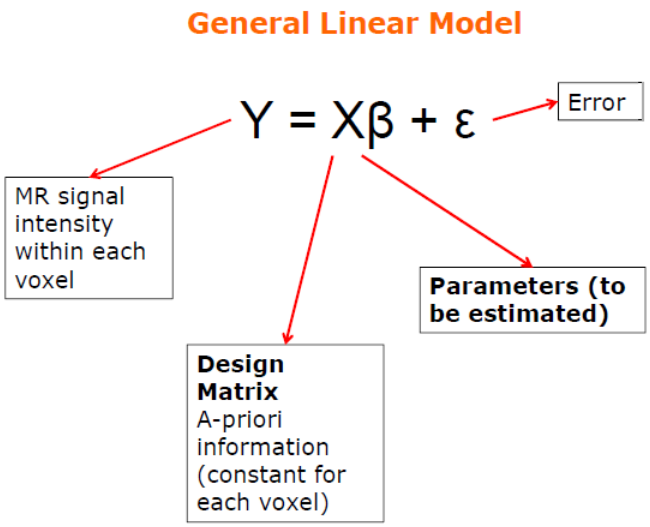

Figure 2.6. Application of General Linear Model to fMRI data [21].

The design matrix specifies the statistical model consisting of the regressors which have to explain the output data Y. This matrix is, thus, the fundamental tool to formulate hypotheses about expected changes of the fMRI signal. Using the General Linear Model (GLM), the statistical model specified in a design matrix is compared with the measured time course at each voxel of the fMR images.

In the practice, if the hemodynamic response function (HRF, fig. 1.10) is convolved with an external stimulus decided by the experimental protocol, it is possible to obtain a reconstruction of the actual BOLD signal [43].

In the present work, for all subjects the design matrix is built convolving the canonical HRF with an event-design gotten from kinematics data onsets. So the design matrix is obtained with two regressors: kinematics-derived onsets during ADF and kinematics-derived onsets during WE.

These onsets are used during the EMG processing to window the recorded signals and to detect the muscle activations (EMG signals) which correspond to the actual movement execution.

The created linear model created (β values) undergoes a statistical analysis through a t-test (H0 = no significant effect of test condition within each voxel). If the p-value obtained for the voxel under analysis is lower than 0.05, the voxel is highlighted as activated. The intensity of the activation map in each voxel is proportional to the statistical significance (false colour coding).

EMG data

fMRI artefacts removing algorithm

For the experimental condition fMRI+K+EMG an algorithm for the removal of the fMRI-induced artefacts from the EMG signal is required. In particular, the artifact reduction algorithm for motion (FARM), developed by van der Meer [38] is applied. FARM is an extension of the AAS algorithm proposed by Allen [29].

Processing of the EMG dataset is performed using a toolbox running on Matlab: EEGLAB [44]. The FARM algorithm consists of the following step:

- ✓ to remove artefacts due to interaction between motion and the main field B_0 (whose frequency has been seen to reach the 30 Hz if the limb movements is fast enough) and to cut-off the zero-frequency of the EMG signal, the data are digitally high-pass filtered at 30 Hz using a least-square FIR (finite impulse response) filter with a 24 dB/Oct (~80dB/dec) slope. Moreover, high-passed EMG data are up-sampled of a 10 factor;
- ✓ EMG data are divided into volume-segments using volume-onset markers: the algorithm functions on each volume-segment individually. In this work, the volume-onsets are 200 (100 for each trial).

  The algorithm separates volume-segments of data into as many slice-segments as the number of slices in an acquired imaging volume. For the current work, the slice number is 36. The slice separation is performed in such a way that slice-segments contain only a single slice-artefact The volume-artefact of the first EPI-volume scan is omitted. Slice-segments have an equally duration of sdurV (slice-duration for volume-segment V).

The basic idea of the FARM artefact correction is to remove all components in the signal that could impair the slice-templates. In addition to the high-pass filter in the pre-processing phase, the algorithm contains two main elements to make it more robust against sudden slice-artefact shape-changes. Firstly, slice-markers are calculated mathematically with optimized values for sdur and this value is used to improve the slice-alignment. Secondly, and mainly important, in the slice-artefact correction, instead of using every slice in a relatively small sliding window, FARM uses a larger sliding window and selects only those slice-artefacts that have the highest correlation. From a sliding window consisting of 50 slice-segments, 12 slice-artefacts with the highest correlation with the slice-artefact to be corrected are selected to create the artefact template to be subtracted from the EMG data [29]. Consequently, the template for any slice-artefact need not be composed of neighbouring slice-artefacts but can also contain slice-artefacts not directly connected in time.

If the shape of the artefact would suddenly change due to motion, then this sub-selection ensures that "motion-impaired" slice artefacts are not used in the slice-template construction because of its low correlation with the currently corrected slice-artefact. It can occur that a slice artefact has a shape that does not resemble any other slice-artefact in the window of 50. In this case, since there are still 12 slice-artefacts picked for the template, the slice-artefact itself will not be corrected optimally. However, because of the selection process, this slice-artefact is also not be able to distort the templates for any other slice-artefacts [38];

- ✓ data processed by FARM are then down-sampled of a 10 factor and digitally low-pass filtered at 250 Hz with a 12 dB/Oct (~40 dB/dec);
- ✓ a principal components analysis (PCA) is applied as last algorithm step. It is implemented as outlined in Niazy [45], to remove residual high frequency artifact residuals in the corrected EMG signal. FARM limits the number principal components (PC's).

Processing

The fMRI-artefact-cleaned EMG data (fMRI+K+EMG) obtained from the FARM are processed as the EMG data acquired in the other two experimental conditions, i.e. EMG-Out and B0+K+EMG.

But, before that, the experimental conditions EMG-Out and B0+K+EMG undergo an additional processing step:

- ✓ application of a band-pass filter (30-250 Hz). This band-pass filtering keeps the most interesting frequency band of the EMG signal, reduces the large motion-artefact noise due to the not-active-shielded cables (which may reach the 25-30 Hz if leads movements are fast enough) and, for the experimental condition B0+K+EMG, removes potential fMRI artefacts due to interaction between cables motion and the main static field B_0. The applied filters are digital IIR (infinite impulse response) filters and have both a Butterworth design: the high-pass filter is a fourth order one (80dB/dec of the slope) and the low-pass filter is a second order one (40dB/dec of the slope). As already specified, to compare EMG data in the three experimental conditions, the band-pass filter design is the same of that used in the FARM algorithm.

Then, all datasets recorded in the three experimental conditions, undergo on common processing steps:

- ✓ rectification of the band-passed EMG to increase the power of the signal [46];
- ✓ application of a low-pass filter (IIR, fifth order Butterworth, f_c = 5 Hz) to obtain the signal envelope;
- ✓ normalization of the signal amplitude into the range 0-1 with reference to the recorded maximum amplitude peak within the each single acquisition [47];
- ✓ windowing of the signal (i.e. detection of every actual muscle activations) based on kinematic onset;
- ✓ time normalization (100 samples every muscular activation, i.e. subsampling at about 50 Hz sampling rate necessary to conduct a meaningful comparison among data population of different numerosity);
- ✓ EMG features extraction.

2.6 Outcome measures

MRI-EMG compatibility test

In order to evaluate the interference between the two systems, MRI scanner and EMG instrumentation, MR images of a phantom are acquired with (MRI+K+EMG) and without (MRI+K) the EMG recording system inside the scanner room. A standard phantom with one-compartment of aqueous paramagnetic solutions is used. During the imaging acquisition session T1-weighted images are obtained for each phantom condition.

Signal-to-Noise Ratio (SNR) is calculated over the 233 slices where the phantom has uniform size, using the standard index for image quality [48], namely the ratio between the mean amplitude of the signal on a homogeneous area and the standard deviation of the background signal amplitude.

Therefore, the ratio between the mean value of a small ROI placed in the most homogeneous of the phantom (around the barycentre) with high signal intensity and the mean of standard deviations for four regions of interest (ROIs) placed outside the object in the image background is computed.

In order to determine the change of the SNR in the images only given by the presence or the absence of the EMG instrumentation, the acquisition parameters of imaging sequence which may change the SNR are kept constant: field of view, slice thickness, volume of voxels, number of acquisitions and number of scans.

The loss of SNR percentage of each slice is computed as following:

$$\Delta\mathrm{SNR} = \frac{\mathrm{SNR_{ref}} - \mathrm{SNR_{test}}}{\mathrm{SNR_{ref}}} * 100; \qquad \text{(eq.2.2)}$$

where SNR_{ref}corresponds to the reference condition (MRI+K) and SNR_{test} corresponds to the integrated set-up condition (MRI+K+EMG).

Finally, the ΔSNR obtained are mediated in order to obtain a single value, able to give information about the MRI-EMG compatibility.

fMRI-EMG compatibility test

To evaluate fMRI-EMG compatibility, SNR of the fMRIs is computed compared between reference (fMRI+K) and test (fMRI+K+EMG) condition in four cortical regions of interest (ROIs) consistently activated during motor tasks executions [49,50], i.e. primary motor cortex (M1), premotor and supplementary motor cortex (PM/SMA), primary somatosensory cortex (S1) and second somatosensory area (SII). The regions are identified in the standardized MNI brain through Brodmann areas, namely M1 corresponds to Brodmann area 4 (b4), PM/SMA to b6, S1 to b2 and b3, and SII to b5 and b7 (fig. 2.7 shows these areas on the anatomical image of one of the analyzed subject, i.e. subject 1).

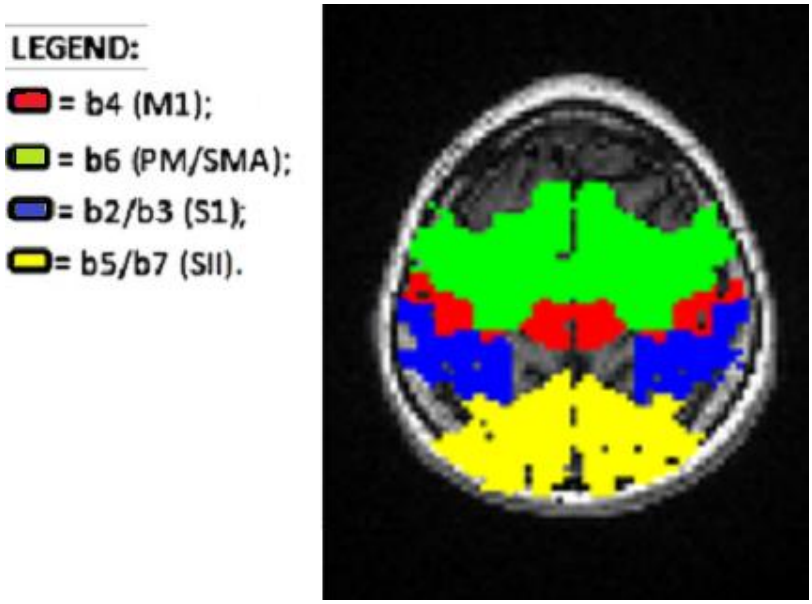

Figure 2.7. ROIs consistently activated in motor tasks execution: b4 = Brodmann area 4; M1 = primary motor cortex; b6 = Brodmann area 6; PM/SMA = premotor and supplementary motor cortex; b2/b3 = Brodmann area 2 + Brodmann area 3; S1 = primary somatosensory cortex; b5/b7 = Brodmann area 5 + Brodmann area 7; SII = second somatosensory area. The represented slice is the number 55 over the 68 of one acquired, normalized.

The ROIs presented in fig. 2.7 and used in the images SNR analysis are standard ones and then suitable to each subject brain only after a normalization to the common standard space. But, because the image normalization is an iterative process, it stops when some optimization conditions are satisfied and not when it reaches the "perfect" normalization.

A check on the normalization of the functional images is made considering for the SNR computation only those ROIs voxels actually comprised in the brain edges of each subject. So, the number of voxels considered is both subject- and condition- (fMRI+K and fMRI+K+EMG) dependent.

At this point, a previous analysis of each ROI homogeneity is made to assess if areas functionally homogeneous are also homogeneous in terms of SNR.

The coefficient of variation (CV, eq. 2.3) for a given experimental condition (fMRI+EMG+K and fMRI+K) is calculated as defined in literature [51]: standard deviation of the SNR across sessions divided by the mean of the SNR across sessions in terms of a percentage where a low value is indicative of good SNR homogeneity for a considered ROI.

$$\mathrm{CV} = \frac{\mathrm{std(SNR)}}{\mathrm{mean(SNR)}} * 100 \qquad \text{(eq. 2.3)}$$

The CV standard deviation is computed for every ROI to compare the CVs obtained for the three subjects in the same experimental condition, i.e. to assess the inter-subject CV reproducibility.

A Mann-Whitney test is applied to compare, for each ROI, the CVs of all the subjects between the two experimental condition, i.e. inter-conditions reproducibility assessment. Separately for each subject and each experimental condition (fMRI+K and fMRI+K+EMG), the SNR of the fMRI images is determined independently for each voxel of each volume on fMRI processed images as the mean signal of the entire time series divided by its standard deviation [6]. A temporal SNR volume results for each acquired session.

The SNR percentage loss between reference and test condition is calculated on the basis of the mean values of SNR for a given ROI.

Then, given that for an MR scanner of 1.5T, the detectable BOLD signal changes are around 1-2%, SNR maps are created for the fMRIs in the two experimental conditions. imposing five SNR thresholds for the detection of as many BOLD signal changes (0.25%, 0.50%, 0.75%, 1%, 2%), where the minimum SNR values are obtained from literature [52] and defined, in eq. 2.4, as follows:

$$SNR = \frac{2*t}{\Delta S*\sqrt{N}} \qquad \text{(eq. 2.4)}$$

In eq. 2.4, t is the t-value for a given α (type I error) and β (type II error), ΔS is the BOLD signal change to be detected and N the number of scanning acquired volumes.

The minimum SNR varies with an inverse linear relationship to the expected BOLD signal change when all other parameters are held constant, as predicted by the eq.3.3.

Below the minimum SNR level, it is not possible to achieve the confidence level for detecting activation for the given imaging parameters. Therefore the computed SNR values can be compared with the proposed minimum threshold and it can be stated that, if the voxel SNR value is over a given threshold, then a corresponding ΔS percentage signal change can be detected in that voxel.

The table 2.1 gathers the minimum temporal SNR required to detect the five sensitivity levels of the BOLD signal change defined above, given that the number of collected volumes is 100 (5 minutes for each motor task so half of the total volumes number acquired during an fMRI sequence of 10 minutes). In fact, we consider that each of the three subjects performs two trials during a whole fMRI sequence for a total of 6 trials for each acquisition modalities (fMRI+K and fMRI+K+EMG).

Table 2.1. Minimum SNR values required to detect associated BOLD signal change. Minimum SNR are calculated with fixed parameters: number of volumes (N) = 100, α = 0.05 (probability to incorrectly reject the null hypothesis when it is in fact true i.e. type I error) and β = 0.95 (probability to not reject the null hypothesis despite being false i.e. type II error).

Change in BOLD signal (Δ S) (%)	**Minimum SNR**
2	36
1	79
0.75	97
0.50	146
0.25	293

The percentages of total ROI voxels where 1% and then 2% of BOLD signal change can be detected are determined and an average of these percentages between ADF and WE period for the same subject is made for both experimental conditions (fMRI+K and fMR+K+EMG). Lastly a comparison between reference and the test condition is conducted on the basis of these ROI's voxels percentage.

EMG-fMRI compatibility

The literature offers many indices, both in time and in frequency, to evaluate the EMG measurement quality and reproducibility. In the present work three time features of the EMG signal are chosen and obtained from the processed signal to compare the reference condition (EMG-Out) with the two experimental test conditions (B0+K+EMG and fMRI+K+EMG).

The first index analyzed is the correlation coefficient among the average EMG waveforms obtained in the three experimental conditions and it gives us an indication on the maintenance of the EMG characteristic form without distortions induced by the MR-environment.

Then other two indices which may characterize the actual EMG measurement are calculated. In detail, for each windowed EMG signal: the peak amplitude and the integrated area under the signal [11].

According to the protocol, 100 EMG activations are obtained for each motor task (ADF and WE) and then as many area and peak amplitude values.

A statistical two-ways ANOVA test is applied on these last two indices for each motor task separately (ADF and WE) to evaluate whether there is a significant inter-condition (EMG-Out, B0+K+EMG, fMRI+K+EMG) and inter-subject means difference. Then, for the same two indices and separately for each subject, an analysis on the EMG variability among experimental conditions is made calculating the coefficient of variation (CV), suitable for EMG intra-subject comparisons on the same muscle [53]. In particular, in the current discussion, CV is computed, for each of the two indices (area and peak amplitude), considering the index average value obtained in every experimental condition as the EMG feature on which to calculate the intra-subject variability. Then, considering, for example, the area index, the CV is defined as follows (eq. 2.5):

$$\mathrm{CV}_{\mathrm{area}} = \frac{\mathrm{std}(\mathrm{area})}{\mathrm{mean}(\mathrm{area})} \qquad \text{(eq. 2.5)}$$

where the mean and the standard deviation are defined with respect to the three experimental conditions which each subject undergoes.

Chapter 3. Results

3.1 MRI-EMG compatibility test

Fig. 3.1 shows the phantom areas used to compute the values of magnetic resonance image SNR and they are the same in reference (MRI+K) and test (MRI+K+EMG) condition.

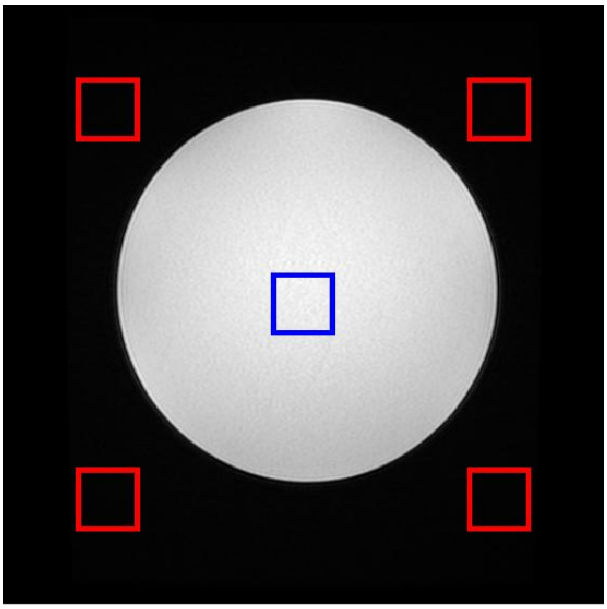

Figure 3.1. Phantom areas used to compute SNR for both reference condition (MRI+K) and test condition (MRI+K+EMG equipment present in the scanner room).

In detail, the fig. 3.2 and 3.3 show respectively the resultant mean amplitude of the signal on the central selected area and the resultant mean standard deviation amplitude of the background signal (the noise) for every slice in the two experimental condition (MRI+K and MRI+K+EMG).

The obtained SNR percentage loss between reference (MRI+K) and test (MRI+K+EMG) condition is (mean ± std): 5.71 ± 3.4 %. In fig. 3.4 are represented the SNR loss for each MRI slice acquired and its average value with the literature reference value coloured in red. As shown, the mean of the SNR loss is below the literature value considered acceptable taking into consideration the MRI data quality.

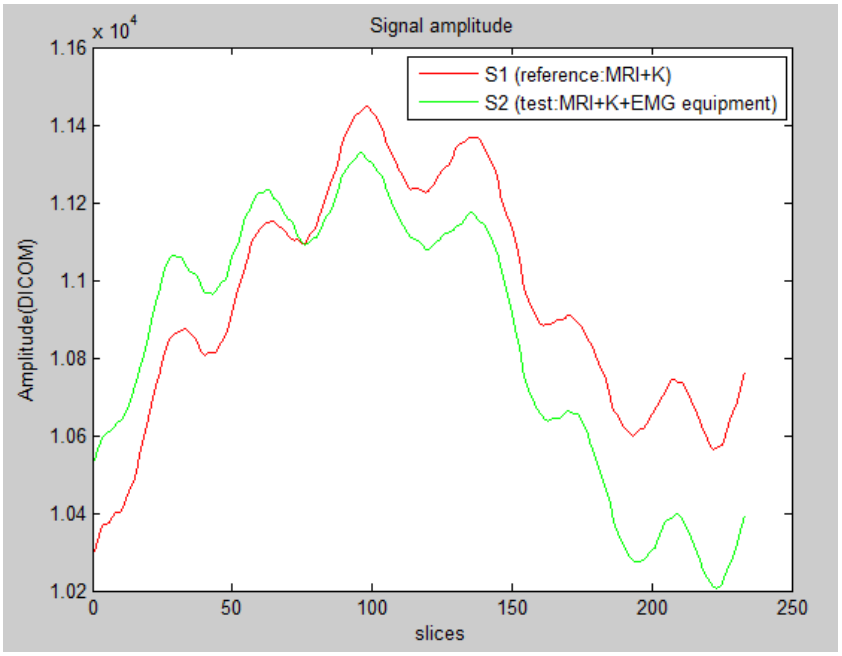

Figure 3.2. Phantom signal trend in reference and test condition.

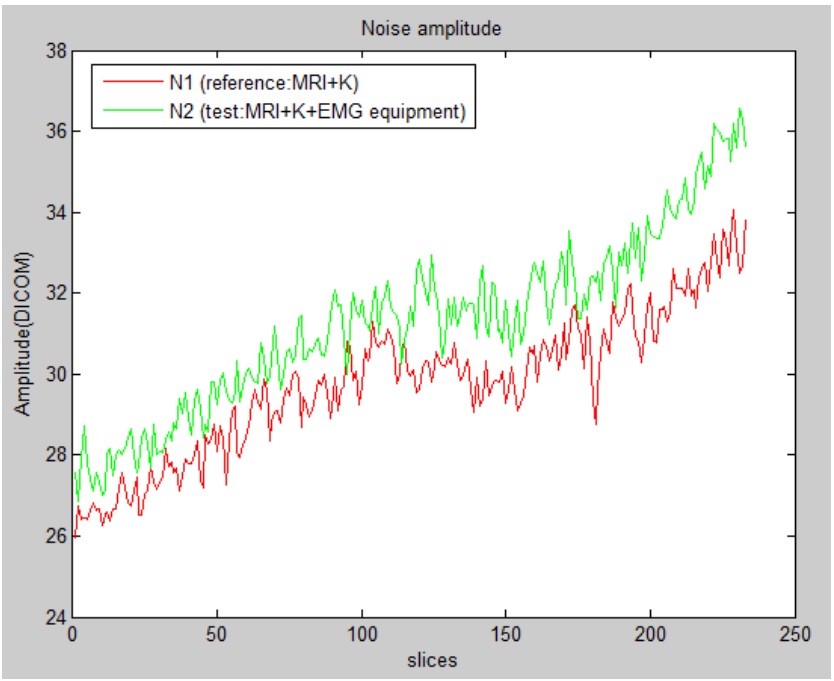

Figure 3.3. Phantom noise trend in reference and test condition.

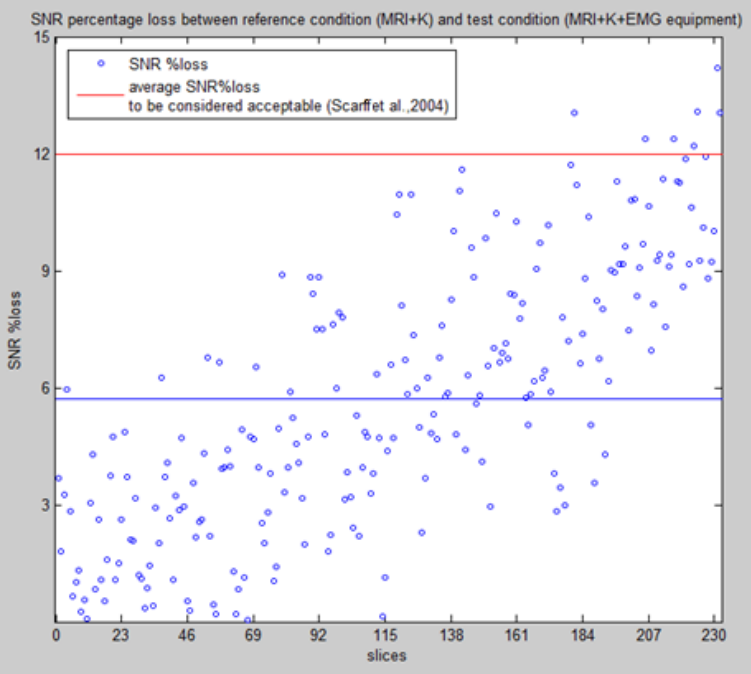

Figure 3.4. Phantom SNR percentage loss between the reference and the test conditions.
The blue line represents the average SNR % loss while the red line is the literature acceptable value.

3.2 fMRI-EMG compatibility test

Definition of Regions of Interest (ROIs)

The percentage of voxels for each ROI, compared to the absolute ROI number, is presented for the reference condition (fMRI+K) and for the test condition (fMRI+K+EMG) in table 3.1. The percentage of voxels excluded for each ROI is, on average, less than 2%.

Table 3.1. Percentage of considered voxels for each ROI for each subject and the average.

NUMBER OF VOXELS		**Subject 1**		**Subject 2**		**Subject 3**		**Average**	
		fMRI+K	**fMRI + K + EMG**	**fMRI+K**	**fMRI + K + EMG**	**fMRI+K**	**fMRI + K + EMG**	**fMRI+K**	**fMRI + K + EMG**
M1 (b4)	3662	99.18 %	98.45 %	99.9 %	99.9 %	97.11%	97.89%	98.73%	98.75%
PM/ SMA (b6)	11641	98.30 %	97.79 %	99.1 %	99.0 %	98.60%	99.08%	98.70%	98.62%
S1 (b2-b3)	4824	99.90 %	99.73 %	100 %	100 %	97.82%	98.33%	99.24%	99.35%
SII (b5-b7)	7847	97.52 %	95.79 %	92.34 %	91.73 %	91.31%	92.89%	93.72%	93.47%

SNR data reproducibility

Table 3.2 reports the CV values (an average between ADF and WE scanning) for every subject and every ROI in the two experimental condition (fMRI+K and fMRI+K+EMG).

Table 3.2. CV average values in the four considered ROIs for the three subjects.

CV(%)	**Subject 1**		**Subject 2**		**Subject 3**	
	fMRI +K	**fMRI + K + EMG**	**fMRI + K**	**fMRI + K + EMG**	**fMRI + K**	**fMRI + K + EMG**
M1(b4)	38%	42%	32%	34%	41%	42%
PM/SMA (b6)	40%	45%	38%	40%	43%	43%
S1 (b2-b3)	30%	38%	28%	29%	36%	39%
SII (b5-b7)	45%	49%	44%	40%	46%	48%

The standard deviation computed for every ROI, to compare the CVs obtained for the three subjects in the same experimental condition is always lower than 5%. The Mann-Whitney test applied to compare the CVs of each subject between the two experimental conditions has always p-value > 0.05 for every ROI. The three subjects and the two experimental conditions have comparable ROIs'homogeneity so an analysis on their average SNR value is significant.The table 3.3 shows an SNR percentage loss between the reference (fMRI+K) and the test (fMRI+K+EMG) condition, computed on the basis of the SNR means in each ROI and assessed by a t-test (p-value < 0.05).

Table 3.3. Functional images SNR percentage loss between the reference and the test condition for the three subjects and an average of this SNR loss.

SNR % LOSS	**Subject 1**	**Subject 2**	**Subject 3**	**Average**
M1 (b4)	16.60%	10.77%	15.43%	14.43% ± 3.08%
PM/SMA (b6)	14.80%	6.18%	10.28%	10.42% ± 4.31%
S1 (b2-b3)	20.03%	15.93%	9.68%	15.21% ± 5.21%
SII (b5-b7) 3	12.13%	21.22%	4.88%	12.74% ± 8.18%

Figure 3.5 presents an exemplifying SNR map, created imposing the five minimum SNR thresholds obtained from literature, in both reference and test condition.

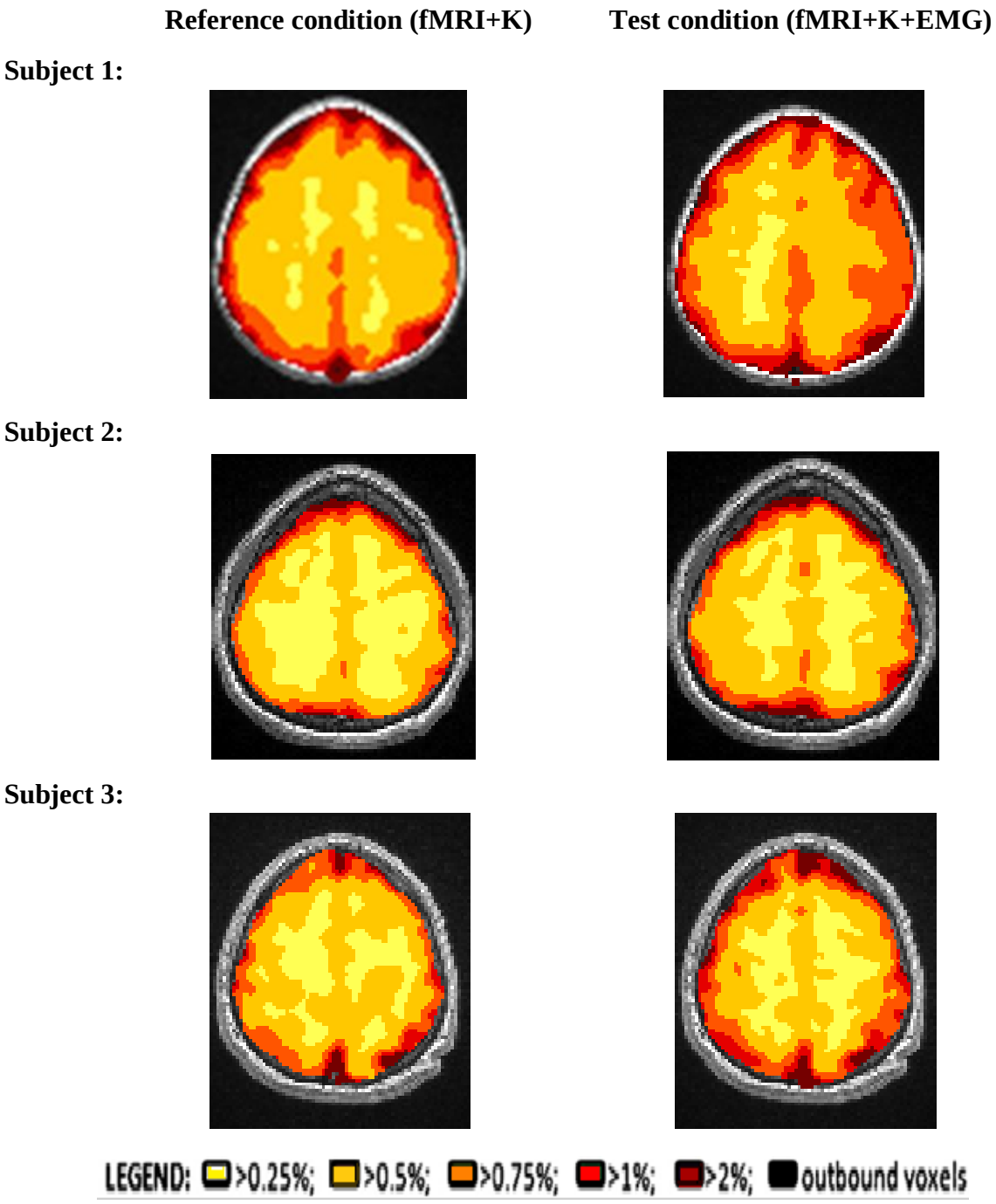

Figure 3.5. SNR map (the slice represented is the number 52 over the 68 of one SNR volume) in reference (fMRI+K) and test (fMRI+K+EMG) condition. The slice elected (52) contains all the four considered ROIs.

Therefore, for the SNR maps shown above, the percentage of voxels for each ROI which have an SNR value high enough to observe a BOLD signal change equal to 1-2% is presented in table 3.4.

Table 3.4. Percentage of each ROI which has an SNR value high enough to allow the detection of a BOLD signal changes of 1% and 2%.

***BOLD* ΔS**		**Subject 1**		**Subject 2**		**Subject 3**		**Average**	
		fMRI+K	**fMRI+K +EMG**	**fMRI+K**	**fMRI+K +EMG**	**fMRI+ K**	**fMRI+K +EMG**	**fMRI+ K**	**fMRI+ K+EM G**
M1 (b4)	1%	92.84 %	88.85 %	99.45 %	97.65 %	93.70 %	95.38 %	95.33%	93.96%
	2%	99.83 %	99. 33%	99.97 %	99. 93%	99.23 %	99.02 %	99.68%	99.43%
PM/SMA (b6)	1%	91.77 %	88.73 %	97.87 %	96.72 %	95.27 %	96.16 %	94.97%	93.87%
	2%	99.97 %	99.86 %	99.99%	99.96 %	99.41 %	99.34 %	99.79%	99.72%
S1 (b2-b3)	1%	98.17 %	94.39 %	99.98 %	99.69 %	96.83 %	96.95 %	98.33%	97.01%
	2%	99.90 %	99.90 %	99.98 %	99.98 %	99.27 %	98.93 %	99.72%	99.60%
SII (b5-b7)	1%	85.33 %	81.05 %	97.25 %	94.67 %	90.20 %	89.24 %	90.93%	88.64%
	2%	99.28 %	98.19 %	99.98 %	99.74 %	98.13 %	97.61 %	99.13%	98.51%

Task-related activation as revealed with the novel experimental set-up

In figure 3.6 are shown the cerebral activation maps of every subject for both motor tasks ADF and WE) obtained considering the functional images acquired in the test condition (fMRI+K+EMG).

Subject 1:

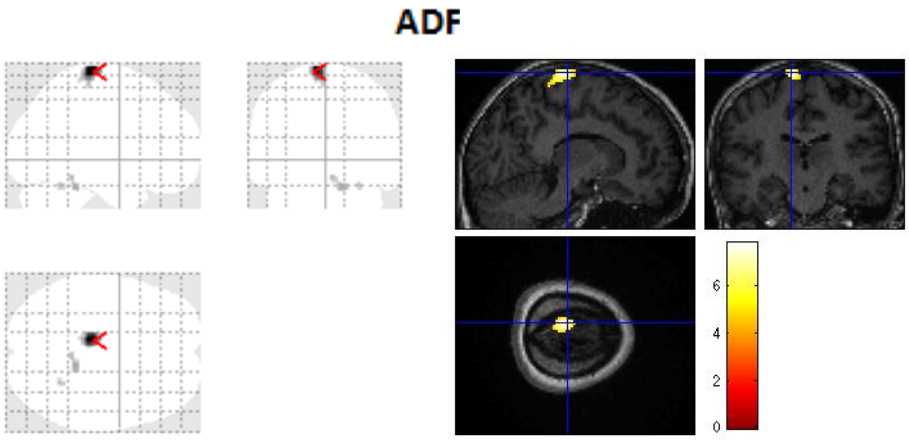

Subject 2:

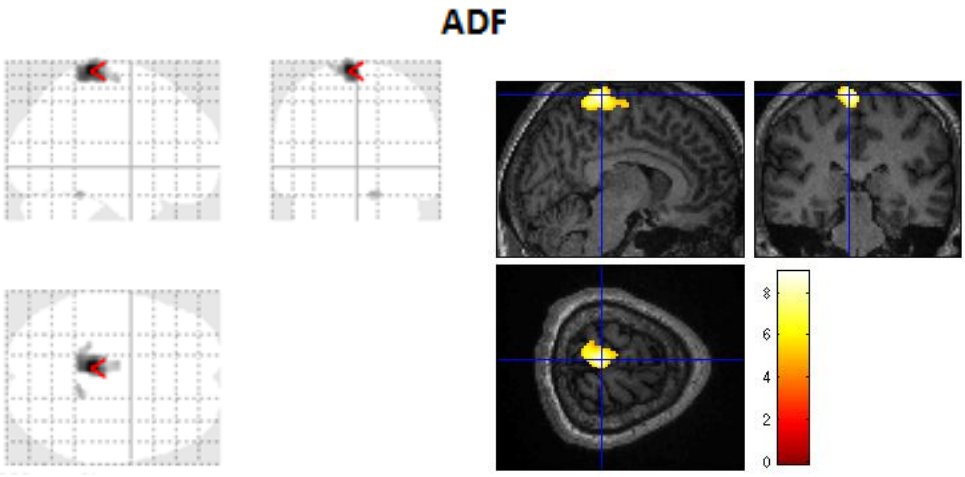

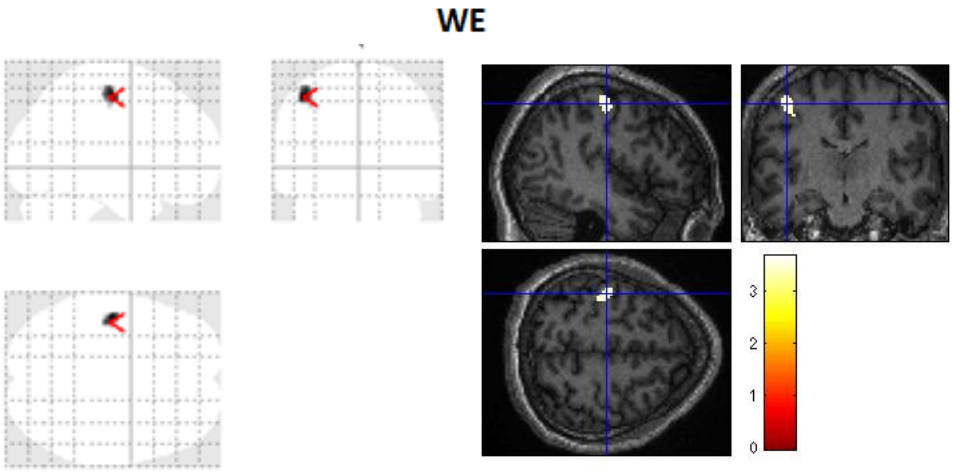

Subject 3:

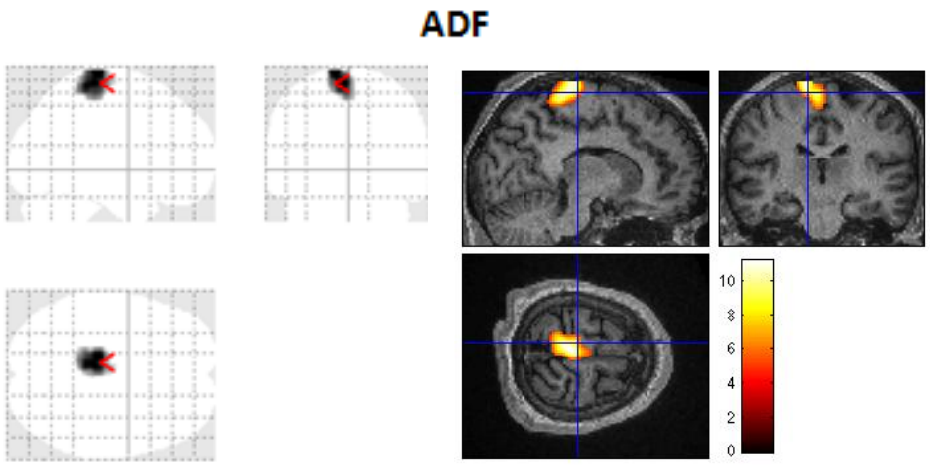

Subject 3: WE

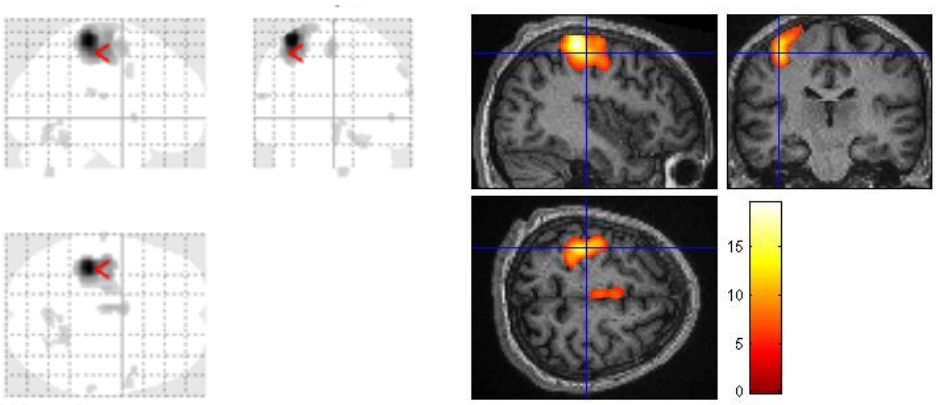

Figure 3.6. Cerebral activation maps obtained during the ADF and WE motor task performance. Event-design matrix with kinematics-derived onsets. The results are FWE corrected (p-value < 0.05) and the cluster number is set at 10.

3.3 EMG-fMRI compatibility test

EMG Processing

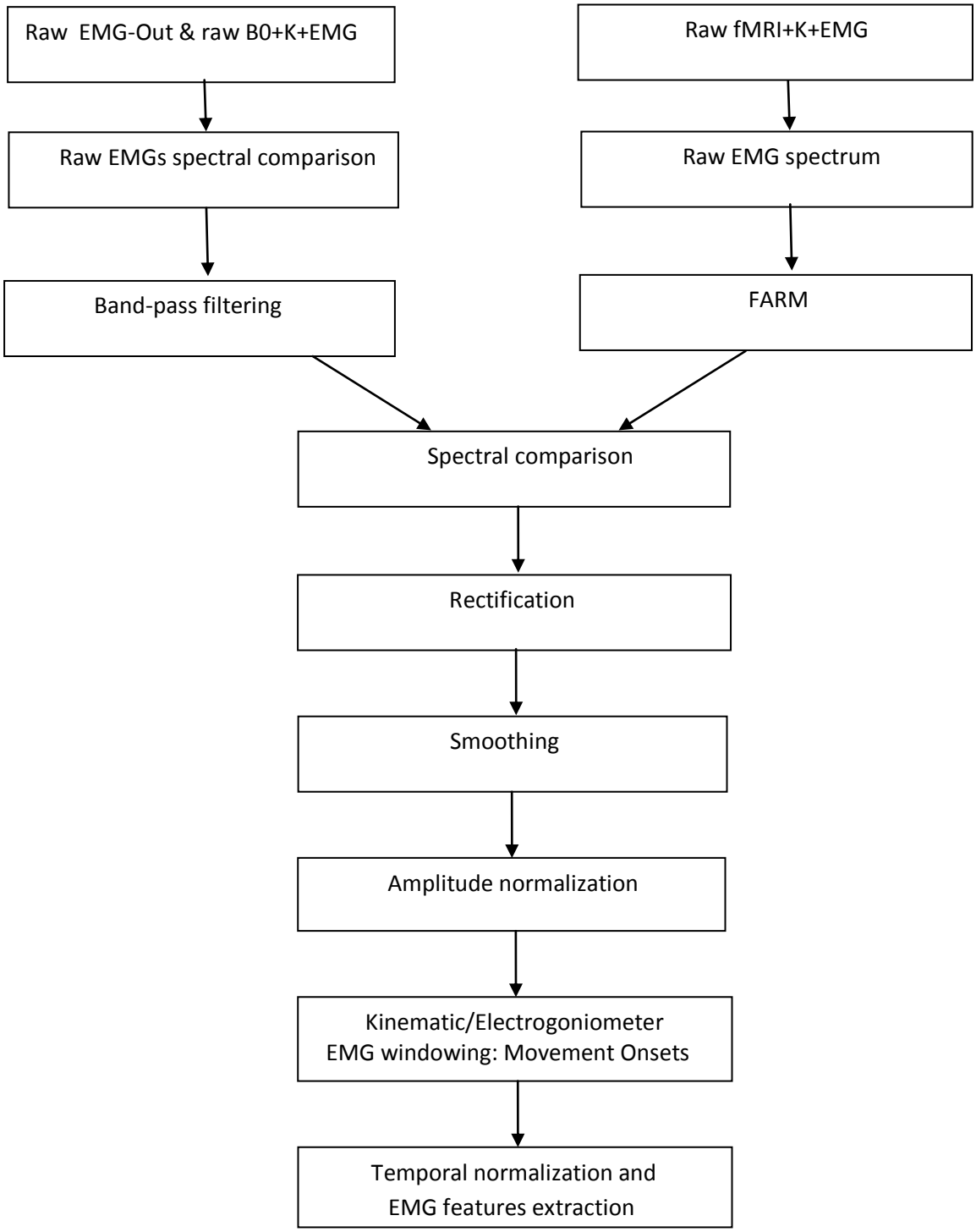

For the principal signal processing steps the EMG data recorded outside the scanner room and those recorded inside the scanner room with the EPI sequence switched on are shown. The data are those of a single subject (subject 3) for a single motor task (ADF).

EMG outside scanner room (EMG-Out):

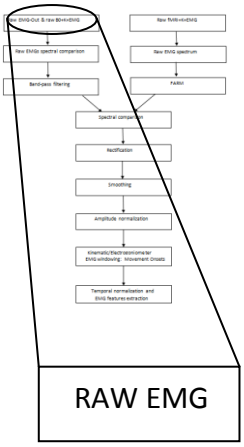

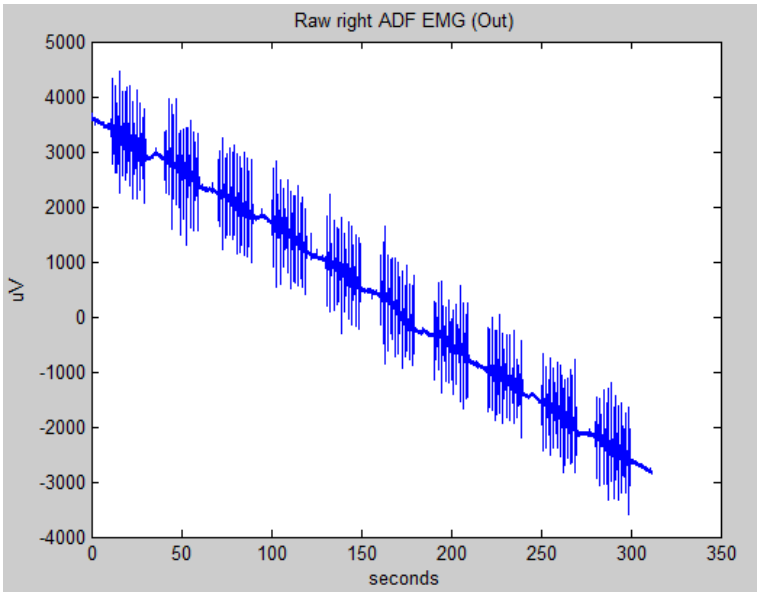

Before filtering the data, the spectrum of condition EMG-Out and that of condition B0+K+EMG are calculated to compare the frequency components. In fact, in literature [38], B0-induced artifacts in EMG signals are documented at frequencies below the 30 Hz.

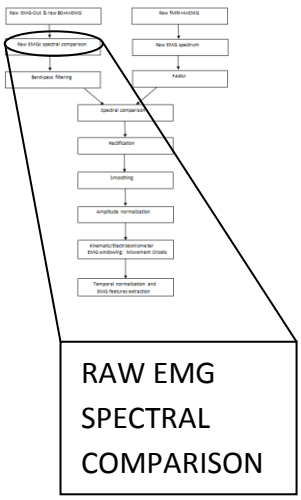

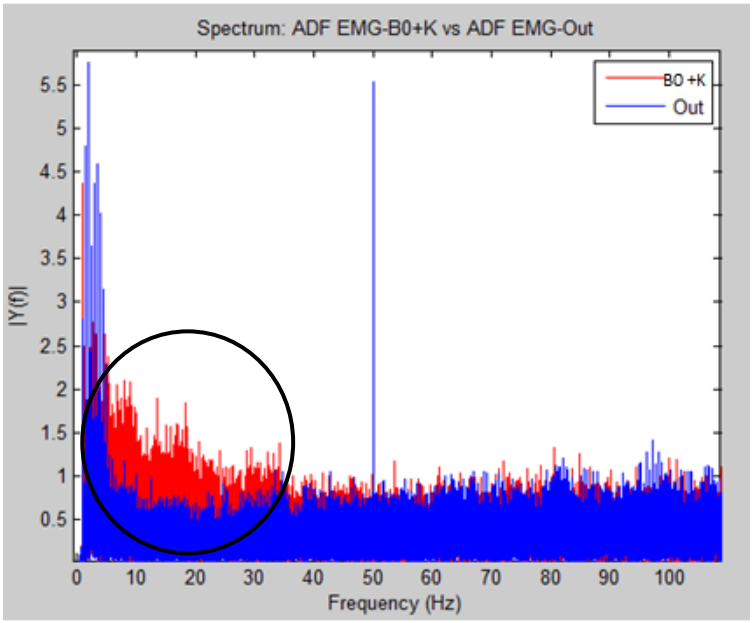

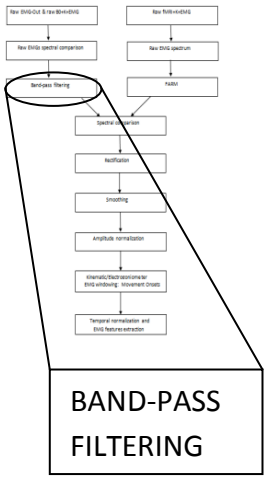

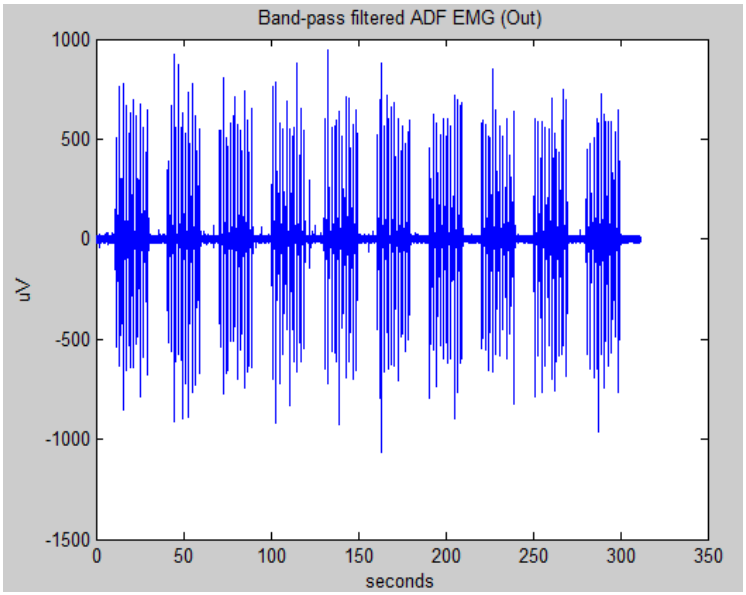

EMG with EPI sequence on (fMRI+K+EMG):

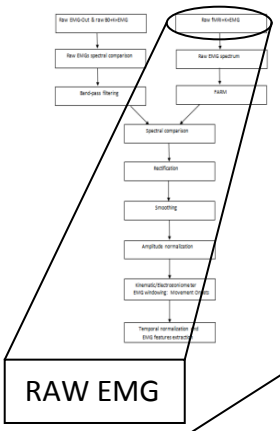

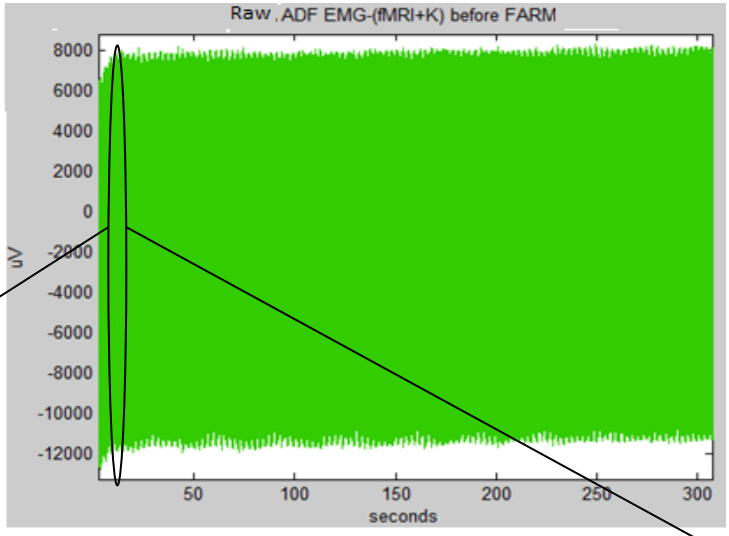

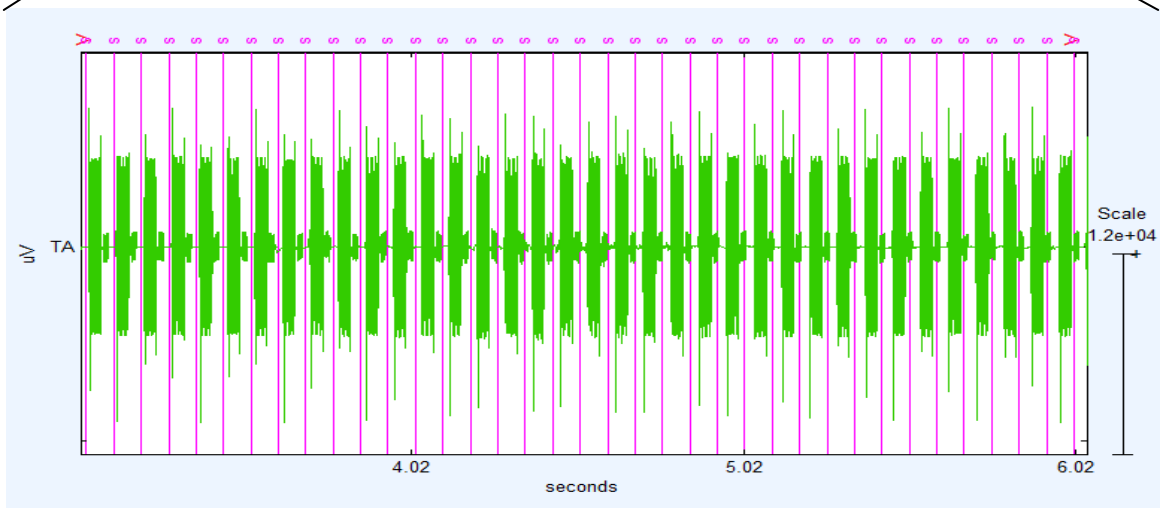

The raw EMG signal in the experimental condition fMRI+K+EMG presents huge artifacts occurring at every acquisition of an fMRI volume slice. The scanning repetition time (TR) is equal to 3 seconds and 36 slices are acquired during this time so a slice is acquired every 0.083 seconds. The spectrum of the raw EMG shows, omitting the direct current, a peak at 12 Hz and a modulation of its harmonics (24 Hz, 36 Hz, etc.). The own spectrum of the EMG signal is hidden by the fMRI artifact components.

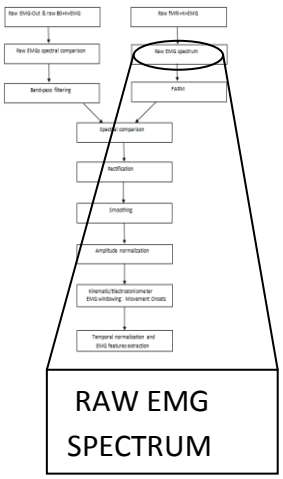

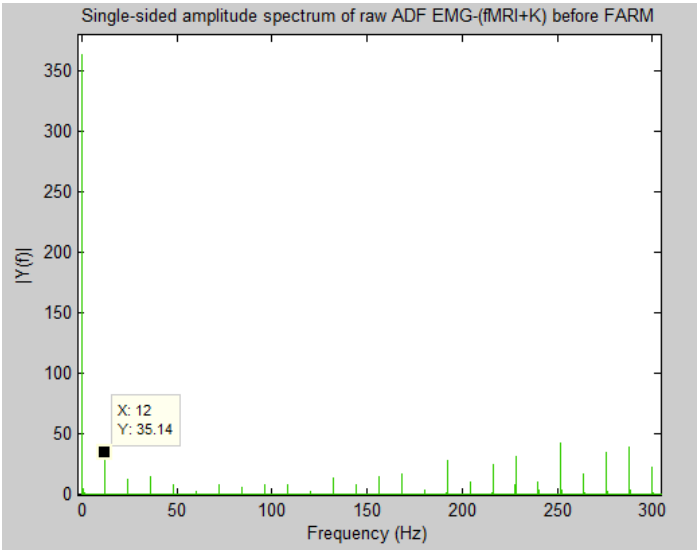

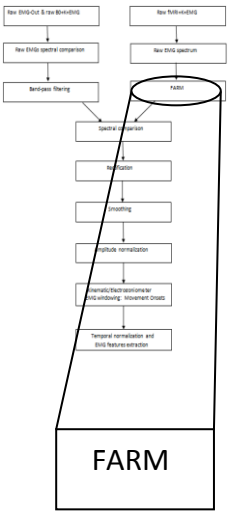

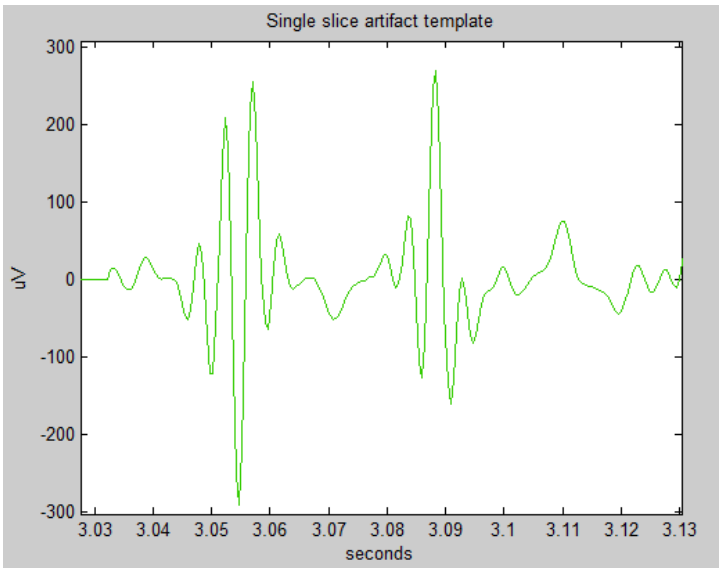

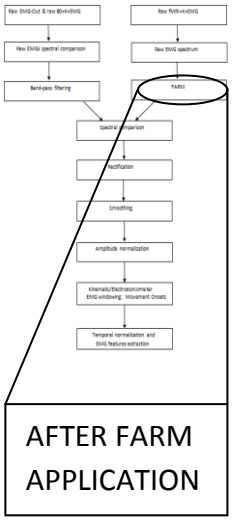

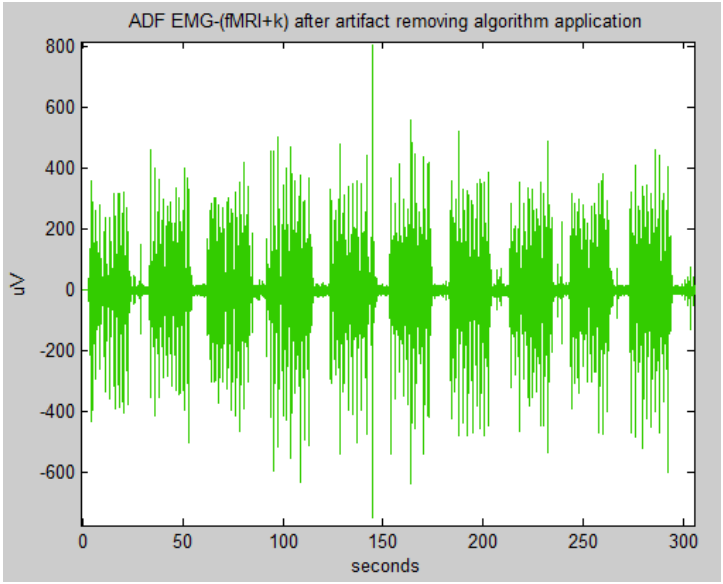

Before effective removal of fMRI slice- and volume-artifacts, the FARM applies an high-pass filtering at 30 Hz to the EMG signal and, after the artifacts subtraction, the EMG is low-pass filtered at 250 Hz.

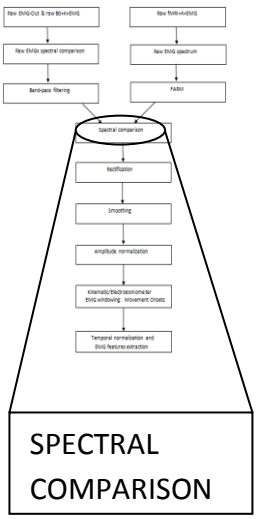

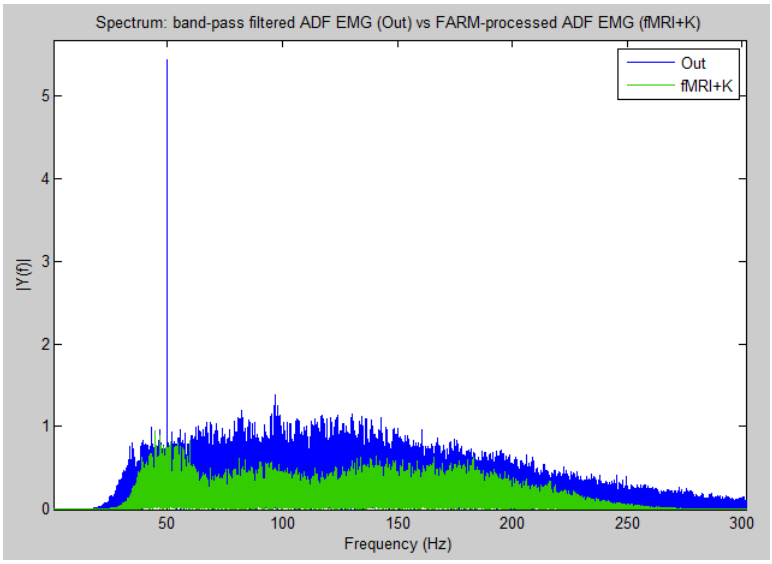

EMG outside scanner room (EMG-Out) and EMG with EPI sequence on (fMRI+K+EMG):

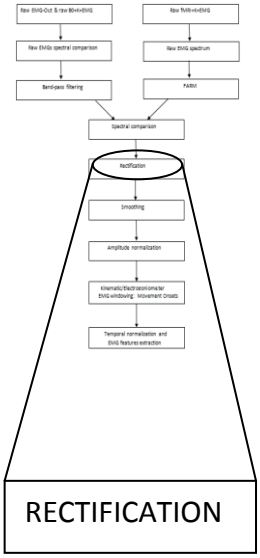

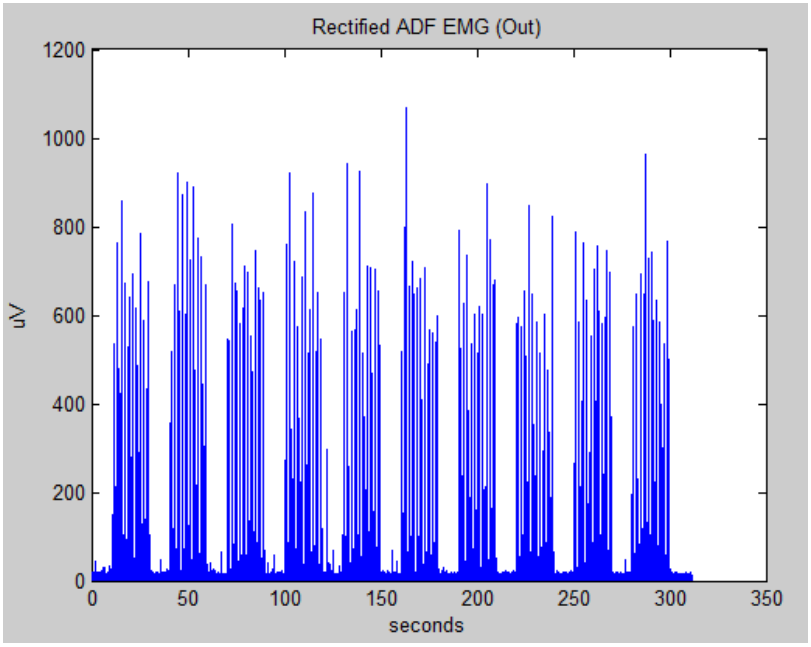

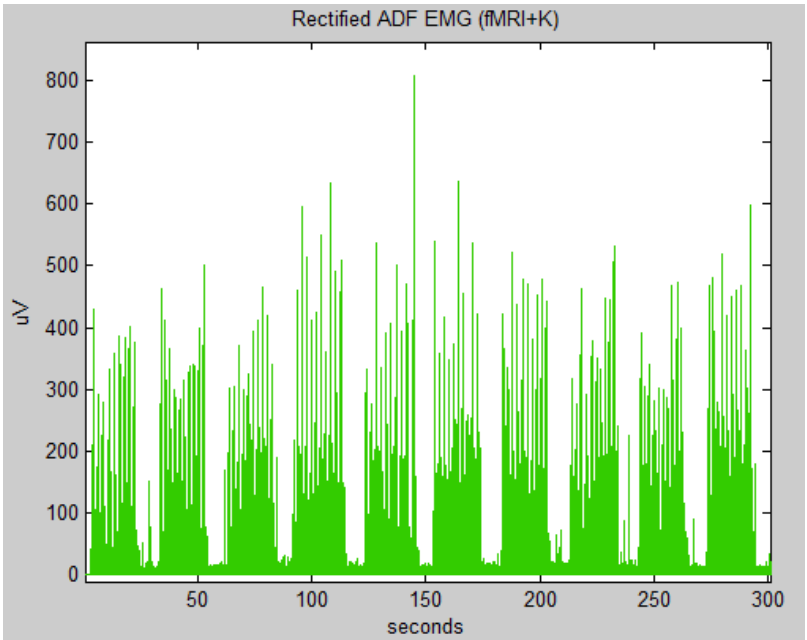

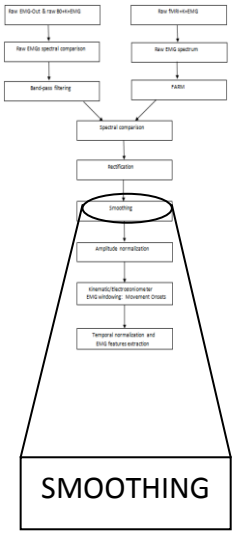
SMOOTHING

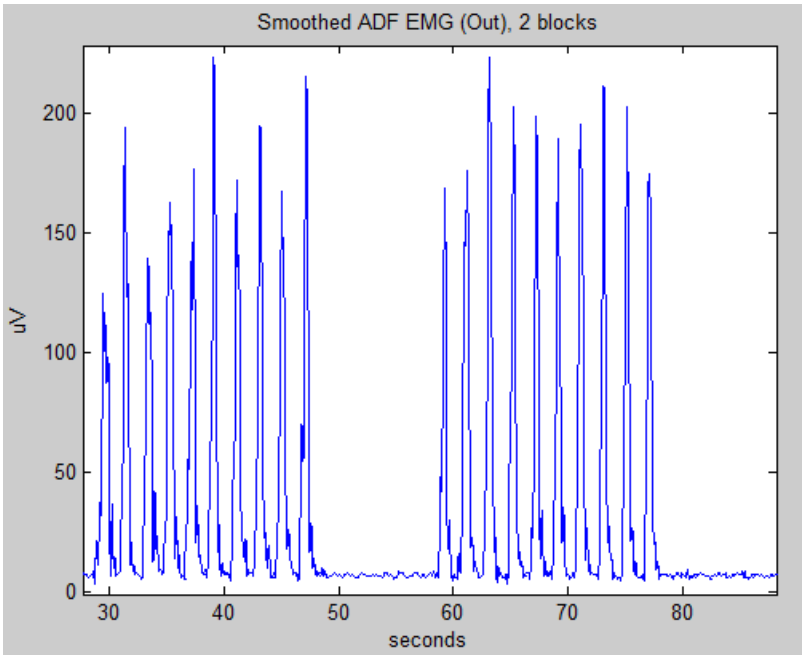
Smoothed ADF EMG (Out), 2 blocks
uV
seconds
0
50
100
150
200
30
40
50
60
70
80

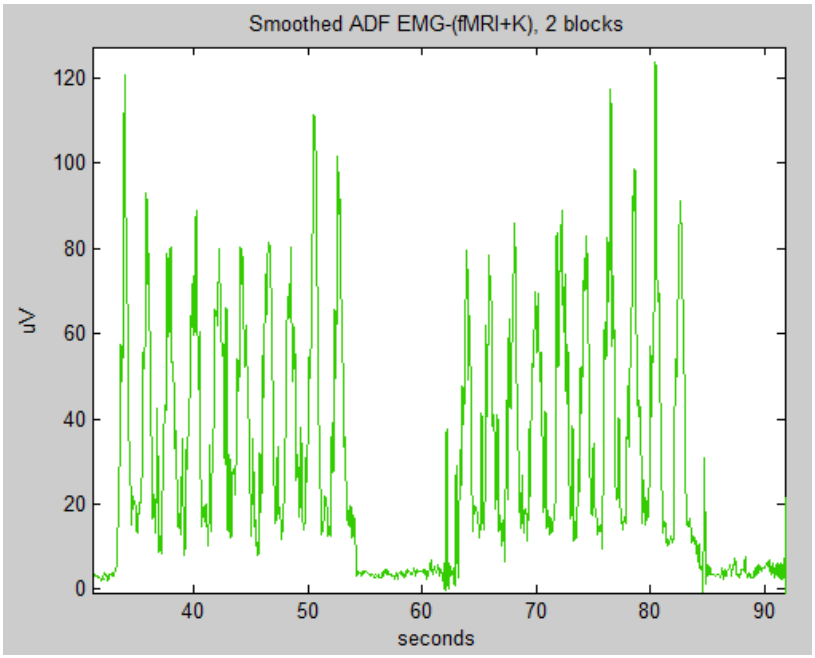
Smoothed ADF EMG-(fMRI+K), 2 blocks
uV
seconds
0
20
40
60
80
100
120
40
50
60
70
80
90

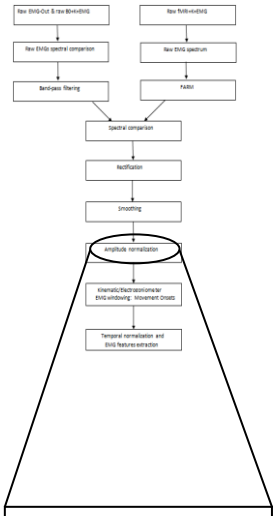

AMPLITUDE NORMALIZATION

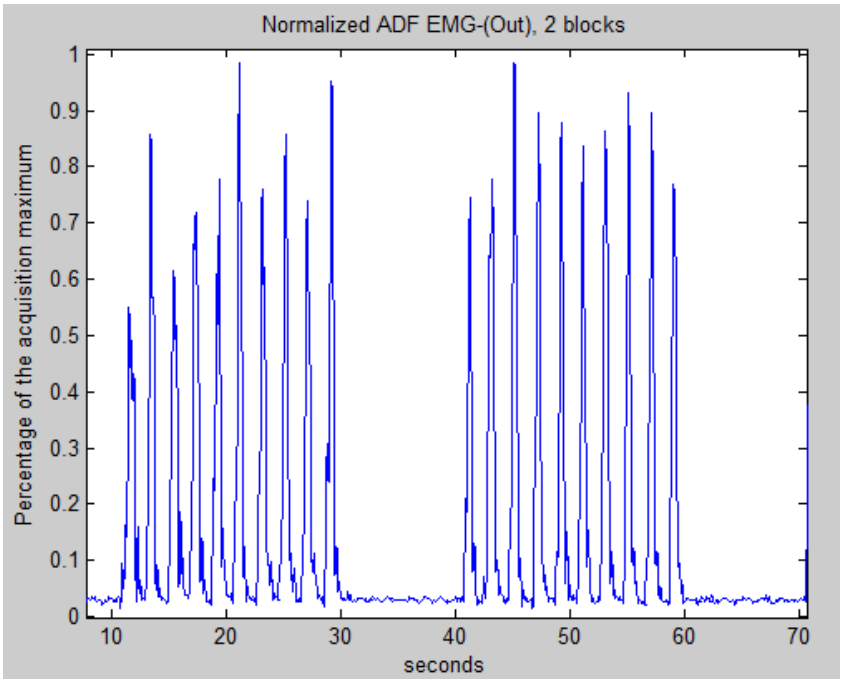

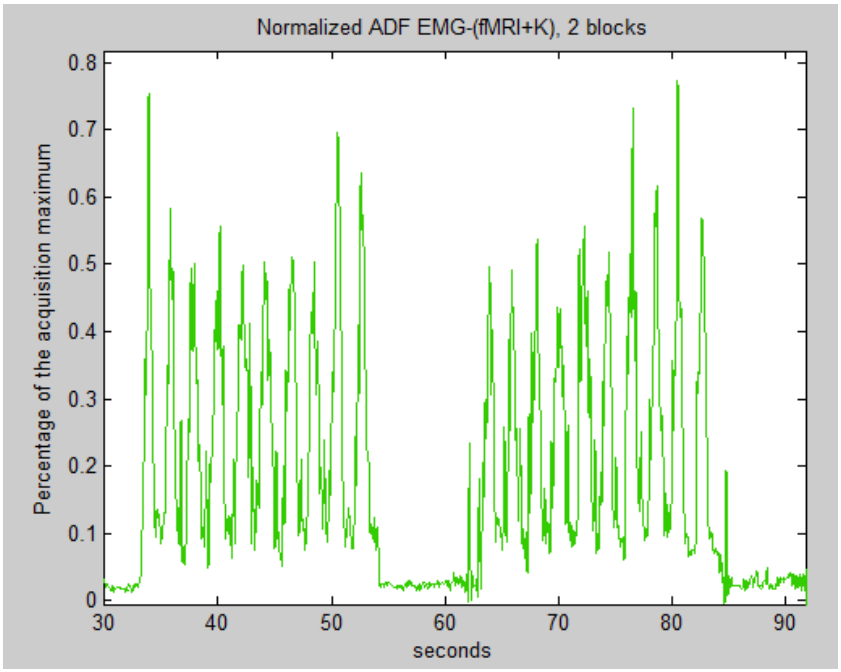

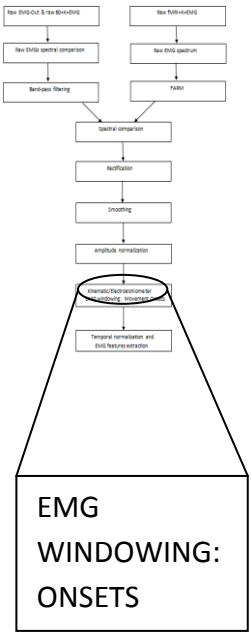

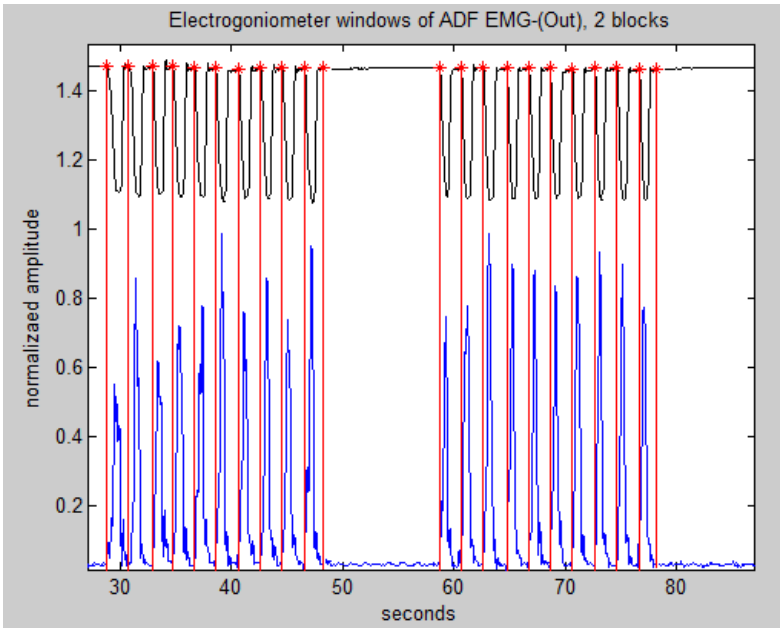

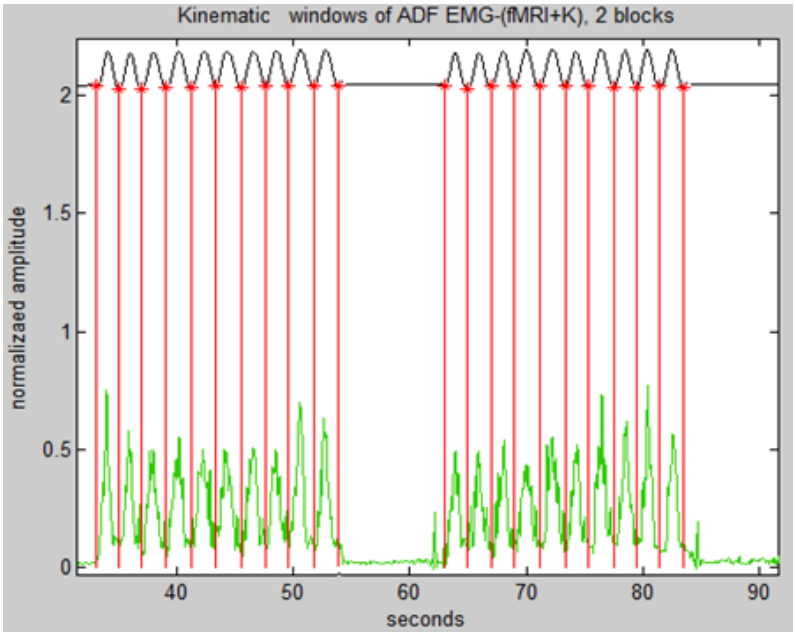

The temporal normalization consists in a sub-sampling to bring each windowed EMG burst to the same sample number, i.e. 100 in the present work, in order to conduct a significant comparative analysis both intra- and inter-subject.

EMG features analysis

The tables 3.5 present the EMG waveform correlation coefficients among the three experimental conditions and separately for the two motor tasks (subject 1 performed only ADF while subject 2 and 3 performed both ADF and WE but the ADF data of the subject 2 aren't available).

Tables 3.5. Above: ADF data. Below: WE data. Correlation coefficients of the EMG waveforms comparing the reference condition (EMG-Out) with the other two test conditions (B0+K+EMG and fMRI+K+EMG).

ADF	**Subject 1**		**Subject 3**	
	correlation coefficient	**p-value**	**correlation coefficient**	**p-value**
(B0+K+EMG)-(EMG-Out)	0.96	$p < 0.05$	0.92	$p < 0.05$
(fMRI+K+EMG)-(EMG-Out)	0.95	$p < 0.05$	0.93	$p < 0.05$

WE	**Subject 2**		**Subject 3**	
	correlation coefficient	**p-value**	**correlation coefficient**	**p-value**
(B0+K+EMG)-(EMG-Out)	0.76	$p < 0.05$	0.98	$p < 0.05$
(fMRI+K+EMG)-(EMG-Out)	0.78	$p < 0.05$	0.95	$p < 0.05$

Figure 3.7 shows an example of the average EMG waveforms in the three experimental conditions (EMG-Out, B0+K+EMG, fMRI+K+EMG), referring to the data of the subject 3 performing the ADF motor task.

Then the two considered indices of the EMG measure, area under the signal and peak amplitude, are calculated for the amplitude-normalized and windowed signal in the three experimental conditions. Tables 3.6 present the mean and standard deviation values of these two indices for each condition (EMG-Out, B0+K+EMG and fMRI+K+EMG) and separately for the two motor task (ADF and WE).

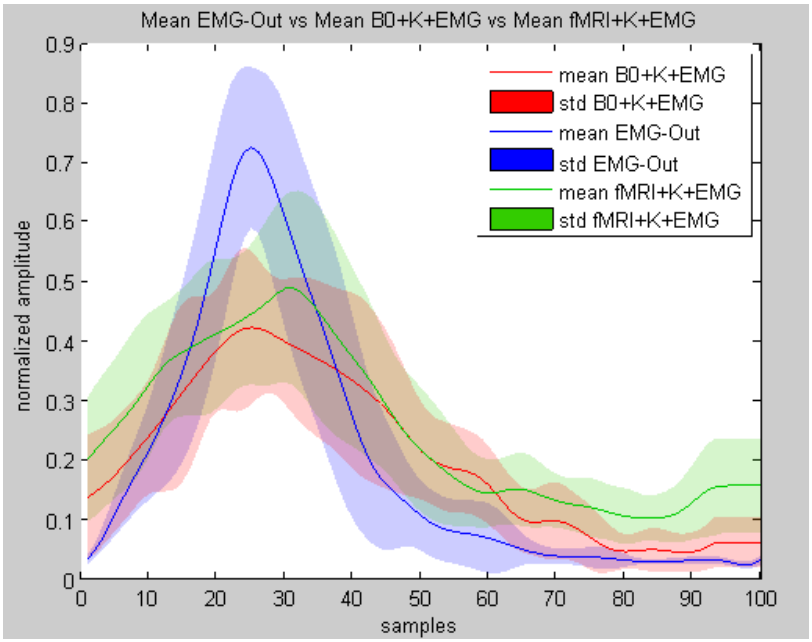

Figure 3.7. Average EMG waveforms in the three experimental conditions (EMG-Out, B0+K+EMG and fMRI+K+EMG) for the ADF motor task performed by the third subject.

Tables 3.6. Above: ADF data. Below: WE data. EMG area and peak amplitude values presented as mean ± std for both the motor tasks.

ADF	**Subject 1**		**Subject 3**	
	Area (arbitrary units)	**Peak amplitude (% of acquisition maximum)**	**Area (arbitrary units)**	**Peak amplitude (% of acquisition maximum)**
EMG-Out	14.37 ± 1.81	0.56 ± 0.08	19.20 ± 2.04	0.78 ± 0.10
B0+K+EMG	19.94 ± 4.65	0.59 ± 0.13	21.47 ± 2.94	0.59 ± 0.14
fMRI+K+EMG	17.05 ± 2.64	0.52 ± 0.11	26.73 ± 3.79	0.63 ± 0.12

WE	**Subject 2**		**Subject 3**	
	Area (arbitrary units)	**Peak amplitude (% of acquisition maximum)**	**Area (arbitrary units)**	**Peak amplitude (% of acquisition maximum)**
EMG-Out	21.22 ± 1.93	0.67 ± 0.13	22.54 ± 3.69	0.79 ± 0.09
B0+K+EMG	11.82 ± 2.33	0.45 ± 0.15	34.44 ± 3.37	0.73 ± 0.11
fMRI+K+EMG	19.99 ± 3.02	0.53 ± 0.12	30.75 ± 3.69	0.59 ± 0.13

The two-ways ANOVA test, used for an inter-condition and inter-subject comparison, gives a p-value < 0.05 for both the motor tasks (ADF and WE).

Tables 3.7 shows the coefficient of variation values for both the area and the peak amplitude among the three experimental conditions (same subject), separately for ADF and WE motor task.

Tables 3.7. Above: ADF data. Below: WE data. CVs among experimental conditions (EMG-Out, B0+K+EMG, fMRI+K+EMG) obtained for the two EMG indices.

ADF	**Subject 1**		**Subject 3**	
	Area	**Peak amplitude**	**Area**	**Peak amplitude**
CV (%)	16%	6%	17%	16%

WE	**Subject 1**		**Subject 3**	
	Area	**Peak amplitude**	**Area**	**Peak amplitude**
CV (%)	29%	20%	21%	14%

Chapter 4. Discussion

The aim of the work was the design and the validation of a novel experimental set-up for the detection of volitional intention during motor tasks functional imaging. The set-up integrates kinematics (for an extraction of movement characteristics), EMG acquisition (for a quantitative measure of the actual motor output performed by the subject) and fMRI scanning (for an evaluation, at the central level, of the sensorymotor activation patterns during motor tasks execution).

A set of procedures have been performed: i) a test on an MRI phantom was made to investigate EMG acquisition system influence on the magnetic resonance images quality. Moreover, three subjects underwent the following experimental protocol conditions: ii) fMRI scanning with only motion capture system working (i.e.,fMRI+K), iii) fMRI scanning with motion capture system and concurrent EMG acquisition (i.e. fMRI+K+EMG), iv) EMG acquisition with motion capture system working inside the scanner room with the fMRI sequence off (static magnetic field B0 on, i.e. B0+K+EMG) and v) stand-alone EMG acquisition performed outside the MRI room (i.e.EMG). Each subject performed the whole protocol once, where two subjects executed two different motor tasks (ankle dorsiflexion - ADF and wrist extension - WE) and one only a single motor task (ADF).

4.1 MRI-EMG compatibility test

We have shown that the SNR loss introduced in the magnetic resonance images by the designed experimental set-up is negligible. In fact, the mean SNR percentage loss over the considered phantom slices is 5.71 ± 3.4 %. Indeed, it is used as reference a literature study [54]: in simultaneous recordings of fMRI and EEG, it is showed that magnetic resonance image SNR, computed as we did, decreased as the number of electrodes increased, and Scarff and colleagues fixed as imaging data quality acceptable an images SNR loss of 11-12%. This value originates from complex device components and necessarily closer to the MR scanner than the experimental set-up used in the present work.

Anyway, it can be considered as general reference (worst case) about the additive noise on the fMRI images due to an additional device introduced in the scanner room.
Mullinger and colleagues evaluated phantom the effect, of the conducting materials in the EEG-caps with 1.5T acquisitions, accepting a SNR reduction of 27% with 32 electrodes [33].
Therefore it can be concluded that the data quality, i.e. the SNR, of the magnetic resonance images is not compromised by the introduction, inside the scanner room, of our experimental set-up which includes two cameras of the motion capture system and the EMG acquisition system (Porti7, TMSi) inlaid in an fMRI artefacts shielding prototype box.

4.2 fMRI-EMG compatibility test

Four cortical ROIs, consistently activated during motor tasks executions, were considered. An homogeneity index (coefficient of variation, CV) is computed for every ROI in the two experimental conditions including fMRI scanning (i.e., fMRI+K and fMRI+K+EMG). This homogeneity analysis is made to create a valuable background for the following SNR considerations which are both inter-subject and inter-condition and mean-based.
All the subjects, given a ROI, present similar CV values for a considered experimental condition (fMRI+K and fMRI+K+EMG). Data reproducibility among subjects in the same experimental condition was verified by the standard deviations calculation which were always (for every ROI) lower than 5%. A statistical comparison of the CV data between the reference (fMRI+K) and the test (fMRI+K+EMG) condition was made too: a Mann-Whitney test is used and a p-value > 0.05 is obtained. So, even if the CVs computed are higher (on average > 40%) than those obtained in literature for the same ROIs (i.e. lower than 30%, [11]) no significant variations in CV values between conditions and among subjects were obtained.
All the subjects show a significant percentage SNR loss between the two conditions (t-test, p-value < 0.05) with the reference one having the highest SNR values as expected. This loss is in the worst case (subject 2, SII) around 21% and in the best case (subject 3, SII) around the 5%.
On average, we can say that the SNR percentage loss between reference and test condition settles below the 16% with a std of 5% for each considered ROI.

Krakow and colleagues [27] show that, the EMG device could radiate spurious electromagnetic noise to its environment and the sensitive receiver coil in MR scanner could pick up this noise resulting in a degradation of the image signal-to-noise ratio. Krakow proves that the use of an appropriate shielding device (aluminum box and RF filter), as we did, for the EMG equipment could remove the presence, in the functional images, of these kinds of noise for a scanner of 1.5T. Although the Krakow's test on a representative range of MR compatible components, subtle changes in the manufacture process (e.g., modification of composition) or differences between manufacturers can cause significant changes of the MR-related material properties and the electromagnetic noise amplitude generated by the specific EMG system.

Despite this general functional images SNR loss between the two scanning conditions, for a given MR scanner of 1.5T, the detectable BOLD signal changes are around 1-2% so it is fundamental that the fMRI SNR loss doesn't affect the possibility of observing these signal variations.

Therefore, SNR maps which indicates the local presence of a minimum SNR to detect BOLD signal changes at five sensitivity levels were created for each condition and each subject separately. These maps show better detection sensitivity in the most internal brain regions, whereas they show a signal drop close to the external part, next to the skull. Such SNR loss at brain edges could be mainly due to motion artefacts (e.g. head motion, but also respiratory artefacts).

The SNR loss between reference and test scanning condition is evident, for all subjects, right at the edges of the brain with a shrinkage of the area with a minimum SNR such as to allow the detection of a BOLD signal change greater than 0.75%.

With respect to the detection of 1-2% BOLD signal changes, it was computed the percentage of the voxels within the four considered ROIs which presents the minimum SNR for distinguishing these BOLD variations, in both reference and test scanning conditions. At least in the 89% of all selected sub-volumes (ROIs) 1% BOLD signal change can be detected and almost in the whole considered ROIs volume 2% signal change can be revealed for both reference and test condition.

The most affected region resulted to be SII (second somatosensory area) that is the most occipital one and the closest to the brain boundary so it includes a significant portion of less sensitive area (>2% signal change detection) in the detectability maps.

For the other ROIs signal sensitivity is higher, always over 93% also for a BOLD signal change of 1%.

In conclusion, for all subjects and all ROIs, there is no significant difference, between the two experimental conditions, in the percentage of ROI area which enable to detect 1-2% of BOLD signal changes for the considered MR scanner. We can therefore be confident that the novel experimental set-up is able to correctly detect the BOLD signal, for statistical parametric maps analysis. Indeed, for each subject, the functional images obtained in the test scanning condition (fMRI+K+EMG) have been processed and then analyzed, creating the statistical parametric maps, to assess the effective cerebral activation due to motor tasks execution.

As it may be seen from the activation maps presented in the Results chapter, the functional images obtained with the developed experimental set-up (i.e., in the test condition) show clear, correct and significant cerebral activation. For all subjects, active ADF and WE elicited evident activation respectively in the leg and hand contralateral (right movements product activation in the left brain hemisphere) primary motor (M1) and primary somatosensory (SI) area. Cerebral activations obtained for the two protocol motor tasks show the somatotopical structure of the motor and somatosensory areas.

In fact, the cortical homunculus (Penfield) for the primary motory and somatosensory cortex shows, in the frontal plane, an activation deeper and closer to the longitudinal fissure for the lower limb movements (ADF) while an activation superficial and farther from the longitudinal fissure for the upper limb movements (WE). In figure 4.1 the described cortical homunculus and the two activations maps obtained for the subject 3 are shown.

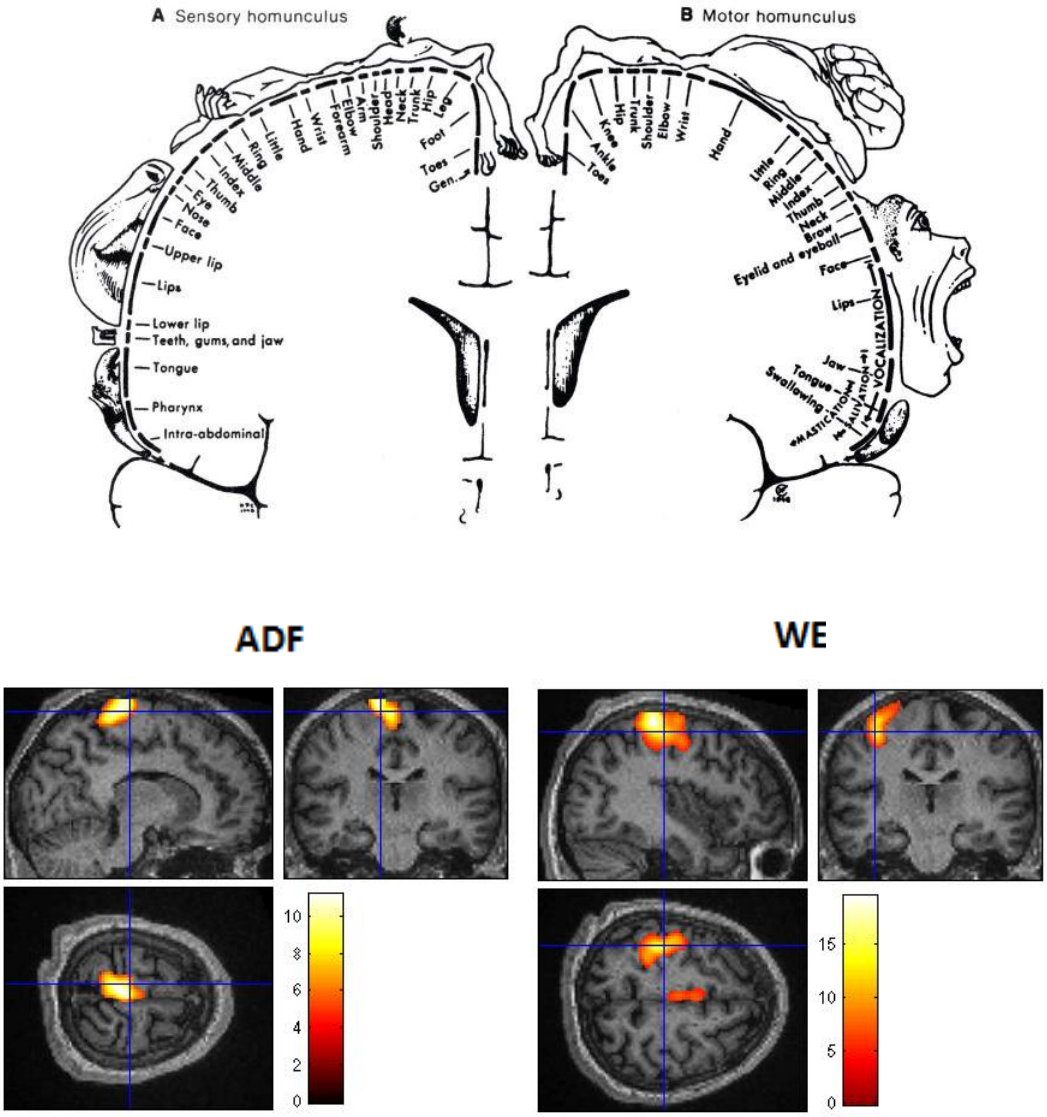

Figure 4.1. Above: Penfield homunculus for both sensory and motor cortex.
Below: cerebral activations elicited in ADF and WE execution for the subject 3.

4.3 EMG-fMRI compatibility test

fMRI artefacts reduction

In the present work the use of a prototype box, explicitly designed to shield the EMG acquisition system from induced fMRI artefacts (above all those induced by radio frequency pulses), however doesn't allow a direct analysis of the EMG signals recorded during fMRI scanning and the application of an fMRI artefacts reduction algorithm was necessary.

The spectral analysis of the raw EMG acquired during an fMRI scanning shows the expected artefact components at 12 Hz (and at its harmonics) [32] which corresponds to the slice-timing of the fMRI, i.e. 0.083 seconds.

As obtained in literature [38], the spectral comparison of raw EMG acquired in the reference (EMG-Out) and in the first test (B0+K+EMG) condition shows that the artefacts induced by the EMG wires movements in the main B0 fields are concentrated at frequencies lower than 30 Hz. So, we can confirm that the high-pass filter applied in the first EMG processing step (fcut = 30 Hz) is suitable to reduce, in the EMG signal, not only the movement artefacts due to the not-active-shielded cables but also the artefacts induced by their movement in B0.

With respect to the fMRI reduction algorithm used in the present work, the rationale for the choice of the FARM algorithm is the following one. The first approaches to the fMRI artefacts issue in EMG acquisitions were based on the EEG–fMRI artefact correction presented by Allen and colleagues [29], i.e. artefact template subtraction, but they have been shown not to be effective if there are movements during the acquisition since they do not account for changes in the shape of fMRI artefacts. So, once identified the fundamental effects of motion on the gradient-artefacts induced in the EMG signal, the choice of the artefacts correction algorithm ended up being the FARM developed by van der Meer and colleagues [38]. The FARM algorithm core still bases on the approach proposed by Allen [29] but effectively deals with the presence of irregularities in the artefacts shape increasing the algorithm artefact reduction performance. The choice of the template subtraction approach to correct EMG data contaminated by fMRI artefacts could be questioned, as there are other techniques available, like individual component analysis (ICA) [2,55] or principal components analysis (PCA) [45], but each of these techniques uses the implicit assumption that the fMRI slice-artifact has a periodic waveform.

Furthermore in PCA and independent component analysis (ICA), being higher-order statistical approaches, the cause of remaining inaccuracies in the corrected EMG are more difficult to assess than with template subtraction alone. By using template subtraction approach, as implemented in FARM, residual artefacts are known to be due to uncommon shapes in the slice-artefact, and no a-priori assumptions are made [38].

The rationale for still using PCA analysis, after the template subtraction, also in FARM, is that the first four principal components always correlated well with the slice-templates; interpretation from the 5th to the last component is increasingly difficult [38].

In the present study FARM performs an effective fMRI artifacts correction on every EMG dataset, except for the ADF data of the second subject, where the application of the algorithm only reduces the amplitude of the noise but doesn't remove enough fMRI superimposed noise to allow a proper EMG activations detection. So, this dataset wasn't processed in the current work.

The amplitude of the fMRI artefacts superimposed on the EMG signal, obviously, depends on the proximity of the analyzed limb site to the scanner bore too. For this reason the EMG recorded during WE presents fMRI artefacts of about an order of amplitude higher, with respect to the those recorded for ADF motor task. However the dataset which isn't well processed by the FARM comes from an ADF task execution during fMRI scanning. This dataset presents the larger artefact noise amplitude, considering the same motor task executed during fMRI scanning, among the three subjects. For this reason it presents, from the spectral point of view, higher spectral lines at the frequency (12 Hz and its harmonics) corresponding to the fMRI slice-timing (0.083 s). Fig. 4.2 shows this dataset and fig. 4.3 compares its spectrum with that of another ADF dataset acquired during fMRI scanning. Apart from this difference in artefacts amplitude, the EMG dataset presents the same artifacts features (fMRI slice shapes) of the other two subjects.

The EMG dataset processed by FARM is shown in fig. 4.4. The active periods (i.e. 20 seconds of muscle contraction with frequency of 0.5 Hz) can be hardly distinguished from rest blocks (10 seconds). Furthermore, the baseline noise amplitude is one order of amplitude higher than the other well corrected datasets. The reason of this failed artefacts removing deals with a wrong slice-artefacts template construction performed by the algorithm. Along the imposed neighbouring in which it is possible to search, the algorithm is not able to estimate further slice-artefacts well correlated with the current slice to be corrected. However, the best template construction doesn't effectively clean the EMG data, meaning that doesn't correctly estimate the artefacts template. Among possible reasons for incomplete template estimation, it can be included excessive cables motion.

Further analysis is required to improve FARM performance, and in particular a detailed analysis of each slice template, especially at the transition from an fMRI acquired volume to the following one, tests on different neighbouring width (which it is now set at 50 slices) and number of slices to construct the slice-artefacts template (set at 12 in the current FARM version) might improve the artefacts removal.

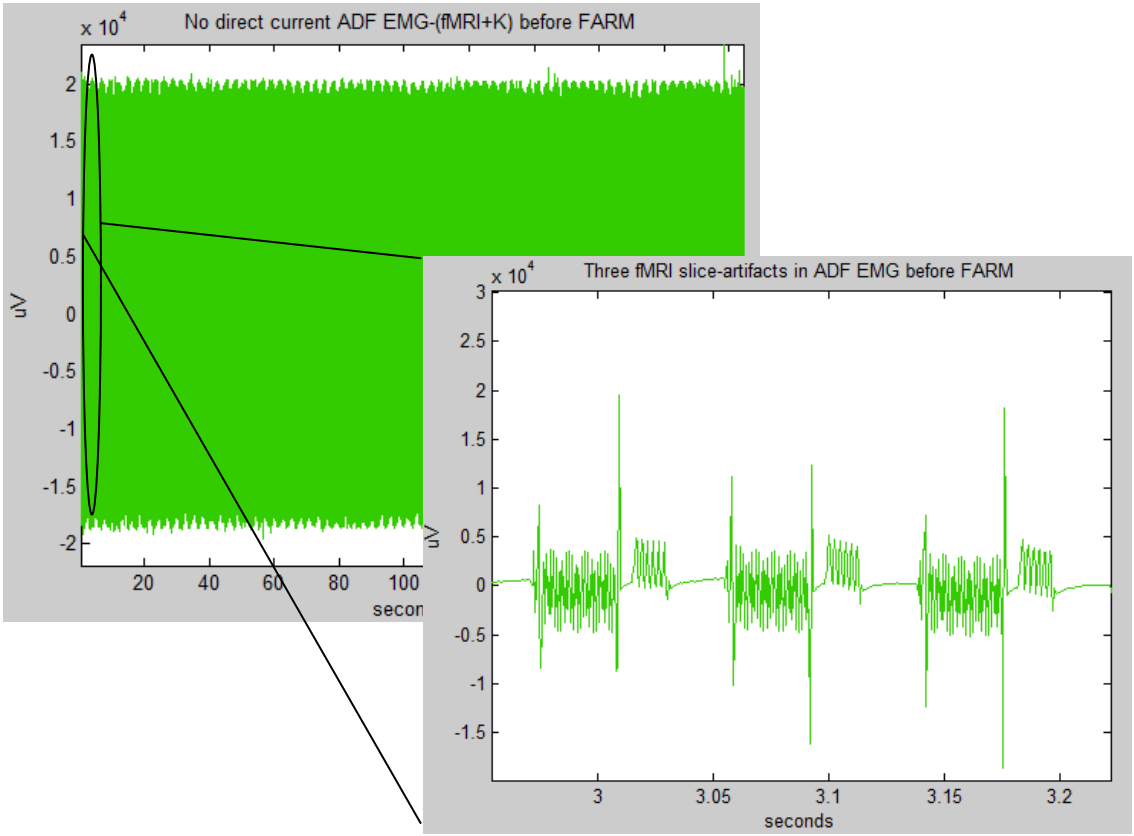

Figure 4.2. EMG dataset, with a zoom on the fMRI-induced artifacts, which isn't well processed by the FARM algorithm (ADF motor task).

RAW DATASET NOT-WELL-FARM-PROCESSED

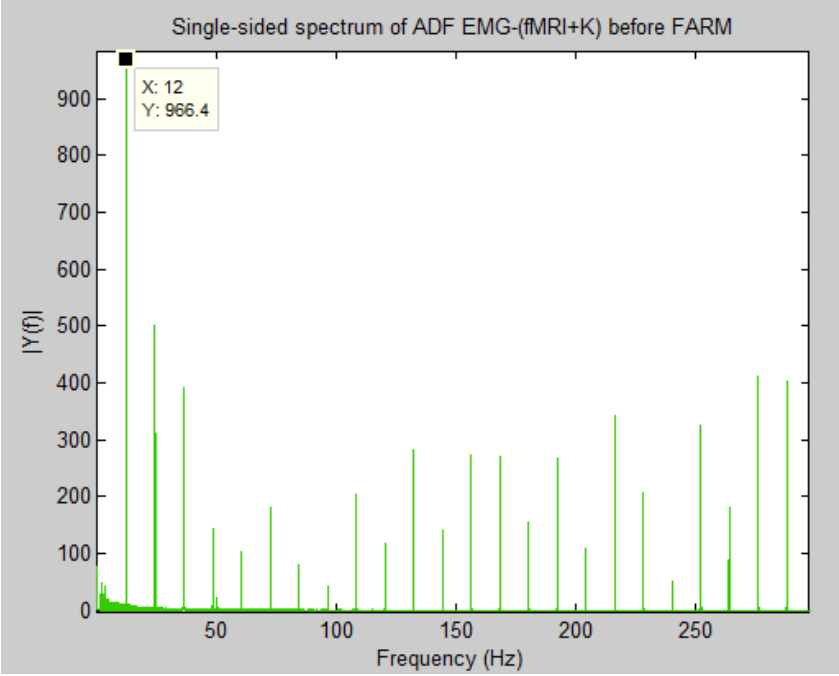

RAW DATASET WELL-FARM-PROCESSED

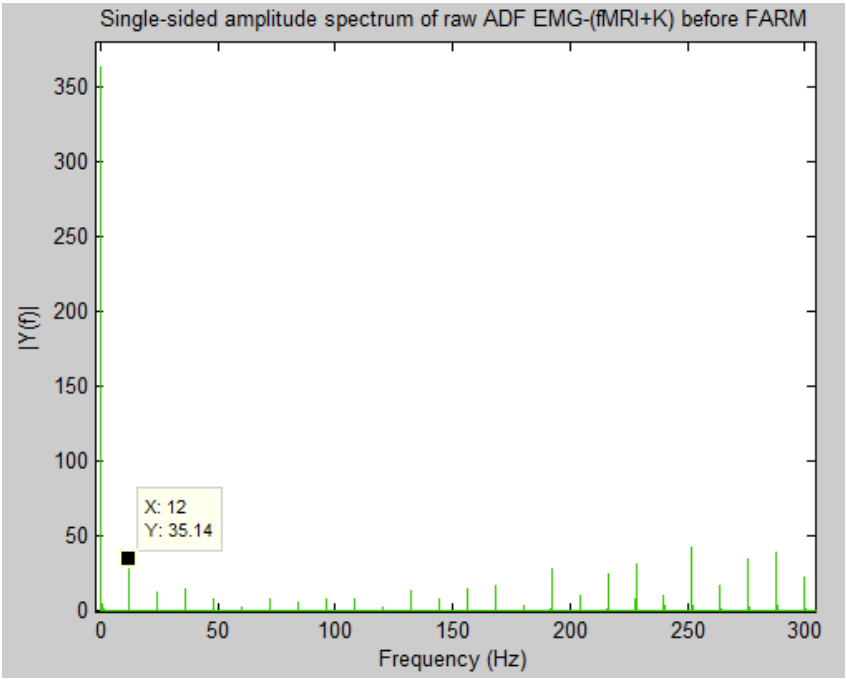

Figure 4.3. Spectral comparison between the raw EMG dataset which isn't well processed by FARM algorithm and one of the raw EMG datasets which are well processed by FARM algorithm. Both EMG are acquired during an ADF motor task execution.

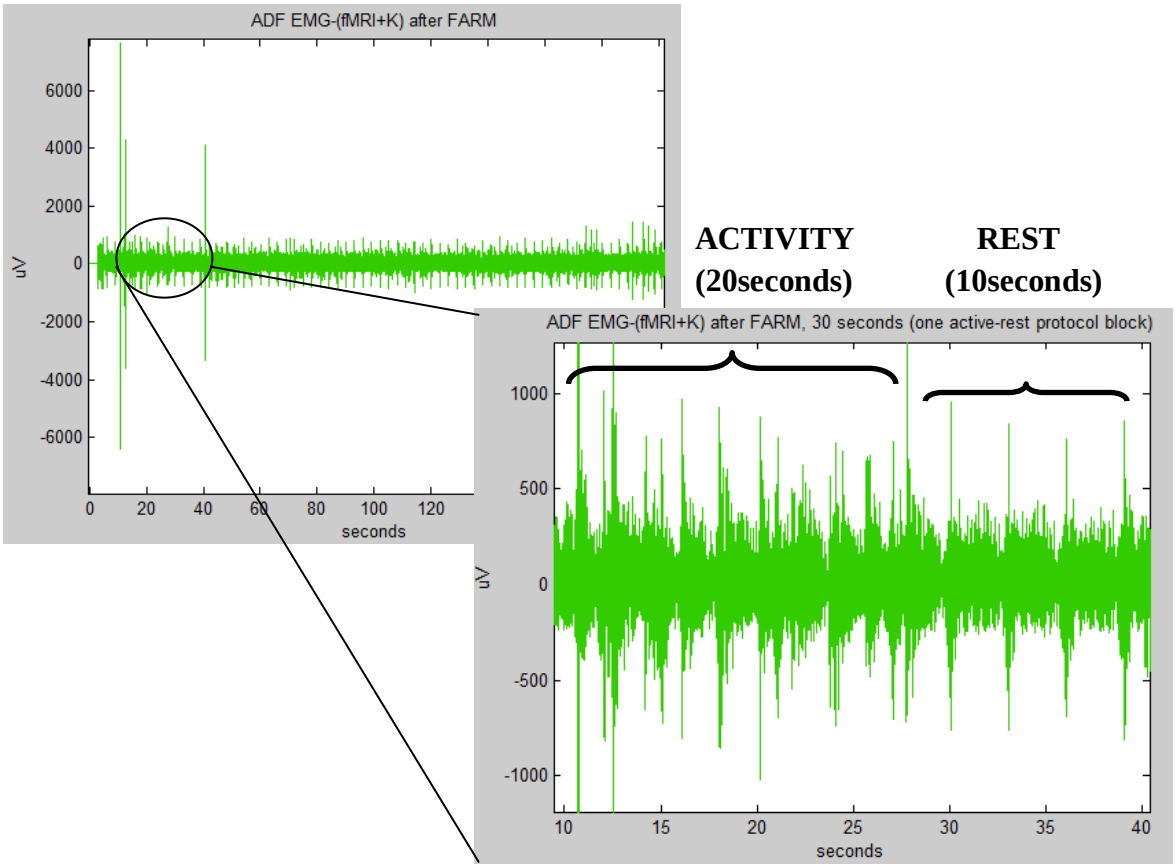

Figure 4.4. FARM-not-well-processed EMG dataset. The artifacts aren't removed effectively (a volume artifact is present every 3 seconds) even if there a reduction in their amplitude and, in the zoom, an hard distinction between active and rest period can be noticed.

EMG features analysis

The literature offers many indices, both in time and in frequency, to evaluate the EMG measurement quality and reproducibility. In the present work three EMG features were chosen to compare the experimental reference condition (EMG-Out) to the other two test conditions (B0+K+EMG and fMRI+K+EMG): correlation coefficient between average EMG signal shape, peak amplitude and area under the EMG curve.

For all the subjects, the mean EMG signal waveforms in the three conditions are highly correlated (p-value < 0.05). In particular, each subject, for each motor task, presents correlation coefficients between the reference condition and the B0+K+EMG condition higher than 0.76 with this being the worst case (the correlation coefficients between the considered condition it's greater than 0.92 for two over three subjects).

With regard to the most important signals correlation, that between the reference condition and the fMRI+K+EMG condition, all the subjects have a correlation similar to that registered for the B0 condition: the correlation coefficient is always higher than 0.75. As the previous correlation, this last value is the worst documented case, with two subjects over three having correlation values above 0.93. The similarity between the correlation of the two investigated conditions shows that the EMG signal acquired inside the considered scanner room with or without the fMRI scanning on it is not affected or significantly distorted in its characteristic waveform.

For what is concerning the other two EMG indices, area under the signal and the maximum peak amplitude, the two-way ANOVA test, applied on each index separately, shows a significant difference (p-value < 0.05) among the three experimental conditions but also among subjects in the same experimental condition. Given the large intra-and inter-subject EMG signal variability, preventively, in the signal processing, the EMG signal was normalized to reasonably perform comparison among conditions. But the most convenient normalization process for dynamic EMG contractions is a questionable point in literature [56,47] and a significant EMG variability, function of the normalization applied, among trials must still be considered [53,57,58,59]. So the variability of the two EMG indices proposed, area and peak amplitude, was calculated for each subject considering the three experimental conditions (EMG-Out, B0+K+EMG, fMRI+K+EMG). The CVs obtained for both indices for the ADF task range from 6% to 17% for the peak amplitude and sets around 17% for the area while for the WE task the CVs range from 14% to 20% for the peak amplitude and from 21% to 29% for the area. Therefore all the CVs computed set below the 30%.

As various studies argue, according to the muscle considered, the type of contraction (isometric, dynamic, maximal, submaximal, etc.) the EMG processing applied and the descriptive EMG feature considered, a wide range of values for the intra-subject coefficient of variation are obtained: from 9% ([53], considering 50% of the maximal isometric contraction of the triceps muscle) to 52% ([57], from a variety of other lower-extremity muscles in slow dynamic exercises).

Araujo and colleagues [59] studied the ADF maximal voluntary isometric contraction (MVIC) in different trials and obtained an intra-subject CV within days of about 22%.

Araujo considers this CV value as a baseline of the variability of the considered EMG signal because of the high reproducibility of the MVIC task in well controlled experiments. In addition to this established intrinsic EMG variability, we have to consider that, in the present work, the contractions weren't controlled strictly as in mentioned literature works but the movement was self-paced in amplitude. Then the assumption that a subject performs all the EMG contractions, acquired in different environmental conditions but, above all, in different temporal moments, with the same commitment and effort (muscle force developed) is very weak. So, even though there is a significant statistical difference, among the three experimental conditions, in the means two presented EMG indices (area and peak amplitude), this discrepancy (tested by CVs) is included in the variability which always affects the intra-subjective reproducibility of EMG signal and therefore can be considered as negligible in this context.

Chapter 5. Conclusions and future perspectives

The inclusion of the EMG acquisition, besides the kinematics data [6], during fMRI scanning provides extra information and offers advantages to studies focused on motor control and rehabilitation.

The movement performed by the tested subject can be analyzed quantitatively at its muscular origin and the peripheral motor output (EMG signal) can be used as a clue to modulate the information of the cerebral activation derived from the functional images. Furthermore, the present study conducts a systematic validation test on a particular experimental set-up, not specifically designed to be MRI-compatible, which includes an EMG acquisition system, suitable, for its technical features, not only to record the muscular activity but also to be an effective functional electrical stimulation (FES) controller on the same muscle. The conducted analysis verify the feasibility, without significant alterations or distortions of any data, of a combined fMRI-motion capture-EMG acquisition with respect to a specific EMG recording system (Porti7, TMSi). The SNR of the functional images obtained with the proposed experimental set-up was analyzed and a negligible SNR percentage loss was verified, demonstrating that the BOLD signal can be correctly detected by the integrated experimental set-up.

The EMG data acquired outside and inside the MR scanner room were compared to evaluate a possible signal degradation. The MR environment introduces artefacts in the EMG signal and therefore the signal has to be pre-processed by an appropriate artefact reduction algorithm which doesn't distort the signal but only remove the greatest amount of induced fMRI artefacts (i.e., FARM algorithm). The artefact-cleaned EMG signals present an high waveform correlation with the reference condition (i.e. EMG acquired outside the scanner room). Further, the area and the peak amplitude of the EMG, representative indices of an EMG measurement, were calculated and their variability between reference and test conditions evaluated. We have shown that no significant bias is induced in the EMG signal when it is acquired with the experimental set-up presented in this work.

In conclusion, the current study validates the application of a novel integrated set-up which allows to detect volitional intention and effective executed movement during motor-tasks functional imaging. Indeed, neuromotor rehabilitation central mechanisms of action are of great interest in the definition of a proper patient training and it is widely accepted that volitional contribution of the subject during the rehab session is a key feature for its success.

The proposed experimental set-up allows to simultaneously record the movement characteristics (i.e., amplitude, velocity, etc.) and the volitional contribution of the subject throughout the session (i.e., muscle contractions, co-contractions, etc.), during functional imaging scanning.

The feasibility of a combined fMRI scanning and possibly also an EMG-piloted FES could increase the information on the motor rehabilitation process and be an effective way to evaluate the changes in cerebral activation patterns in studies on patients affected by different kinds of motor disabilities.

References

1. Glaser J. (2012). fMRI Artifact Correction in EEG and EMG Data [diploma thesis]. Vienna University of Technology, Institute of Computer Technology.
2. MacIntosh B.J., Baker S.N., Mraz R., Ives J.R. (2007). Improving Functional Magnetic Resonance Imaging Motor Studies Through Simultaneous Electromyography Recordings. Human Brain Mapping 28: 835–845.
3. van Roostelaar A.F., Remco R., de Jong B.M., Hoogduin J.M., Tijssen M., MauritisM.N. (2007). fMRI analysis for motor paradigms using EMG-based designs: a validation study. Hum Brain Map 28: 1117–27.
4. Richardson MP, Grosse P, Allen PJ, Turner R, Brown P. (2006). BOLD correlates of EMG spectral density in cortical myoclonus: description of method and case report. Neuroimage; 32 (2): 558–65.
5. van Rootselaar A.F., Maurits N.M., Renken R., Koelman J., Hoogduin J.M., Leenders K.L., et al. (2008). Simultaneous EMG-functional MRI recordings can directly relate hyperkinetic movements to brain activity. Hum Brain Map; 29 (12): 1430–41.
6. Gandolla M., Ferrante S., Casellato C., Ferrigno G., Molteni F., Martegani A., Frattini T., Pedrocchi A. (2011). fMRI Brain Mapping During Motion Capture and FES Induced Motor Tasks: Signal to Noise Ratio Assessment**.** Medical Engineering & Physics 33, 1027-1032.
7. Lemieux L., Allen P.J., Franconi F., Symms M.R., Fish D.R. (1997). Recording of EEG during fMRI Experiments: Patient Safety. Magn. Reson. Med.38(6): 943-952.
8. Lazeyras F., Zimine I., Blanke O., Perrig S., Seeck M. (2001). Functional MRI with Simultaneous EEG Recording: Feasibility and Applicatin to Motor and Visual Activation. Journal of Magnetic Resonance Imaging 13: 943-948.
9. Meriläinen V. (2002). Magnetic Resonance Imaging with Simultaneous Electroencephalography Recoding: Safety Issues [diploma thesis]. Helsinki University of Technology, Department of Electrical and Communications Engineering.
10. Jiang N., Falla D., D'Avella A., Graimann B., Farina D. (2010) Myoelectric Control in Neurorehabilitation. Crit Rev Biomed Eng 38(4):381–391.

11. Francis S., Lin X., Aboushoushah S., White T.P., Phillips M., Bowtell R., Constantinescu C.S. (2009). fMRI Analysis of Active and Electrically Stimulated Ankle Dorsiflexion. NeuroImage44: 469-479.
12. Merletti R., Botter A., Troiano A., Merlo E., Minetto M.A. (2009): Technology and Instrumentation for Detection and Conditioning of the Surface Electromyographic Signal: State of the art. Clinical Biomechanics 24: 122–134.
13. Kiryu T. (1999). Measurement and Analysis of Surface EMG using Multi-Channel Array Electrode [lecture]. Nigata University.
14. De Luca C.J. (2002).Surface electromiography: detection and recording. DelSys Incorporated.
15. Ravariu C. (2011). Novel Methods in Electrophysiology Aided by Electronic Devices and Circuits. Contributions to: Applied Biomedical Engineering by Dr.GargiuloG. (Ed.), ISBN: 978-953-307-256-2, InTech, DOI: 10.5772/21443.
16. Tachtsidis I. (2010). Other Neuroimaging Methods in Epilepsies: Brain Optical Imaging and More. Contributions to: Atlas of Epilepsies by Panayiotopoulos C.P. Springer-Verlag London Limited.
17. Aliverti A. (2014). Basic Principles and Technologies for Nuclear Medicine and Magnetic Resonance Imaging (MRI) [lecture]. Polytechnic University of Milan, Department of Electronics, Information and Bioengineering.
18. Cohen M.S. (1999). Echo-planar imaging (EPI) and functional MRI. Functional MRI, Springer Verlag, Berlin.
19. Rother J., Schreiber A., Kraemer F.M., Janz C., Hennig J. (1998). Functional Magnetic Resonance Imaging (fMRI). Magnetism in Medicine: A Handbook, pp. 350-372. Wiley-VHC, Berlin.
20. Ogawa S., Menon R.S., Kim S.G., Ugurbil K. (1998). On the Characteristics of Functional Magnetic Resonance Imaging of the Brain. AnnuRevBiophysBiomolStruct. 27: 447-74.
21. Baselli G. (2014). Functional Magnetic Resonance Imaging (fMRI) [lecture]. Polytechnic University of Milan, Department of Electronics, Information and Bioengineering.

22. MHRA (Medicines and Healthcare products Regulatory Agency) (2014). Safety Guidelines for Magnetic Resonance Imaging Equipment in Clinical Use. UK Department of Health.
23. Kwan-Hoong Ng, Ahmad A.C., Nizam M.S., Abdullah B.J.J. (2003). Magnetic Resonance Imaging: Health Effects and Safety. Proceedings of the International Conference on Non-Ionizing Radiation at UNITEN (ICNIR2003) - Electromagnetic Fields and Our Health (October 2003).
24. Heiland S. (2008). From A as in Aliasing to Z as in Zipper: Artifacts in MRI. Clinical Neuroradiology 18: 25-36.
25. Wood M.L. (1997). Artifact Identification and Elimination. RSNA Categorical Course in Physics: The Basic Physics of MR Imaging, pp. 56-69.
26. Rosenkranz, K.., Lemieux, L. (2010). Present and future ofsimultaneous EEG-fMRI. Magnetic Resonance Materials in Physics, Biology and Medicine, 23 (5-6), 309–316.
27. Krakow K, Allen PJ, Symms MR, Lemieux L, Josephs O, Fish DR.(2000). EEG recording during fMRI experiments: Image quality. Hum.Brain.Mapp.;vol.10:10–15.
28. van Duinen H., Zijdewind I., Hoogduin H., Maurits N. (2005).Surface EMG measurements during fMRI at 3T: accurate EMG recordings after artifact correction. Neuroimage 27:240–246.
29. Allen P.J., Josephs O., Turner R. (2000). A method for removing imaging artifact from continuous EEG recorded during functional MRI. Neuroimage 12:230–239.
30. Allen P.J., Polizzi G., Krakow K., Fish D.R., Lemieux L. (1998). Identification of EEG events in the MR scanner: the problem of pulse artifact and a method for its subtraction. Neuroimage 8:229–239.
31. Ritter P., Becker R., Graefe C., Villringer A. (2007). Evaluating gradient artifact correction of EEG data acquired simultaneously with fMRI. Magnetic Resonance Imaging 25: 923–932.
32. Hoffmann A., Jager L., Werhahn K..J., Jaschke M., Noachtar S., Reiser M. (2000). Electroencephalography during functional echo-planar imaging: detection of epileptic spikes using post-processing methods. MagnReson Med44:791–798.

33. Mullinger K., Yan W.Y., Bowtell R. (2011). Reducing the gradient artefact in simultaneous EEG-fMRI by adjusting the subject'saxial position. NeuroImage 54: 1942–1950.
34. Laudon, M. K., Webster, J. G., Frayne, R., and Grist, T. M.(1998). Minimizing interference from magnetic resonance imagers during electrocardiography. IEEE Trans. Biomed. Eng.45:160–163.
35. Felblinger J., Slotboom J., Kreis R., Jung B., and Boesch C.(1999). Restoration of electrophysiological signals distorted by inductive effects of magnetic field gradients during MR sequences. Magn.Reson. Med. 41: 715–721.
36. Widrow B., Glover J. R., McCool J. M., Kaunitz J. (1975).Adaptive noise cancellation: Principles and applications. Proc. IEEE 63: 1692–1716.
37. Mandelkow H., HalderP., Boesiger P., Brandeis D. (2006). Synchronisation facilitates removal of MRI artefacts from concurrent EEG recordings and increases usable bandwidth. Neuroimage 32 (3): 1120–1126.
38. van der Meer J.N, Tijssen M.A.J., Bour L.J., Van Roostelaar A.F., Nederveen A.J. (2010). Robust EMG–fMRI artifact reduction for motion (FARM). Clinical Neurophysiology 121: 766–776.
39. Casellato C, Ferrante S, Gandolla M, Volonterio N, Ferrigno G, Baselli G, et al.(2010). Simultaneous measurements of kinematics and fMRI: compatibility assessment and case report on recovery evaluation of one stroke patient. J NeuroEngRehabil7:49.
40. Tang A.M., Kacher D.F., Lam E.Y., Wong K.K., Jolesz F.A., Yang E.S. (2008). Simultaneous ultrasound and MRI system for breast biopsy: compatibility assessment and demonstration in a dual modality phantom. IEEE Trans Med Imaging 27: 247–54.
41. Bonmassar, G., Angelone, L., Segonne, F., Purdon, P., Potthast, A., Fischl, B., Wald, L., Ives, J., George, J., Belliveau, J.(2002). SAR Computations in a realistic and high-resolution model of the head with EEG Electrodes in place. Human Brain Mapping; Jun. 2–6; Sendai, Japan.
42. Rorden C., Brett M. (2000). Stereotaxic Display of Brain Lesion. 12:191-200.

43. Prendin A. (2010). Quantification of Maps Activation of Functional Magnetic Resonance Images for the Study of Schizophrenia [Diploma thesis] .University of Padua, Faculty of Engineering, Department of Informatic Engineering.
44. Delorme A., Makeig S. (2004). EEGLAB: an open source toolbox for analysis of single-trial EEG dynamics including independent component analysis. J Neurosci Methods; 134 (1): 9–21.
45. Niazy R.K., Beckmann C.F., Iannetti G.D., Brady J.M., Smith S.M. (2005). Removal of FMRI environment artifacts from EEG data using optimal basis sets. Neuroimage; 28 (3): 720–37.
46. Basmajian J.V. and De Luca C.J. (1985). Muscles alive: their functions revealed by electromyography (5th edition). Baltimore: Williams & Wilkins.
47. Halaki M. and Ginn K. (2012). Normalization of EMG Signals: To Normalize or Not to Normalize and What to Normalize to? Computational Intelligence in Electromyography Analysis – A Perspective on Current Applications and Future Challenges [chapter7]. Edited by Ganesh R. Naik, ISBN 978-953-51-0805-4, 460 pages, Publisher: InTech.
48. Kaufman L, Kramer DM, Crooks LE, Ortendahl. (1989) Measuring signal-to noise ratios in MR imaging. 173:265-267.
49. Johannsen, P., Christensen, L.O., Sinkjaer, T., Nielsen, J.B., 2001. Cerebral functional anatomy of voluntary contractions of ankle muscles in man. J. Physiol. 535, 397–406.
50. Dai T.H et al (2001). Relationship between muscle output and functional MRI-measured brain activation. Exp. Brain Res. 140, 290–300.
51. Tjandra T. et al. (2005). Quantitative assessment of the reproducibility of functional activation measured with BOLD and MR perfusion imaging: implications for clinical trial design. Neuroimage 27, 393–401.
52. Parrish TB, Gitelman DR, LaBar KS, Mesulam MM. (2000). Impact of signal-to-noise on functional MRI. Magn Reson Med ; 30:161–73.
53. Yang J.F. and Winter D.A. (1983). Electromyography reliability in maximal and submaximal isometric contractions. Arc Phys Med Rehab 64: 417-420.

54. Scarff CJ, Reynolds A, Goodyear BG, Ponton CW, Dort JC, Eggermonta JJ. (2004). Simultaneous 3-T MRI and high-density recording of human auditory evoked potentials. NeuroImage, 23:1129-1142.
55. Mantini D., Perrucci M.G., Cugini S., Ferretti A., Romani G.L., Del Gratta C. (2007). Complete artifact removal for EEG recorded during continuous fMRI using independent component analysis. Neuroimage; 34 (2): 598–607.
56. Mathiassen SE (1997) A checklist for normalisation of surface EMG amplitude. Proceedings of the Second General SENIAM Workshop Chapter 2. Eds: Hermens H, Hagg G, Freriks B. Stockholm, Sweden.
57. Knutson L.M. et al. (1994). A study of various normalization procedures for within day electromyographic data. J Electromyogr Kines 4: 47-59.
58. Christ C. et al. (1994). Reliability of selected parameters of isometric muscle function associated with testing 3 days x 3 trials in women. J Strength Cond Res 8: 65-71.
59. Araujo R.C. et al. (2000). On the inter- and intra-subject variability of the electromyographic signal in isometric contractions. Electromyogr. Clin. Neurophysiol. 40, 225-229.